PROVENANCE AND THERMAL HISTORY OF DETRITAL SANDSTONES OF THE SCOTIAN BASIN, OFFSHORE NOVA SCOTIA, USING THE APATITE FISSION TRACK AND $^{40}Ar/^{39}Ar$ METHODS

by

ALEXANDER MICHAEL GRIST

Submitted in partial fulfillment of the

requirements for the degree of

MASTER OF SCIENCE

at Dalhousie University

Halifax, Nova Scotia

August 1989

DALHOUSIE UNIVERSITY

DEPARTMENT OF GEOLOGY

The undersigned hereby certify that they have read and recommend to the Faculty of Graduate Studies for acceptance a thesis entitled "Provenance and Thermal History of Detrital Sandstones of the Scotian Basin, Offshore Nova Scotia, Using the Apatite Fission Track and $^{40}Ar/^{39}Ar$ Methods", by Alexander Michael Grist, in partial fulfillment of the requirements for the degree of Master of Science.

Dated Nov. 29, 1999

Supervisor: ___

Readers: ___

___

___

D A L H O U S I E U N I V E R S I T Y

DATE November 28, 1989

AUTHOR Alexander Michael Grist

TITLE Provenance and Thermal History of Detrital Sandstones of the Scotian Basin, Offshore Nova Scotia, using the Apatite Fission Track and $^{40}Ar/^{39}Ar$ Methods.

Department or School Geology

Degree M.Sc. Convocation February Year 1990

Permission is herewith granted to Dalhousie University to circulate and to have copied for non-commercial purposes, at its discretion, the above title upon the request of individuals or institutions.

Signature of Author

For my grandmother, Marguerite Driscoll.

Table of Contents

Table of Figures

Table of Tables

ABSTRACT

Apatite fission track analysis and $^{40}Ar/^{39}Ar$ age spectrum analysis have been carried out on sandstone drillcores taken at depths of 2 to 5 km from 9 hydrocarbon exploration wells in the Scotian Basin. K-feldspar argon spectra from the Early Cretaceous Missisauga and Logan Canyon Formations, which are unaffected by present-day burial heating at depths of less than 4 km, give mainly Precambrian ages (800-1000 Ma), and are similar to spectra from the Grenville Province of the Canadian Shield. K-feldspar and muscovite argon spectra from the Jurassic Mohican Formation give mainly late Paleozoic ages (250-350 Ma), and are similar to spectra from plutons on the Nova Scotian mainland. Muscovite argon spectra from the Missisauga Formation give Cambrian-Carboniferous ages, indicating that the sources of K-feldspar and muscovite had quite different thermal histories. At depths of greater than 4 km K-feldspar argon diffusion is apparent, and estimates of argon loss range from 1 or 2 to over 30 percent.

Apatite fission track ages are generally younger than stratigraphic ages, and tend to zero at a depth of 4 km (corresponding to formation temperatures of approximately 125°C). Fission tracks in samples from the Mic Mac J-77 and Erie D-26 wells are more annealed than present-day formation temperatures would predict, and are interpreted to have been affected by warm convecting fluids subsequent to deposition.

The provenance data are used to explain the deposition of the Mohican Formation in terms of a model of simple flank uplift and erosion of Acadian-age sources on the Nova Scotian mainland. The deposition of the Missisauga Formation can be approximated by a more complex model of an extensive fluviodeltaic system that combines sediments from at least two sources. K-feldspars are dominantly derived from the Canadian Shield, but the micas are derived from the Avalon Uplift, south of Newfoundland.

Acknowledgements

The author gratefully acknowledges the people who have provided much valuable assistance throughout the course of this project. In particular I would like to thank my supervisor, Peter H. Reynolds, for his inspiration, tireless patience and many useful discussions, and the thesis committee, Chris Beaumont, Marcos Zentilli, and Lubomir Jansa, for useful discussions and for constructive reviews of early thesis drafts. I would also like to thank Ray Donelick and Casey Ravenhurst, who assisted in all aspects of the fission track dating, Keith Taylor, who assisted with the argon analyses, and Bill Paterson, for the use of his computer.

1 Introduction

1.1 Introduction and purpose of study

Over the past thirty years the Scotian Basin, offshore Nova Scotia, Canada (Figure 1.1), has been the site of extensive hydrocarbon exploration activity (Wade et al., 1983, Grant et al., 1986). Deep drilling has resulted in the discovery and delineation of fifteen significant oil and gas/condensate-bearing structures. The largest of these, the Venture Gas Field, is thought to contain gas reserves in excess of 40 billion m^3, and the total gas reserves in the basin are estimated to be over 510 billion m^3, establishing the Scotian Basin as one of Canada's future hydrocarbon resource producing regions (Sherwin, 1972, Wade et al., 1983, Grant et al., 1986).

The generation and destruction of hydrocarbons are thermally controlled processes. Maximum generation of liquid hydrocarbons from liptinic matter occurs between temperatures of 60° and 120°C (Dow, 1977). Maximum generation of natural gas from humic matter occurs between temperatures of 100° and 150°C (Ibid). The accurate evaluation of hydrocarbon resource potential depends not only on an understanding of the nature of the organic source materials and of the processes of migration and entrapment, but also of the thermal evolution of the source and reservoir rocks. A number of techniques have been developed to assess thermal maturation levels based on solid organic, molecular organic, and mineral indicators as well as mineral-water interactions (see Naeser and McCulloh (1989) for a review

of these techniques). Figure 1.2 shows a generalized correlation of five thermal maturation indices with the zones of petroleum generation and destruction (from Dow, 1977).

The most widely employed solid organic thermal maturation index is obtained by measuring the optical reflectance of vitrinite (Ro) (Dow, 1977). Another routinely used solid organic thermal maturation index is obtained from Rock-Eval pyrolysis, based on the measurement of the total amount of hydrocarbons contained in source rock pores (expressed in mg hydrocarbon/ g rock)(Peters, 1986). A molecular organic thermal maturation index is obtained by measuring the degree of aromatization of certain steroids and isomerization of steranes and hopanes (A-I) (Mackenzie and McKenzie, 1983; Mackenzie et al., 1985; Beaumont et al., 1985).

Two of the mineral thermal maturation indices are apatite fission track analysis (Green et al., 1988; Gleadow et al., 1983), and K-feldspar $^{40}Ar/^{39}Ar$ age spectrum analysis (McDougall and Harrison, 1988; Harrison and Burke, 1989). The latter are unique among the maturation indices in that they have the potential to provide an absolute chronology of thermal events. All of the maturation indices have limited applicability, and because no simple equivalence can be drawn between them, it is fruitful to employ several independent techniques in order to obtain a better understanding of the thermal evolution of sedimentary basins for the purposes of hydrocarbon exploration as well as for theoretical models of basin development.

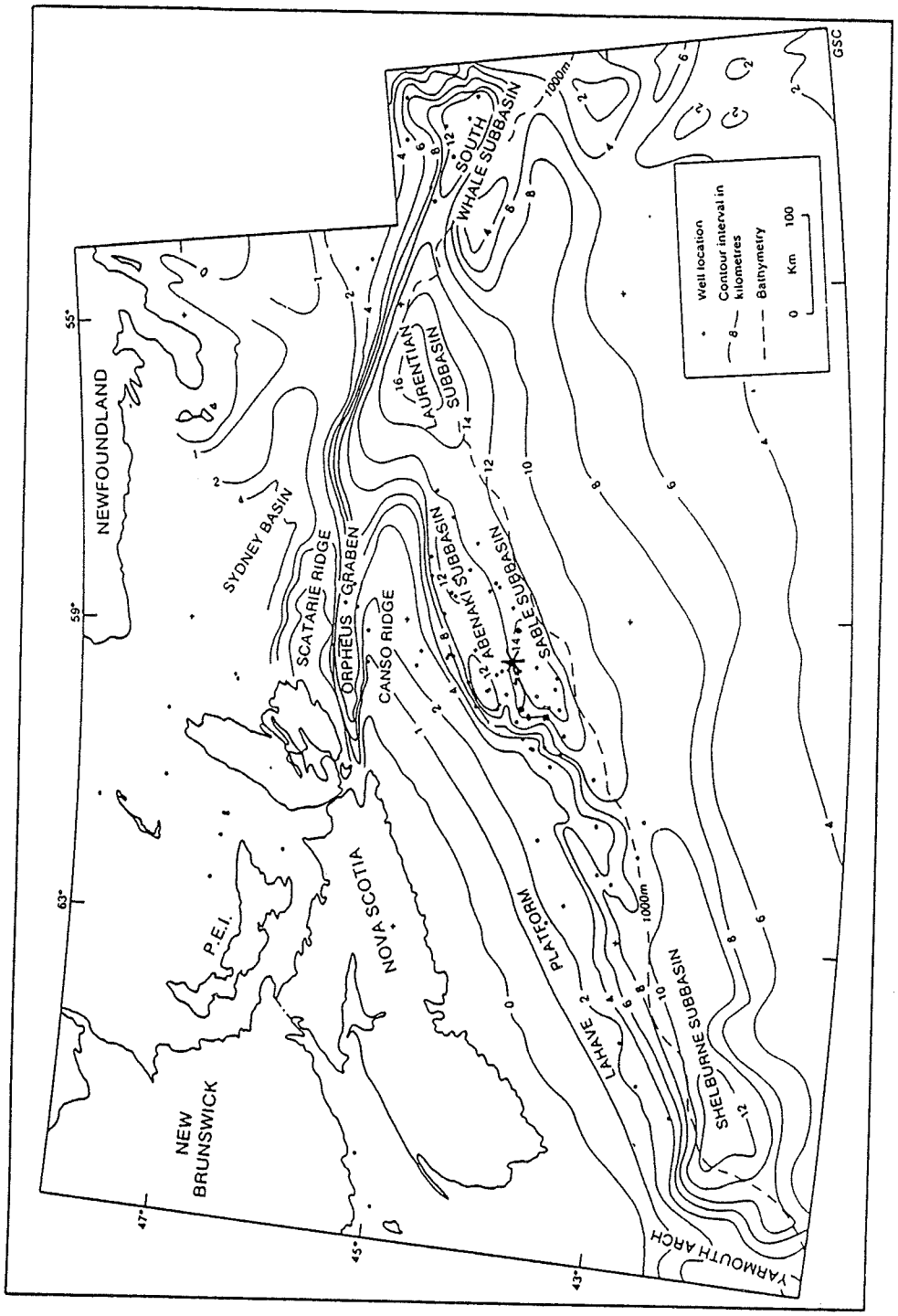

Figure 1.1. Mesozoic-Cenozoic depocenters within the Scotian Basin. The asterisk marks the location of the Venture Gas Field (modified from Grant et al., 1986).

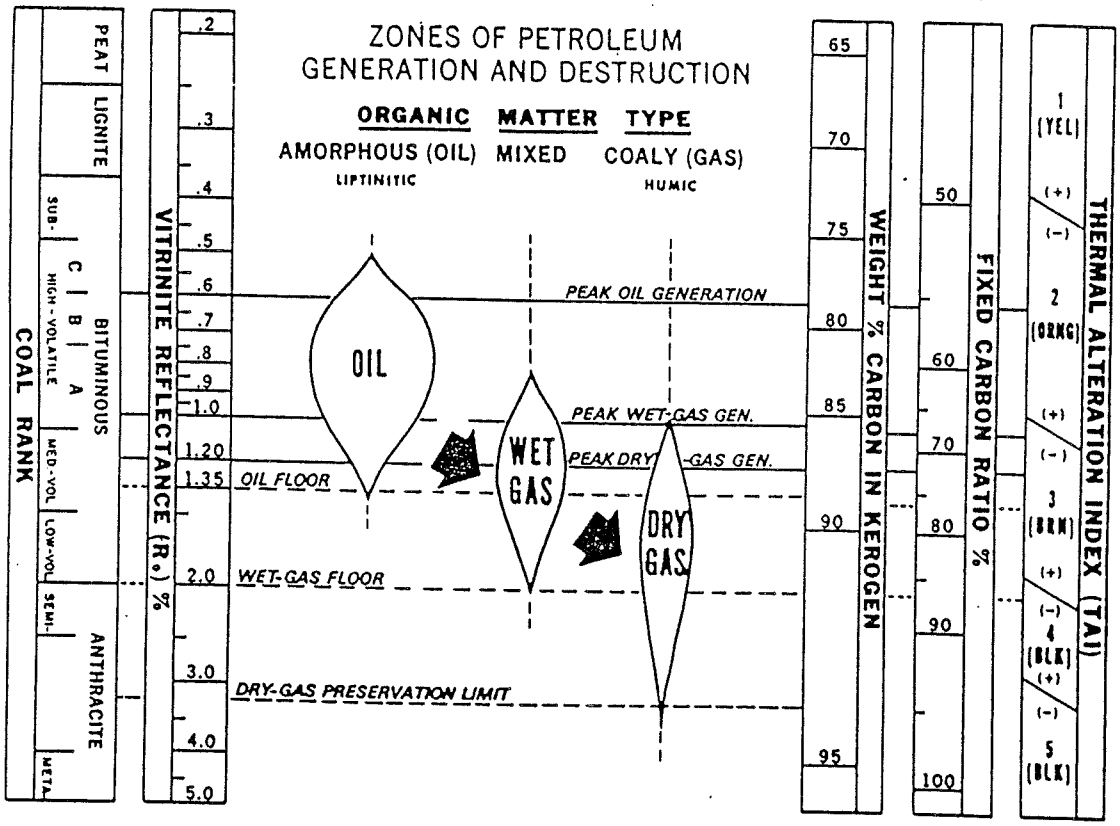

Figure 1.2. Correlation of five thermal maturation indices with the zones of petroleum generation and destruction (from Dow, 1977).

The purpose of this thesis is to present the results of apatite fission track and $^{40}Ar/^{39}Ar$ age spectrum analyses performed on mineral separates from sandstones from the Scotian Basin. The fission track and $^{40}Ar/^{39}Ar$ data are used to assess the relative degree of thermal maturity of samples, and to estimate the maximum temperatures that they have experienced. The $^{40}Ar/^{39}Ar$ method also provides valuable information about the provenance of the detrital grains that is used to constrain depositional models. The fission track and $^{40}Ar/^{39}Ar$ results are compared with Ro (Avery, 1978, 1983, 1985, 1986, 1988), and A-I (Mackenzie et al., 1985) data as well as with geophysical and geological data from other workers in order to increase our understanding of the thermal history of the hydrocarbon-bearing strata of this region.

1.2 Regional geology of the Scotian Basin

1.2.1 Location and tectonic setting

The region offshore Nova Scotia is underlain by a series of connected Mesozoic-Cenozoic sedimentary depocenters and adjoining stable platform areas that are collectively referred to as the Scotian Basin. This region makes up a part of the much larger chain of sedimentary basins that form the Atlantic passive margin of North America from Florida to Baffin Island. The Scotian Basin includes all of the structural elements between the Yarmouth Arch in the southwest, and the Scatarie Ridge and Avalon Uplift in the north-northeast, and wedges out distally over oceanic crust to the southeast (Figure 1.1). The geology and stratigraphy of the Scotian Basin have been described

in detail by McIver (1972), Amoco Canada Ltd. and Imperial Oil Ltd. (1973), Jansa and Wade (1975), Gradstein et al. (1975), Given (1977), Wade (1978, 1981), McWhae (1981), and Wade and McLean (in press). Additional reviews have also been written by Grant et al. (1986), and Noguera (1987). The following sections are based on the observations and interpretations of these authors.

The Scotian Basin comprises the Shelburne, Abenaki, Sable, Laurentian, and South Whale Subbasins (Figure 1.1). These subbasins have been the principal sedimentary depocenters, in which have accumulated up to 16 km of sediments. The northwest (landward) and west flanks of the Scotian Basin are occupied by three positive structural elements - the Canso Ridge, LaHave Platform, and Yarmouth Arch - which are covered by less than 4 km of sediments. A northeast-trending basement hinge zone separates these stable elements from the principal subbasins. On the southeast (seaward) flank of the chain of subbasins, there are numerous salt-cored, mobile, diapiric masses. The maximum concentration of these is contained in a narrow belt (approximately 60 km wide and 640 km long) beneath the continental slope, referred to as the Sedimentary Ridge Province (Jansa and Wade, 1975) or as the Slope Diapiric Province (Wade and McLean, in press). The Orpheus Graben is developed along the seaward extension of the Cobequid-Chedabucto fault system (on the Nova Scotian mainland), forming an additional subbasin north of the Canso Ridge and

has a total accumulated sediment thickness of up to 8 km. Sedimentation has been relatively continuous in all regions of the Scotian Basin from Late Triassic to recent time.

1.2.2 Stratigraphy and geologic history

As discussed by Given (1977), the Mesozoic and Early Cenozoic development of the Scotian Basin generally conforms to the model of an Atlantic-type continental margin (Falvey, 1974), evolved by the rifting and subsequent break-up of a continent by seafloor spreading. Basement in the Scotian Basin is comprised of metamorphic rocks of the Cambro-Ordovician Meguma Series and Devono-Carboniferous intrusive rocks. During the initial stages of continental break-up, a northeast-southwest trending rift valley system was developed in the Paleozoic basement (Jansa and Wade, 1975). The configuration of the basement blocks probably controlled sedimentation during the early stages of basin development (from Late Triassic to Early Cretaceous time; Given, 1977). The grabens that were formed became the sites of initial fluvio-deltaic deposition of terrestrial, clastic red beds of the Upper Triassic-Lower Jurassic Eurydice Formation (see Figure 1.3). The Argo Formation (McIver, 1972) overlies and interfingers with the Eurydice Formation. The Argo Formation consists of thick salt masses that were deposited in an arid, restricted marine environment. The Argo Formation attains its maximum thicknesses in the Orpheus Graben and in the Slope Diapiric Province.

Overlying the Argo Formation are dolostones of the Iroquois Formation (McIver, 1972), and coeval dolomitic, kaolinitic, silty sandstones and interbedded shales of the Mohican Formation (Given, 1977). The Iroquois and Mohican Formations were deposited during the first major regressive phase in the development of the Scotian Basin in a restricted marine environment. Across much of the Scotian Basin an unconformity exists between the top of the Argo Formation and the base of the Iroquois and Mohican Formations. Development of this unconformity was accompanied by basaltic volcanism, including extrusion of the North Mountain Basalt. The North Mountain Basalt has yielded K-Ar radiometric ages of between 190 and 202 Ma (Hayatsu, 1979; Wark and Clarke, 1980; Hodych and Hayatsu, 1989). According to Falvey's (1974) model, the deposition of the Mohican Formation immediately followed the development of a break-up unconformity associated with the final separation of the North American and African plates and the initiation of seafloor spreading (Jansa and Wade, 1975; Wade and McLean, in press).

The Late Jurassic in the Scotian Basin was a period of major transgression, and the open marine environment resulted in the concurrent development of several different facies. Along the edge of the LaHave Platform marine to locally deltaic clastics of the Mic Mac Formation interfinger with a carbonate bank sequence, the Abenaki Formation. These formations attain their greatest thicknesses in the

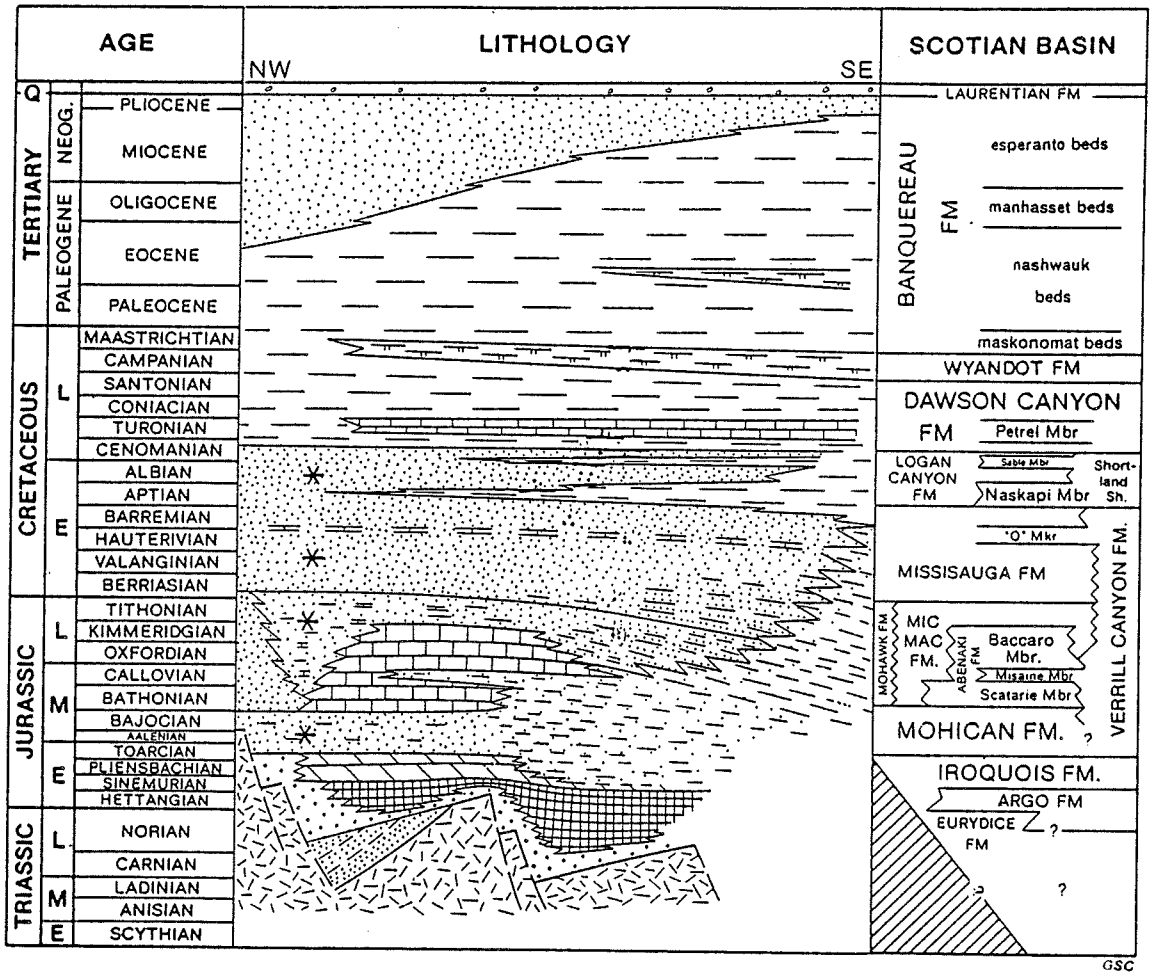

Figure 1.3. Generalized stratigraphy of the Scotian Shelf (from Grant et al., 1986). Formations marked with an asterisk were sampled for this project.

Sable and Abenaki subbasins respectively, and are flanked landward by the terrigenous clastics of the Mohawk Formation and seaward by thick shales of the Verrill Canyon Formation. The Verrill Canyon Formation shales (and equivalent shales within the Mic Mac and Missisauga Formations) are the source rocks for most of the hydrocarbons discovered in the Scotian Basin (Powell, 1982).

At the Jurassic-Cretaceous boundary, a second major regressive event occurred in association with the final separation of the Iberian and North American plates (Wade and McLean, in press). The area south of Newfoundland, (the Avalon Uplift; Jansa and Wade (1975)) was elevated and underwent severe erosion causing a sediment oversupply in the eastern part of the Scotian Basin. During Berriasian - Barremian time a large fluvio-deltaic system developed which covered most of the eastern Scotian Shelf and southwestern Grand Banks. The sediments attained a maximum thickness of over 2 km in the vicinity of Sable Island (the Sable Island delta; Wade and McLean, in press). The deposits of this system, now the Missisauga Formation, conformably overlie the Mohawk, Abenaki, and Mic Mac Formations, and grade basinward into the Verrill Canyon Formation shales. The type section for the lower member of the Missisauga Formation is between 4149 and 5100 m in the Venture H-22 well (Wade and McLean, in press).

A widespread transgression submerged the Scotian Shelf during Aptian time and resulted in the deposition of the Naskapi (shale) Member of the Logan Canyon Formation conformably over the Missisauga Formation (Jansa and Wade, 1975). Overlying the Naskapi

Member, are the Cree, Sable, and Marmora Members of the Logan Canyon Formation. These consist of alternating thick shale and sandstone-shale units deposited in a broad coastal plain and shallow shelf environment during Aptian-Cenomanian time (Wade and McLean, in press). The onset of a period of prolonged transgression during deposition of the Logan Canyon Formation is marked by a progressive, upward decrease in the sand:shale ratio that continues into the overlying shales of the Dawson Canyon Formation. The transgression culminated in the deposition of the Wyandot Formation chalk during Companian-Maastrichtian time. During Paleocene-Eocene time, deep-water sedimentation conditions prevailed, forming prograding shale wedges and reworking Cretaceous shelf-edge sediments into the Banquereau Formation. From Oligocene to Pliocene time shallower-water depositional environments prevailed resulting in an increased sand:shale ratio within the Banquereau Formation.

Throughout most of the Late Cretaceous and Tertiary Periods the Scotian Shelf was generally unstable. This was in part a result of the accumulation of thick, water-saturated sediments adjacent to thinner coeval sediments beneath the slope, and partly a result of the presence of large masses of deeply buried, mobile salt (Wade and McLean, in press). These factors have resulted in minor structural activity, general seaward tilting, and development of numerous growth faults and rollover structures (Jansa and Wade, 1975). During Pliocene-Pleistocene time, the shelf was intermittently subareally exposed by

glaciation. Over most of the shelf the uppermost lithostratigraphic unit is the Laurentian Formation, a coarse clastic sequence consisting mainly of drift and proglacial material (Jansa and Wade, 1975).

The formations chosen for study in this project were the Mohican, Mic Mac, Missisauga, and Logan Canyon Formations. Because they were deposited largely under deltaic facies conditions, they contain the most-abundant sandstones, and therefore could be expected to supply apatite and feldspar grains of suitable size for analysis. In addition, these formations (especially the Missisauga Formation) are quite extensive, and range in depth from less than 2 to greater than 5 km, and therefore could be expected to display considerable variability in levels of maturation. The major fluvial-deltaic clastic sequences of the Mic Mac, Missisauga, and Logan Canyon Formations also constitute the most important hydrocarbon reservoir units in the Scotian Basin.

Little is known about the provenance of the Scotian Basin sandstones. Sediment transport directions for the various formations are largely presumed, based on the distribution of facies during deposition (Jansa and Wade, 1975; Given, 1977). Jansa and Wade (1975) postulated a north-northwesterly direction for the source of the Mohican Formation sediments, in the direction of the LaHave Platform and mainland Nova Scotia. Given (1977) proposed at least two source areas for the Mic Mac Formation. In the vicinity of Sable Island, the source direction was inferred to be to the northwest, in the direction of southern Cape Breton Island. During deposition of the Missisauga Formation, the principal source direction was to the north and

northeast, in the direction of northeastern Cape Breton, and the Cabot Strait. The Missisauga delta was probably fed by an ancestral St. Lawrence drainage system that drained much of the northwestern part of the Canadian Shield (Wade and McLean, in press). During deposition of the Logan Canyon Formation (Aptian - Cenomanian time) sediment transport continued to be primarily from north to south, continuing the pattern established during deposition of the Missisauga Formation.

1.3 Introduction to argon dating

A very thorough and up-to-date treatment of the $^{40}Ar/^{39}Ar$ method and its use in geochronology/thermochronology can be found in McDougall and Harrison (1988). The following is a brief introduction to the $^{40}Ar/^{39}Ar$ technique that has been obtained mainly from McDougall and Harrison (1988), and also Harrison and Burke (1989), and Faure (1986).

Developed by Merrihue and Turner (1966), the $^{40}Ar/^{39}Ar$ dating technique is a modification of conventional K-Ar dating, based on the branching decay scheme of ^{40}K to ^{40}Ar and ^{40}Ca. In a closed system, the total number of radiogenic ^{40}Ar and ^{40}Ca atoms formed during time t can be expressed as:

$$Ar^{40} + Ca^{40} = K^{40}\left(e^{\lambda t} - 1\right)$$

where λ is the total decay constant of ^{40}K, and K^{40}, Ar^{40}, and Ca^{40} are the present-day atomic abundances of these isotopes. The amount of

radiogenic argon produced during time t is:

$$Ar^{40} = \frac{\lambda_e}{\lambda} K^{40}\left(e^{\lambda t} - 1\right) \qquad 1$$

where λ_e is the partial decay constant for the ^{40}K to ^{40}Ar branch.

The $^{40}Ar/^{39}Ar$ dating technique is based on the formation of ^{39}Ar by irradiation of ^{39}K with fast neutrons in a nuclear reactor. During irradiation, ^{39}K is converted to ^{39}Ar through the emission of a positron, changing one proton to a neutron (^{39}K (n,p) ^{39}Ar). Because the $^{40}K/^{39}K$ ratio is everywhere today the same, the number of ^{39}Ar atoms generated by the irradiation is proportional to the ^{40}K present in the sample. (^{39}Ar has a half-life of 269 years and can be treated as stable over the period of analysis.) The number of ^{39}Ar atoms formed by the irradiation can be expressed as:

$$Ar^{39} = K^{39} T \int \phi_\epsilon \sigma_\epsilon d\epsilon \qquad 2$$

where T is the irradiation time in seconds, ϕ_ϵ is the neutron flux density at energy ϵ, and σ_ϵ is the capture cross section of ^{39}K nuclei for neutrons of energy ϵ, and the limits of the integration are determined by the range of neutron energies.

Dividing equation 1 by equation 2 one obtains the ratio ^{40}Ar:^{39}Ar:

$$\frac{Ar^{40}}{Ar^{39}} = \frac{\lambda_e K^{40}\left(e^{\lambda t} - 1\right)}{\lambda K^{39} T_b \int \phi_\epsilon \sigma_\epsilon d\epsilon} \qquad 3$$

To avoid the difficulties in evaluating all of the variables in equation 3, the J parameter was introduced by Mitchell (1968).

$$J = \frac{\lambda K^{39} T}{\lambda_e K^{40}} \int \phi_\epsilon \sigma_\epsilon d\epsilon$$

When the above is substituted into equation 3 the latter becomes:

$$\frac{Ar^{40}}{Ar^{39}} = \frac{e^{(\lambda t)} - 1}{J} \qquad 4$$

J is evaluated by irradiation of a standard sample of known age (used as a flux monitor). By rearrangment of equation 4 we have:

$$J = \frac{e^{(\lambda t_m)} - 1}{\left(\frac{Ar^{40}}{Ar^{39}}\right)_m} \qquad 5$$

where t_m and $(Ar^{40}/Ar^{39})_m$ are the age and (measured) argon isotopic ratios of the monitor mineral. The age of a sample is given by:

$$t = \frac{1}{\lambda} \ln\left(\frac{Ar^{40}}{Ar^{39}} J + 1\right) \qquad 6$$

The standard used as the flux monitor mineral in this study is the MMhb-1 (McClure Mountain) hornblende; its age is given by Alexander et al. (1978) as 519 $\pm$ 3 Ma.

In conventional K-Ar dating samples are heated to a high temperature until completely outgassed. The amount of ^{40}Ar produced is determined by the degree of dilution of a small amount of an added tracer (^{38}Ar). Potassium concentration is determined from measurements made on a separate aliquot of the sample, and a single age is then calculated. In the $^{40}Ar/^{39}Ar$ technique samples are progressively outgassed via a series of increasing temperature steps (usually in 50

C° increments). At each temperature the evolved gas is collected, and an apparent age (or step age) is calculated from the measured $^{40}Ar:^{39}Ar$ ratio.

The standard format for presenting the results of a stepwise degassing experiment is a plot of the apparent ages of gas fractions against the cumulative percent ^{39}Ar released (Turner, 1968). Such a diagram is known as an age spectrum, and it can provide useful information on the internal distribution of argon in the sample. Under the assumption that mineral structures have been preserved during laboratory preparation and heating, and that argon loss mechanisms are the same in the laboratory setting as they are in nature, the resulting argon spectrum can be used to distinguish between low-activation energy and high activation-energy sites, and can be interpreted in terms of the thermal history of the sample (McDougall and Harrison, 1988; Harrison and Burke, 1988).

Because spectra usually contain a variety of apparent ages, they need to be interpreted with care. K-feldspar spectra frequently display gradients of increasing apparent ages (e.g. Reynolds et al., 1987; McDougall and Harrison, 1988). These gradients can result from slow cooling (e.g. of an igneous pluton, Harrison and McDougall, 1980), or from an episode of argon loss due to a thermal (reheating) event (Turner, 1968; Reynolds et al., 1987; Zeitler, 1987), or from a combination of slow cooling followed by a thermal event (Harrison, 1983; McDougall and Harrison, 1988).

In the case of slow cooling, the total gas age represents the best estimate of the actual age of the sample. In the case of a partial thermal overprint, the total gas age is intermediate between the cooling age and the age of the overprint, and therefore does not have geologic significance. In the theoretical age spectra of partially outgassed samples calculated by Turner (1968), Huneke (1976), and Harrison (1983) the time at which the outgassing event occurred is given by the age of the first, infinitesimal fraction of gas evolved during laboratory heating. However, in actual age spectra there is usually an offsetting effect that is caused by reactor-induced ^{39}Ar recoil loss. Recoil associated with the ^{39}K (n,p) ^{39}Ar reaction causes a small amount of the ^{39}K that is situated near the edges of diffusion domains to be lost upon conversion, thereby increasing the $^{40}Ar/^{39}Ar$ ratio, and the apparent age of the initial heating steps (which typically account for 1-2 percent of the total gas). Consequently, the precise age of a partial resetting event is usually not preserved in an age spectrum. The final fractions of gas released provide a lower limit to the original cooling age of the sample.

The interpretations of argon spectra are usually based on the single-site diffusion models developed by Turner (1968), Huneke (1976), and Harrison (1983). Solid diffusion is thermally activated and the ease of diffusion as a function of temperature is described by a simple Arrhenius relationship (McDougall and Harrison, 1988).

$$\frac{D}{a^2} = \frac{D_o}{a^2} e^{(-Ea/RT)} \qquad 7$$

In this equation D is the diffusion coefficient (a term that combines the molecular permeability of the system and the solubility of the diffusant), a is the effective diffusion radius, D_o is the frequency factor (the diffusion coefficient as the temperature approaches infinity), T is the absolute temperature (degrees Kelvin), E_a is the activation energy, and R is the ideal gas constant.

Dodson (1973) demonstrated that the transition of a cooling system from fully-open to fully-closed (daughter products are immobile) occurs over a narrow temperature range (approximately 50 - 100C°), thus defining an effective closure temperature (T_c) for the system.

$$Ea/RT_c = \ln\left(A\tau\frac{D_o}{a^2}\right)$$

where τ is the time constant (the time taken for D to diminish by a factor of e^{-1}), and A is a numerical constant determined by the geometric shape of the system. The closure temperature of a system is thus strongly dependent on its activation energy, frequency factor, and effective diffusion radius, all of which are in turn dependent on the structural state of the specific mineral grains being analyzed. These diffusion parameters must be evaluated before T_c can be calculated.

Fick's Second Law is based on the similarity of thermal diffusion to thermally induced mass diffusion, and states that the partial derivative of the concentration with respect to time is equal to the sum of the second partial derivatives of the concentration with respect to the spatial coordinates, multiplied by the diffusion coefficient. In

cartesian coordinates the diffusion equation has the form:

$$\frac{\partial C}{\partial t} = D\left(\frac{\partial^2 C}{\partial x^2} + \frac{\partial^2 C}{\partial y^2} + \frac{\partial^2 C}{\partial z^2}\right)$$

A number of numerical solutions to this equation have been developed (ie. Crank, 1975; Jain, 1958; Jost, 1960; and Reichenburg, 1953), which describe diffusion out of simple geometric forms (ie. sphere, cylinder, plane-sheet, and cube). These solutions express the fraction of gas lost by diffusion (f) in terms of the compound parameter D/a^2 (or D/l^2) and the diffusion time, t. The solutions to the diffusion equation can be applied in laboratory step-heating experiments, where t and f are measured and used to calculate D/a^2. However, the use of such experiments to model diffusion in complex natural systems is subject to a number of restrictions, as indicated in McDougall and Harrison, 1988. These include:

1) The phase must remain stable throughout the experiment.

2) The effective diffusion radius must be known, or be derivable from the experiment.

3) The shape of the particles in the aggregate must conform to the shape assumed in the solution of the diffusion equation.

4) The aggregate must contain only one effective grain size.

5) Only one mineral phase can be present.

6) The initial distribution of argon must be uniform.

7) The heating must be isothermal.

Hydrous phases (such as biotite and hornblende) have been found to decompose structurally during vacuum extraction heating, and are

therefore not acceptable for diffusion experiments of this type. Similarly, the resorption of perthite lamellae in K-feldspars during heating becomes significant at temperatures over 750°C, thus limiting the range of temperatures over which this mineral provides useful data. Berger and York (1981) used a method to obtain values for the D_o/a^2 and E_a parameters for a given sample directly from that sample's $^{40}Ar/^{39}Ar$ step heating data. This method, also applied in the present thesis (to K-feldspar data), is described below.

One solution of the diffusion equation, for a sphere of radius a (applicable for $0 < f < 0.85$) is:

$$f \sim \left(\frac{6}{\sqrt{\pi}}\right)\left(\frac{Dt}{a^2}\right)^{1/2} - \left(\frac{3Dt}{a^2}\right) \qquad 8$$

This quadratic equation may be rearranged and solved explicitly for Dt/a^2:

$$\frac{Dt}{a^2} = \frac{2}{\pi} - \frac{f}{3} - \frac{2}{\pi}\sqrt{1 - \frac{\pi f}{3}}$$

Figure 1.4 depicts a step-heating experiment. At temperature T(1):

$$\frac{D(1)t(1)}{a^2} = \frac{2}{\pi} - \frac{f(1)}{3} - \frac{2}{\pi}\sqrt{1 - \frac{\pi f(1)}{3}}$$

At time t(1) the temperature is increased to T(2). The sample then begins to diffuse at a faster rate. At T(2):

$$\frac{D(2)t(2)}{a^2} = \frac{2}{\pi} - \frac{f(1)}{3} - \frac{2}{\pi}\sqrt{1 - \frac{\pi f(1)}{3}}$$

and

$$D(2)\frac{t(2)'}{a^2} = \frac{2}{\pi} - \frac{f(1)+f(2)}{3} - \frac{2}{\pi}\sqrt{1 - \frac{\pi(f(1)+f(2))}{3}}$$

The times t(2)' and t(2) are not known, but t(2)' - t(2) is Δt(2), which is the heating time for the second step. Therefore, on subtraction:

$$\frac{D(2)\Delta t(2)}{a^2} = \frac{2}{\pi} - \frac{f(2)}{3} - \frac{2}{\pi}\left(\sqrt{1 - \frac{\pi(f(1)+f(2))}{3}} - \sqrt{1 - \frac{\pi f(1)}{3}}\right)$$

Division by Δt(2) gives $D(2)/a^2$. The calculation is repeated iteratively for subsequent heating steps, thus providing a set of values of D/a^2 as a function of temperature. Values for f(1), f(2), etc. are obtained from the step-heating data. The calculation is usually based on the ^{39}Ar released, but radiogenic ^{40}Ar can also be used. The data are normally plotted as 1000/T (K^{-1}) versus $\log(D/a^2)$. On this type of plot the Arrhenius equation (equation 7) is simply the standard equation of a line (ie. y = mx + b):

$$\log\left(\frac{D}{a^2}\right) = \frac{-.4343 E a_a (1000)}{RT} + \log\left(\frac{D_o}{a^2}\right)$$

The activation energy of the system (E_a) can be derived from the slope of the line, and the y-intercept gives $\log(D_o/a^2)$.

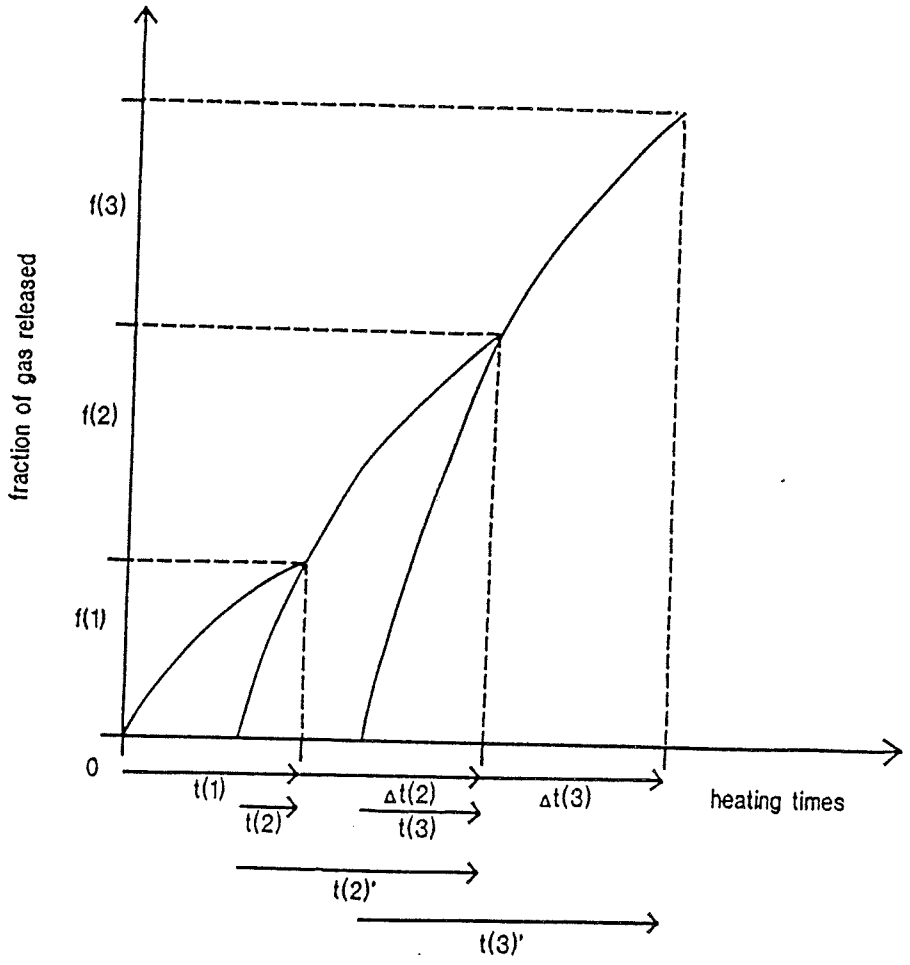

Figure 1.4. Diagram illustrating the Berger and York method of calculating the diffusion parameters. Laboratory extraction heating times increase along the horizontal axis. The fractions of gas evolved during each of the heating steps are shown on the vertical axis (f(1) + f(2) ... + f(n) = 1). The times t(1), ⊿t(2), and⊿ t(3) are actual laboratory heating times, and hence are known. The times t(2), t(2)', t(3), and t(3)' are the (theoretical) times required for diffusion of equivalent fractions of gas if extraction heating all been done at the elevated temperatures T(2), and T(3), respectively (see text for a complete description of the method).

1.4 Introduction to fission track dating

A spontaneous fission track is a submicroscopic damage zone resulting from the spontaneous fission of the nucleus of an atom (usually of the abundant isotope of uranium, ^{238}U). Figure 1.5 (from Fleischer et al., 1965) illustrates the formation of a fission track. Following a fission event, mutual repulsion of the two highly positively-charged fission fragments forces them apart, and as they separate they strip electrons from the surrounding medium leaving a trail of positively-charged ions. In crystalline, insulating solids mutual repulsion between the secondary positively-charged ions forces them into the surrounding crystal lattice, and a single fission track is formed (typically a few tens of angstroms in diameter and 10-20 microns long) that is stable at low temperatures (Faure, 1986).

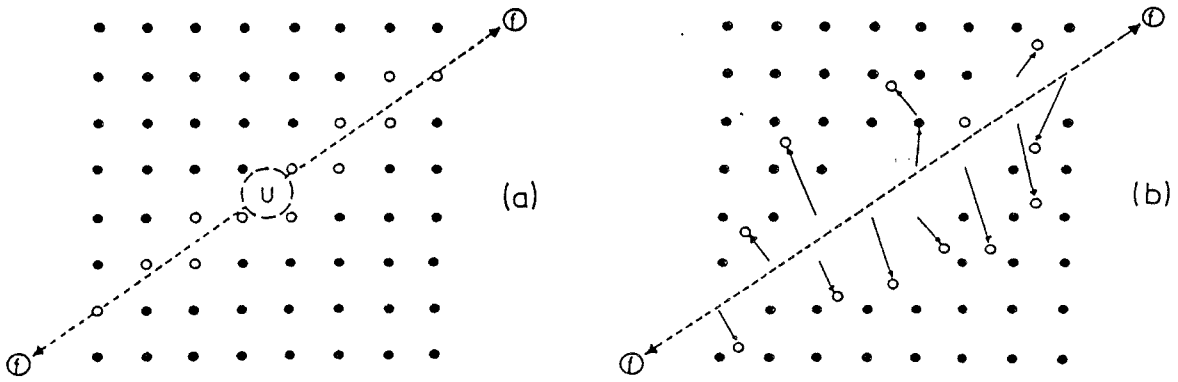

Figure 1.5. The ion spike model for the formation of fission tracks (from Fleischer et al., 1965).

Fission tracks were first observed by Silk and Barnes (1959) using scanning electron microscopy. Subsequently, Price and Walker (1962) discovered that tracks could be enlarged by etching and thereby observed using an optical microscope. Price and Walker (1963) proposed a fission track dating technique based on the assumption that the number of spontaneous fission tracks accumulated in a given time in a substance depends only on the initial concentration of ^{238}U and the rate of decay of ^{238}U by spontaneous fission.

Several techniques have been developed for determining fission track ages, including the population method, subtraction method, re-polish method, re-etch method, and external detector method (Hurford and Green, 1982). All of these methods involve a procedure for the determination of the uranium concentration in samples by inducing fission in a portion of the ^{235}U nuclei by irradiation with thermal neutrons in a nuclear reactor. This produces a second, or induced set of fission tracks, and because the ratio ^{238}U:^{235}U is constant in nature (see below), provides an indirect means of measuring the concentration of ^{238}U. Only the external detector method (using the zeta calibration, as described below) is routinely used in the Dalhousie University laboratory, and the fission track ages reported in this study were all determined by this method. Figure 1.6 illustrates the steps involved in obtaining a fission track age using the external detector method. A brief description of the external detector method and the zeta calibration (Hurford and Green, 1983) follows.

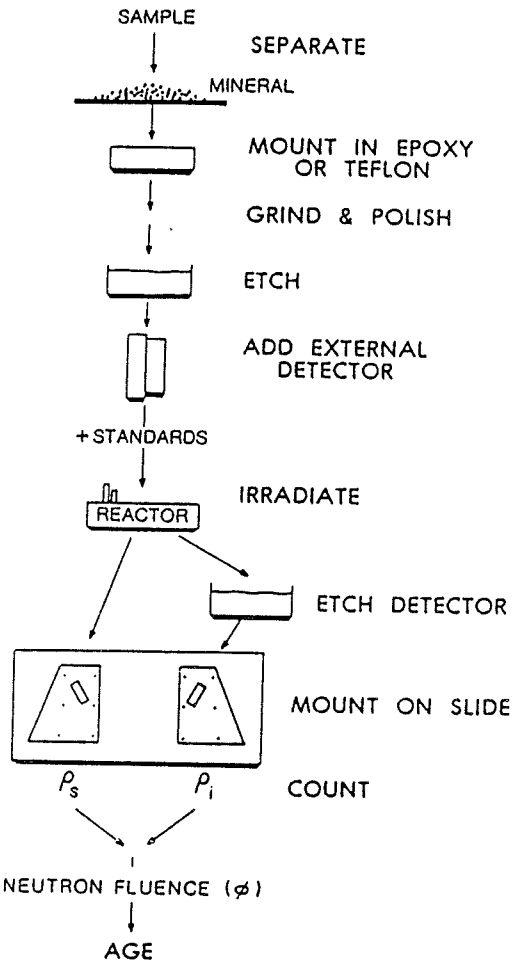

Figure 1.6. The steps involved in obtaining a fission track age using the external detector method (from Naeser et al., 1988).

The fundamental fission track age equation (Price and Walker, 1963) is:

$$t = \frac{1}{\lambda_d} \ln\left(1 + I\Phi\sigma g \frac{\rho_s}{\rho_i}\frac{\lambda_d}{\lambda_f}\right)$$

where:

t = the fission track age of the system (Ma),

I = the atomic ratio $^{235}U/^{238}U$ (7.252×10^{-3}; Steiger and Jager, 1977),

λ_d = the total decay constant for ^{238}U (1.55125 x 10^{-10} a^{-1}; Ibid),

λ_f = the decay constant for spontaneous fission of ^{238}U (approximately 8 x 10^{-17} a^{-1}; Friedlander et al., 1981),

σ = the thermal-neutron fission cross-section for ^{235}U (5.802 x 10^{-26} cm^2),

Φ = the thermal-neutron fluence during irradiation,

g = the geometry factor (0.5 for the external detector method), and

ρ_s/ρ_i = the spontaneous-to-induced fission track density (densities in tracks/unit area).

With the external detector method, spontaneous tracks are counted on a polished and etched internal surface of a mineral grain. Induced tracks are counted in the corresponding area of a low-uranium muscovite detector that is held against the polished surface of the grain mount during irradiation. Thus spontaneous and induced track densities are determined for the same surface of each individual crystal. In this method spontaneous tracks have resulted from the passage of fission fragments across an internal surface, from both above and below, thus producing a 4π geometry, but induced tracks result from the one-way passage of fission fragments from the mineral into the external mica detector, giving a 2π geometry. This is the basis for the 0.5 geometry factor (g) used above.

The zeta calibration was introduced by Fleischer et al. (1975) (see also Hurford and Green, 1982) as a technique for solving the age equation which circumvents the need for explicit evaluation of λ_f and absolute determination of the reactor neutron fluence Φ. Zeta is

defined as follows:

$$Z = \frac{e^{(\lambda_f t_{STD})} - 1}{\lambda_d g \rho_d \left(\frac{\rho_s}{\rho_i}\right)_{STD}}$$

where ρ_d is the induced track density in a uranium-bearing glass dosimeter, and t_{STD} is the age of the standard (a mineral that has a known fission track age). In this study SRM963a (614) glass dosimeters obtained from the U. S. National Bureau of Standards were used. The standard used was the Fish Canyon Tuff apatite. Its age is given by Hurford and Hammerschmidt (1985) as 27.8 $\pm$ 0.2 Ma.

Substitution into the fundamental age equation gives:

$$Z = \frac{I \Phi \sigma}{g \rho_d \lambda_f}$$

Since ρ_d is proportional to Φ, the Φ/ρ_d term (and hence the entire $I\Phi\sigma/g\rho_d\lambda_f$ term) is constant even when the neutron flux varies.

The age of a sample is given by:

$$t = \frac{1}{\lambda_d} \ln\left(1 + \lambda_d Z \frac{\rho_s}{\rho_i} \rho_d g\right)$$

Annealing of fission tracks is a thermally controlled process. Tracks fade by diffusion of displaced ions back into lattice vacancies. Fleischer et al. (1965) showed that temperature was the dominant factor governing the long term stability of fission tracks. Green et al. (1986) presented a qualitative description of thermally-induced annealing of fission tracks in apatite in which they showed that during laboratory heating, mean track lengths were progressively reduced (and track length distributions broadened) from an initial length (l_o) of 16.5

microns to a mean of 10.7 microns (l/l_o = 0.65). Further annealing produced unetchable gaps in the tracks, causing them to break-up into discontinuous portions. Partial to complete annealing reduces the spontaneous track density and hence, the fission track age of a sample.

The degree of temperature sensitivity of various minerals to diffusion processes is usually expressed in terms of closure temperatures (Dodson, 1973), nominal temperatures below which radiogenic daughter products are effectively retained over geologic periods of time. Two estimates of the closure temperature for retention of fission tracks in apatite are 105 $\pm$ 25°C (Harrison and McDougall, 1980) and 60° to 125°C (Gleadow et al., 1983).

In a study that employed apatite fission track analysis as a paleotemperature indicator for hydrocarbon exploration in the Otway Basin, southeastern Australia, Green et al. (1988) list five temperature-sensitive parameters that can be evaluated. These are:

1) the fission track age,
2) the variation of apparent fission track age with depth,
3) the single grain age distribution,
4) the variation of mean confined track length with depth, and
5) the distribution of confined track lengths.

To facilitate comparison with other basin studies, these same parameters are described in the application of fission track analysis to the Scotian Basin.

2 Sampling, sample preparation, and laboratory procedures

2.1 Sampling procedures

Sampling of sandstone drillcores for this project was carried out with the permission of the Canadian Oil and Gas Lands Administration (C.O.G.L.A.). All sampling was done at the C.O.G.L.A. core laboratory at the Bedford Institute of Oceanography, Dartmouth, Nova Scotia. Samples were obtained on three separate occasions. The first group of samples was obtained in October, 1986, from the Shell Mic Mac J-77, and Mic Mac H-86 wells. The second group of samples was obtained in July, 1987, from the Mobil et al. Venture B-13, Venture B-43, and Venture H-22 wells. The third group of samples was obtained in January, 1988, from the Shell Erie D-26, Mobil Sable Island No. 1 (C-67), Husky-Bow Valley et al. Chebucto K-90, and Mobil et al. Bluenose 2G-47 wells. A summary of the depths, formations, and estimated interval temperatures is given in Table 2.1. Figure 2.1 shows the locations of the sampled wells. Figures 2.2 - 2.10 are illustrations of the sampled wells, which show the well stratigraphy, cored intervals, and locations at which samples were obtained for use in this study.

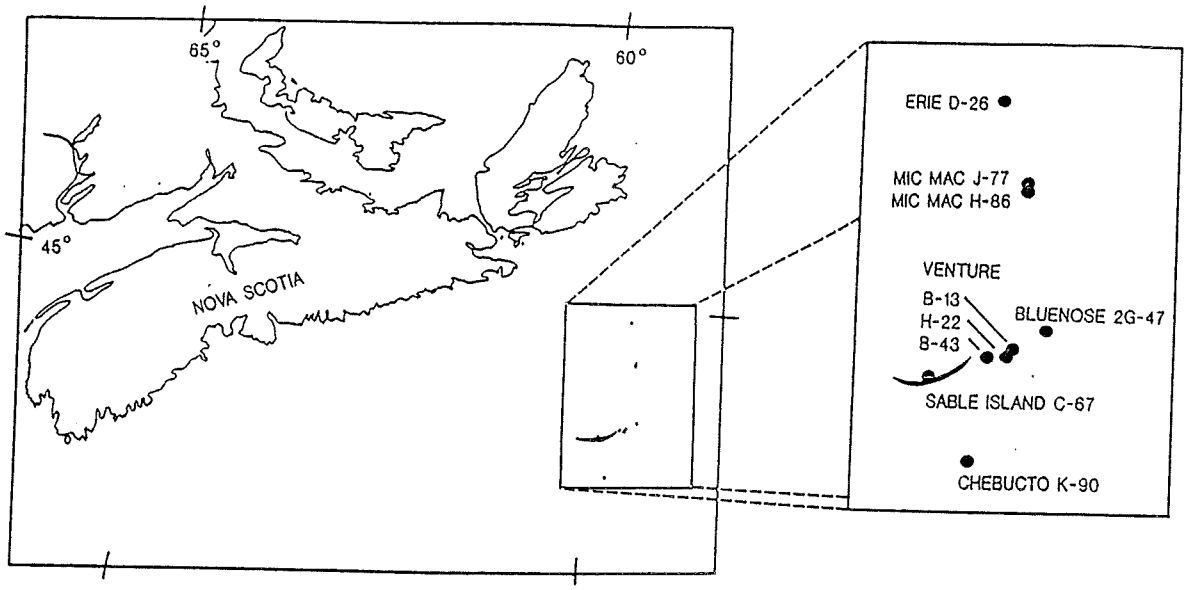

Figure 2.1. Map showing the locations of the wells sampled for this project.

Table 2.1. A summary of the wells sampled for this study. Depths are B.R.T. (below rotary table). Erie D-26 is located on the Canso Ridge. Mic Mac J-77 and H-86 are within the Abenaki Subbasin. The other six wells are within the Sable Subbasin. Interval temperature estimates are based on Issler (1983), and have an uncertainty of ± 8°C.

Well Name	Formation(s) Sampled	Depth (m)	Temperature (degrees C)
Sable Island C-67	Logan Canyon, Missisauga	2471 - 3377	73 - 97
Mic Mac J-77	Missisauga	2814 - 2823	84
Chebucto K-90	Missisauga	4278 - 4287	126
Venture B-13	Missisauga	4697 - 4967	137 - 144
Venture B-43	Missisauga	4424 - 4967	129 - 136
Venture H-22	Missisauga, Mic Mac	4710 - 5410	138 - 155
Erie D-26	Mic Mac	1955 - 1959	60
Bluenose 2G-47	Mic Mac	5112 - 5129	137
Mic Mac H-86	Mohican	4715 - 4725	138

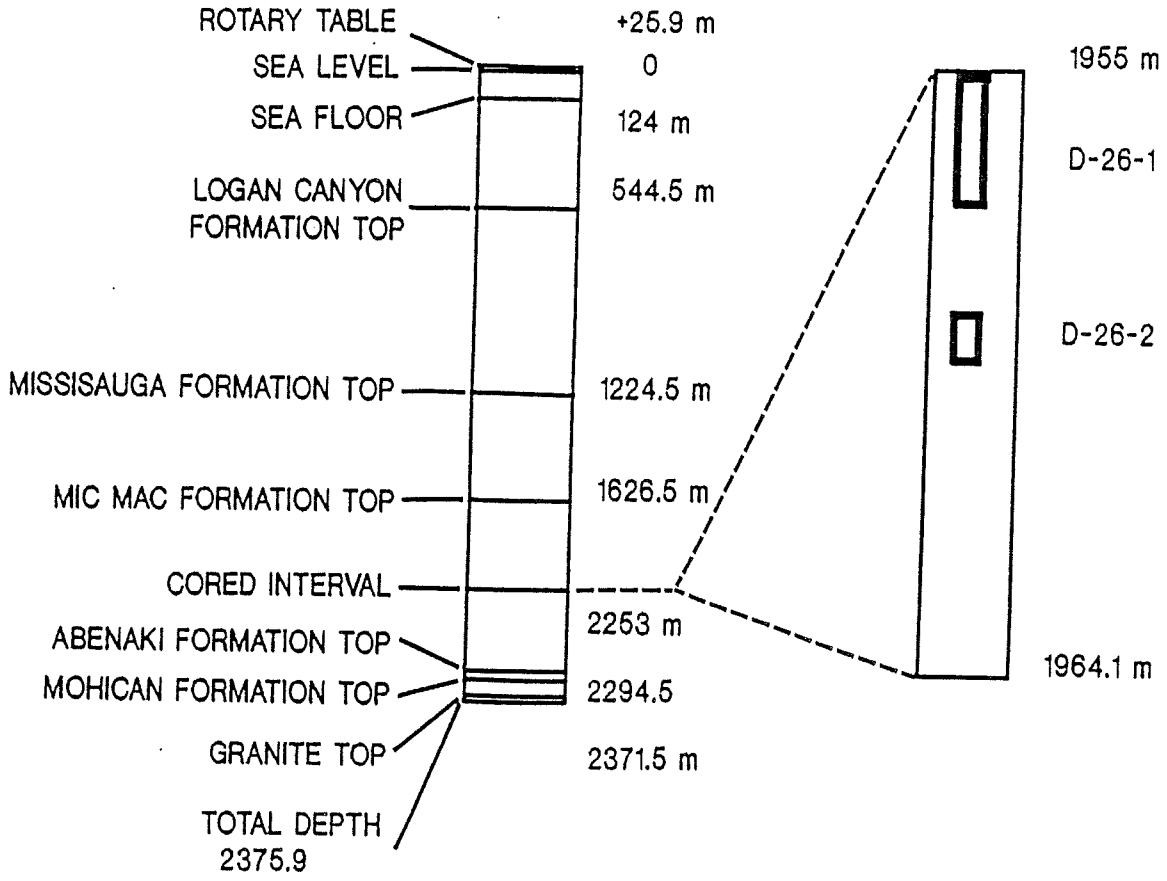

Figure 2.2. Stratigraphy and sample locations (shown with dark rectangles) for the Shell Erie D-26 well. Rotary table elevation is above sea level. All depths to formation tops are relative to the rotary table. The scale of the well sketches in Figures 2.2 - 2.10 are all 1:25,000

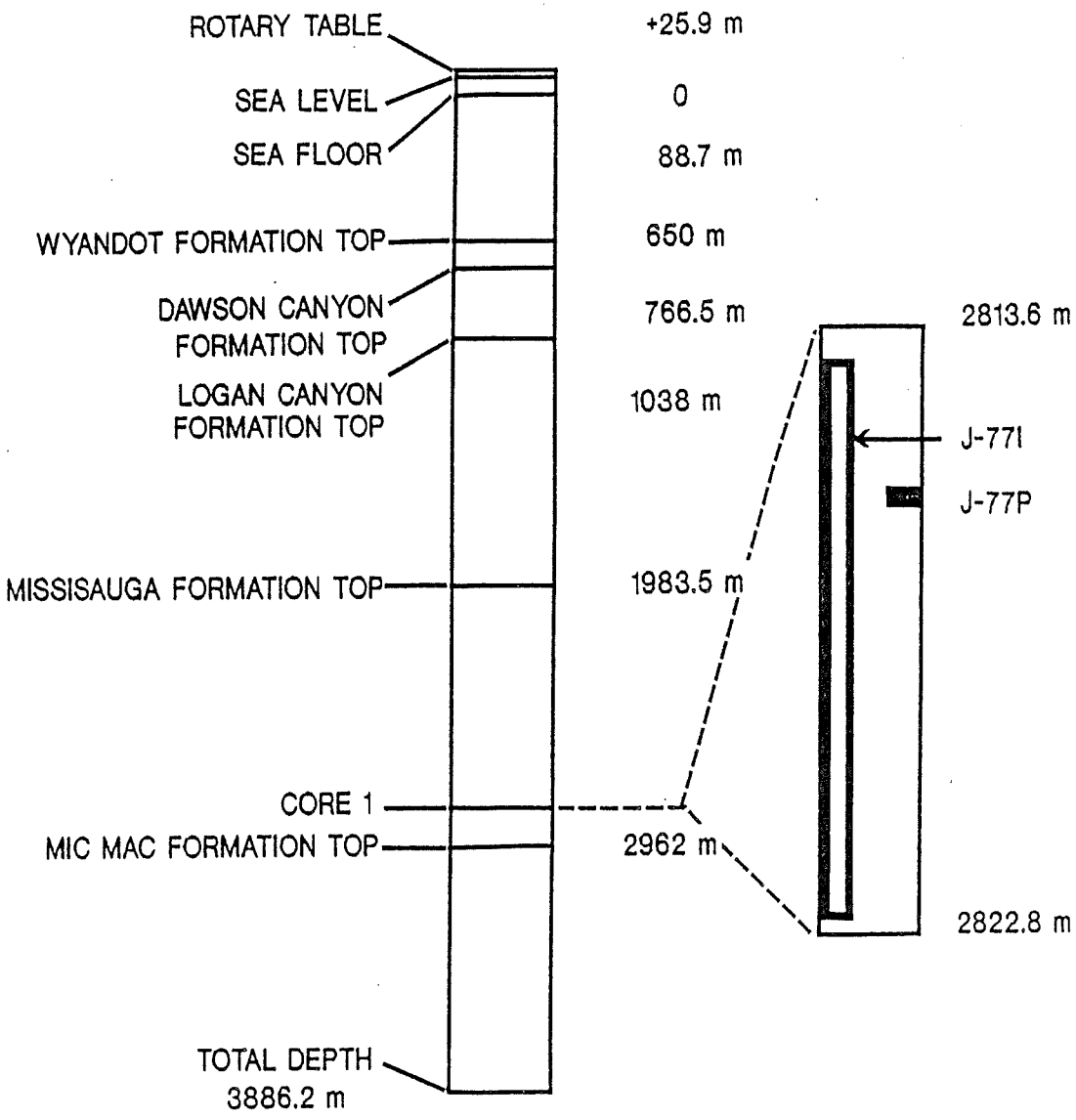

Figure 2.3. Stratigraphy and sample locations (shown with dark rectangles) for the Mic Mac J-77 well.

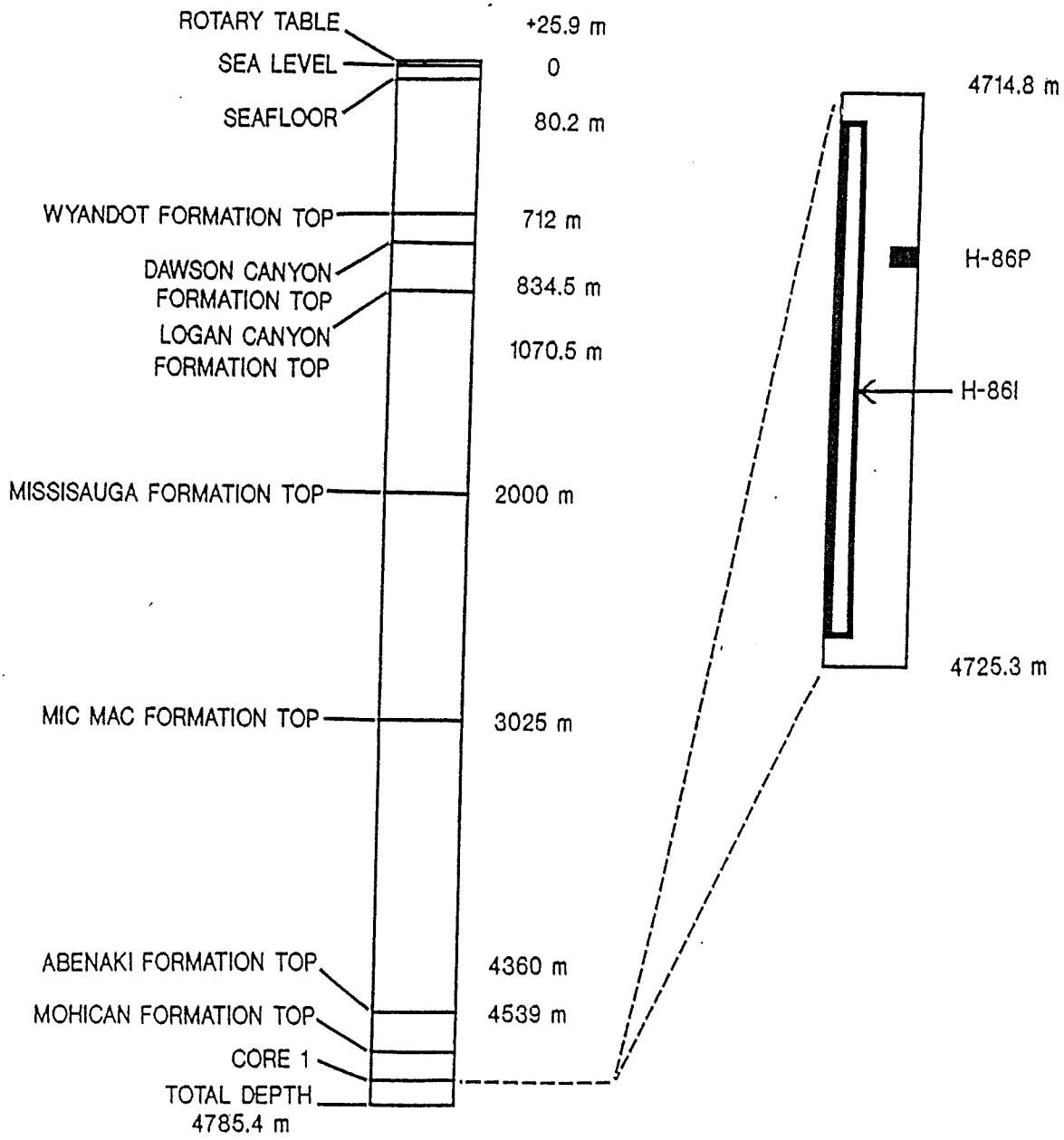

Figure 2.4. Stratigraphy and sample locations (shown with dark rectangles) for the Mic Mac H-86 well.

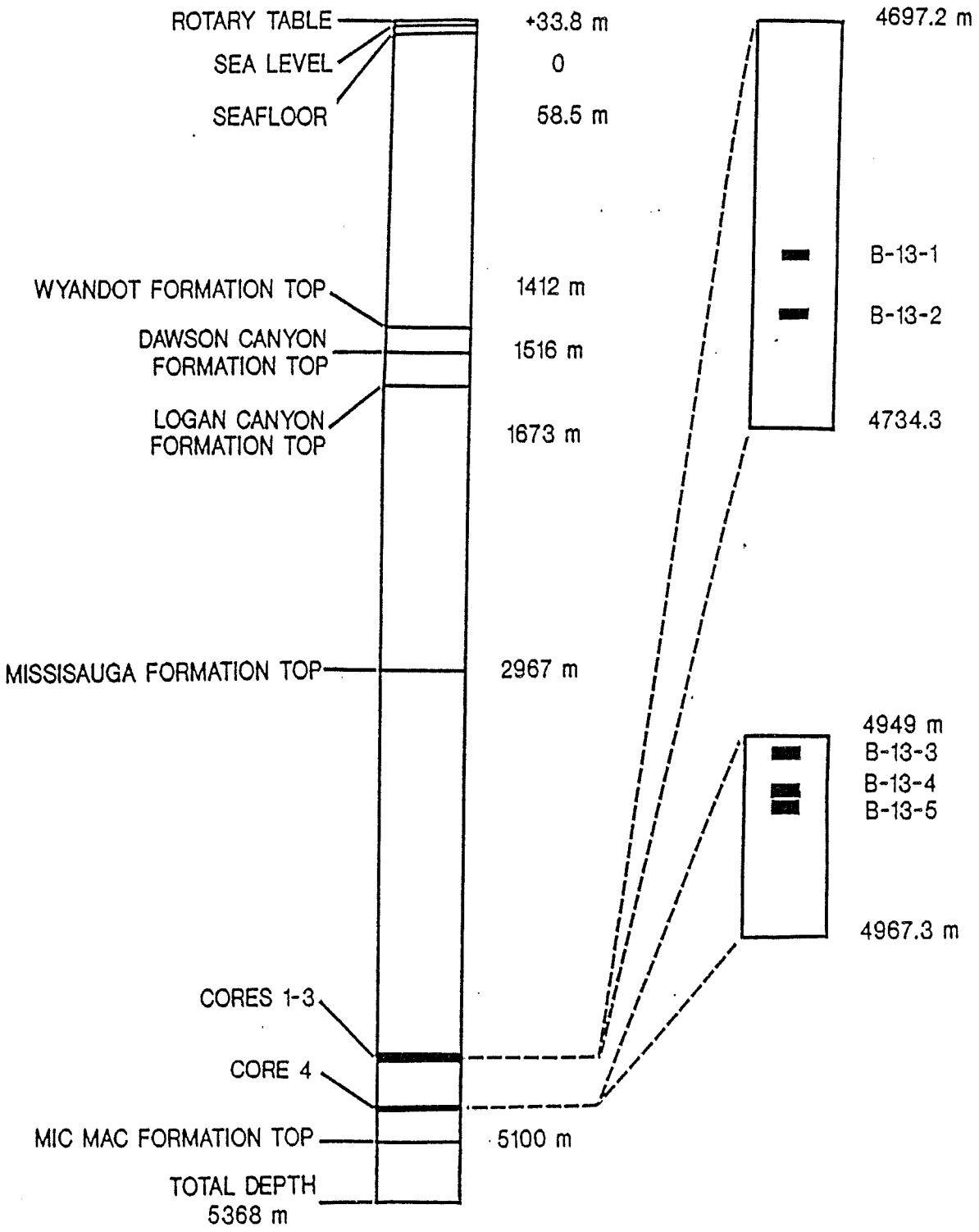

Figure 2.5. Stratigraphy and sample locations (shown with dark rectangles) for the Venture B-13 well.

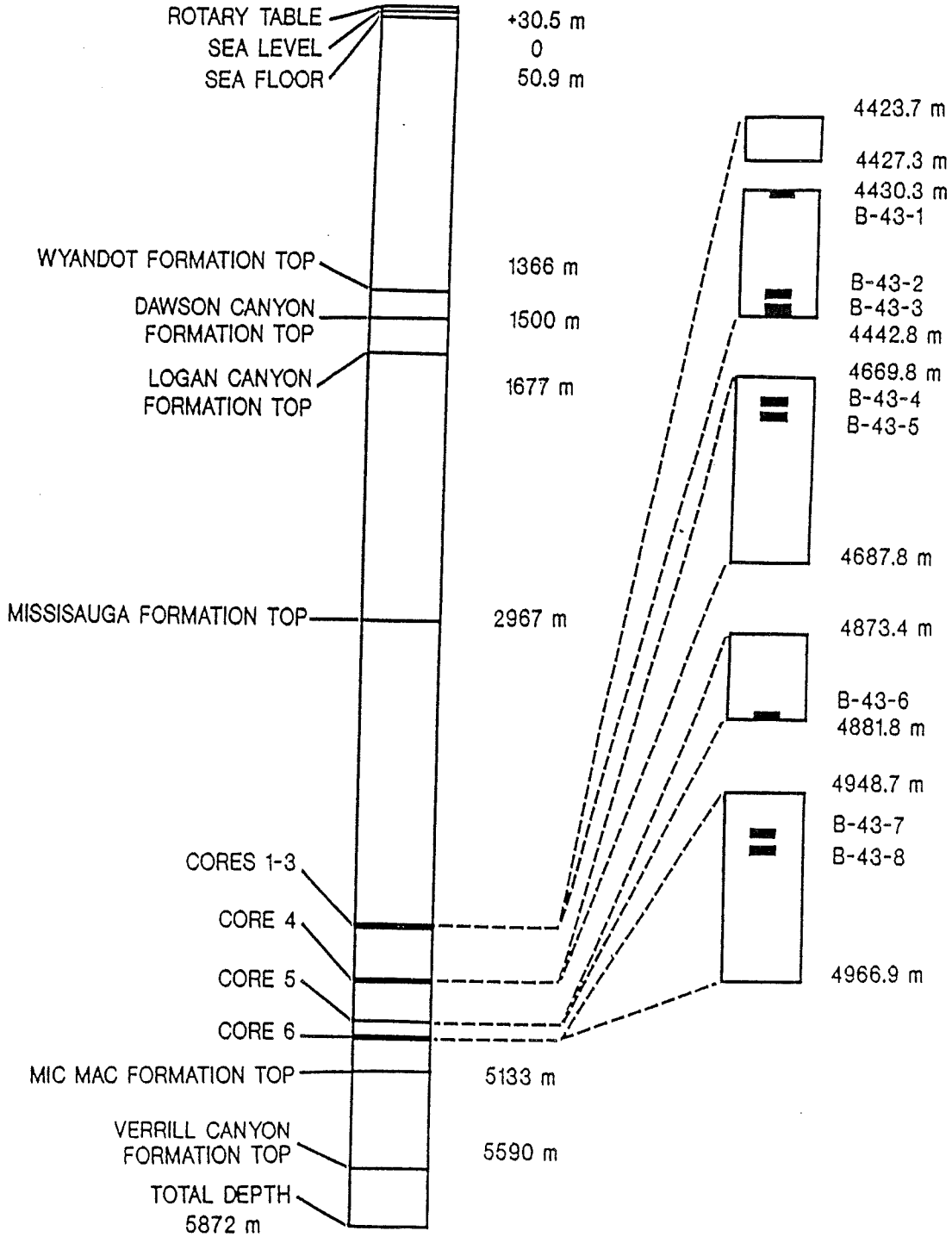

Figure 2.6. Stratigraphy and sample locations (shown with dark rectangles) for the Venture B-43 well.

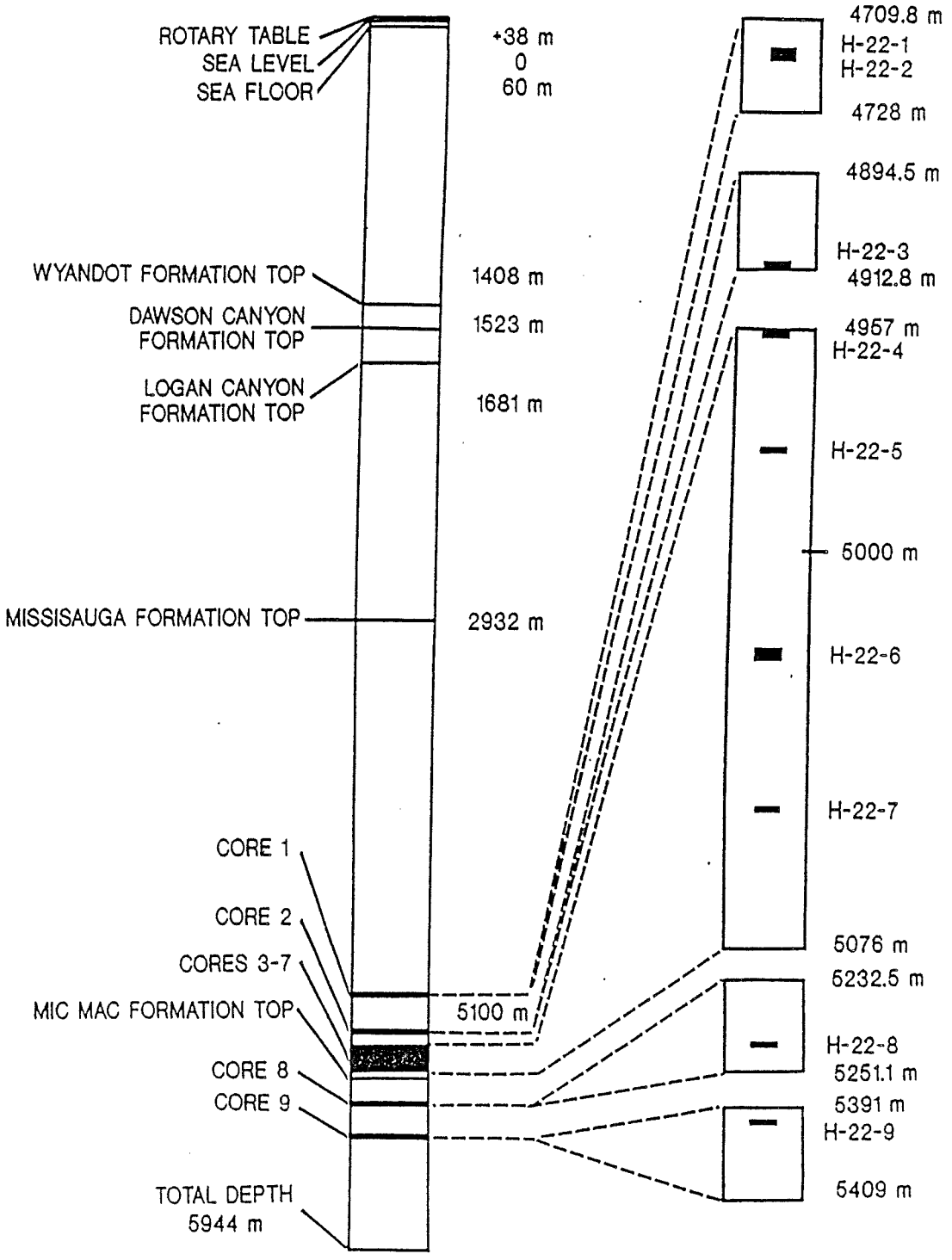

Figure 2.7. Stratigraphy and sample locations (shown with dark rectangles) for the Venture H-22 well.

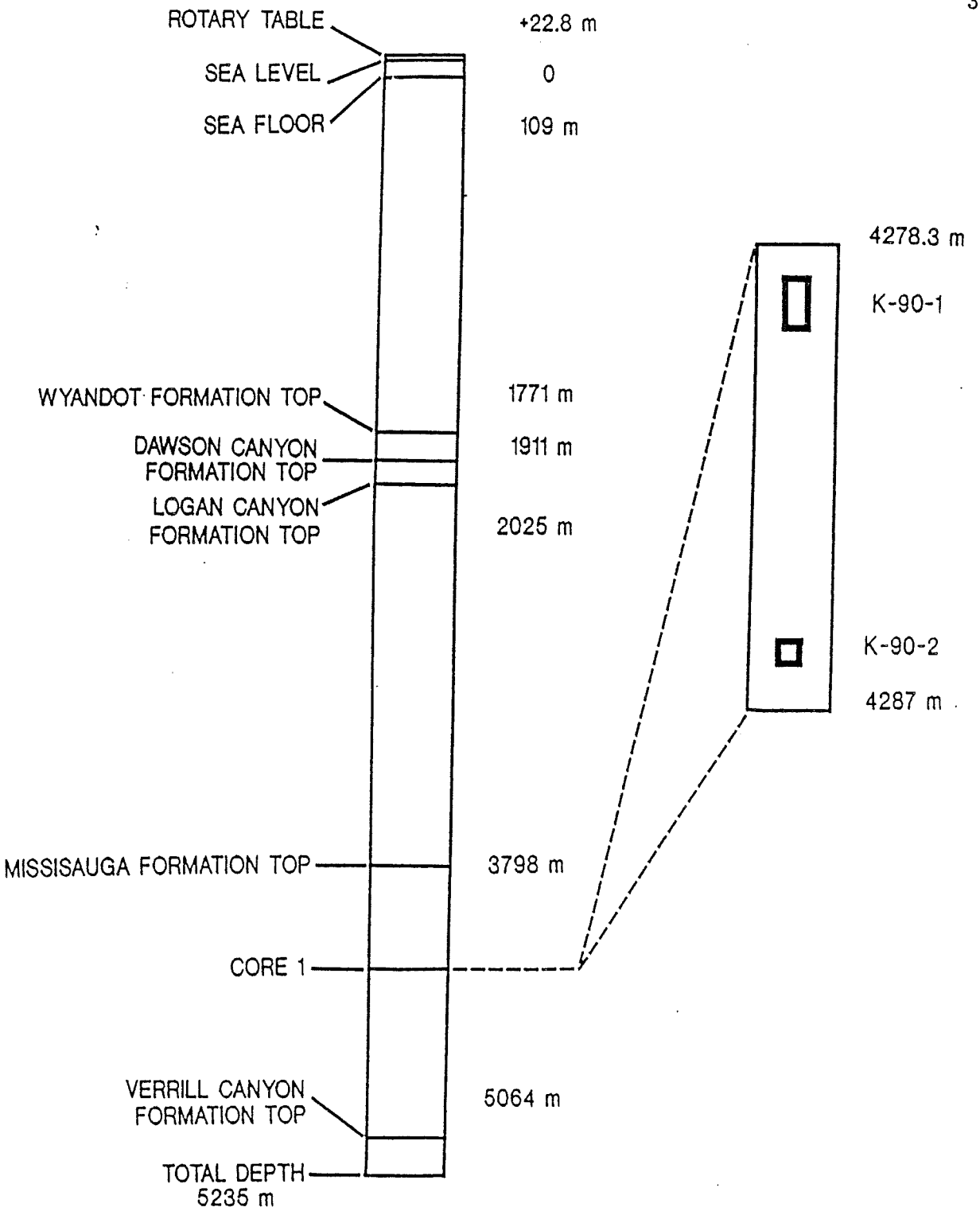

Figure 2.8. Stratigraphy and sample locations (shown with dark rectangles) for the Chebucto K-90 well.

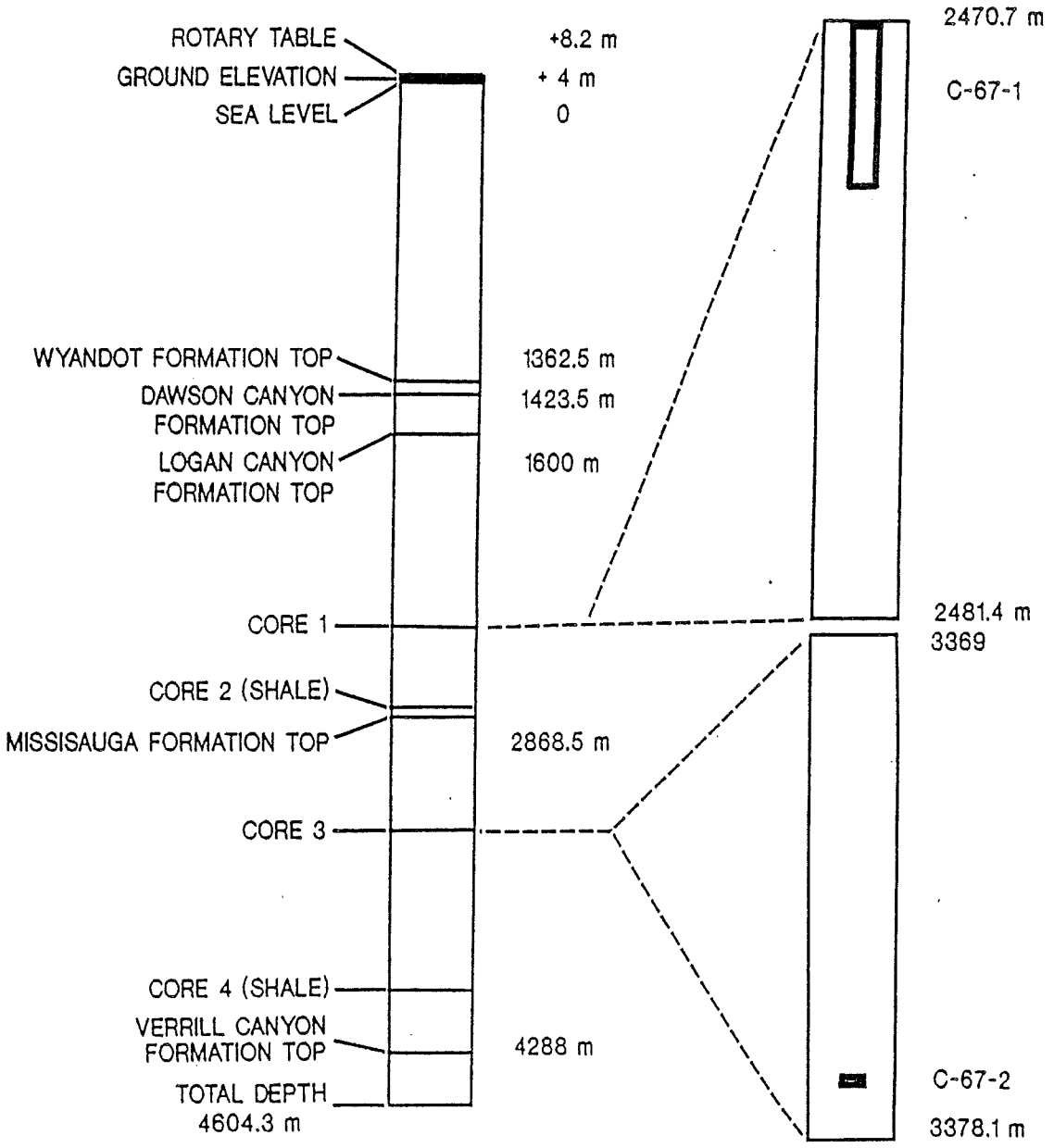

Figure 2.9. Stratigraphy and sample locations (shown with dark rectangles) for the Sable Island C-67 well.

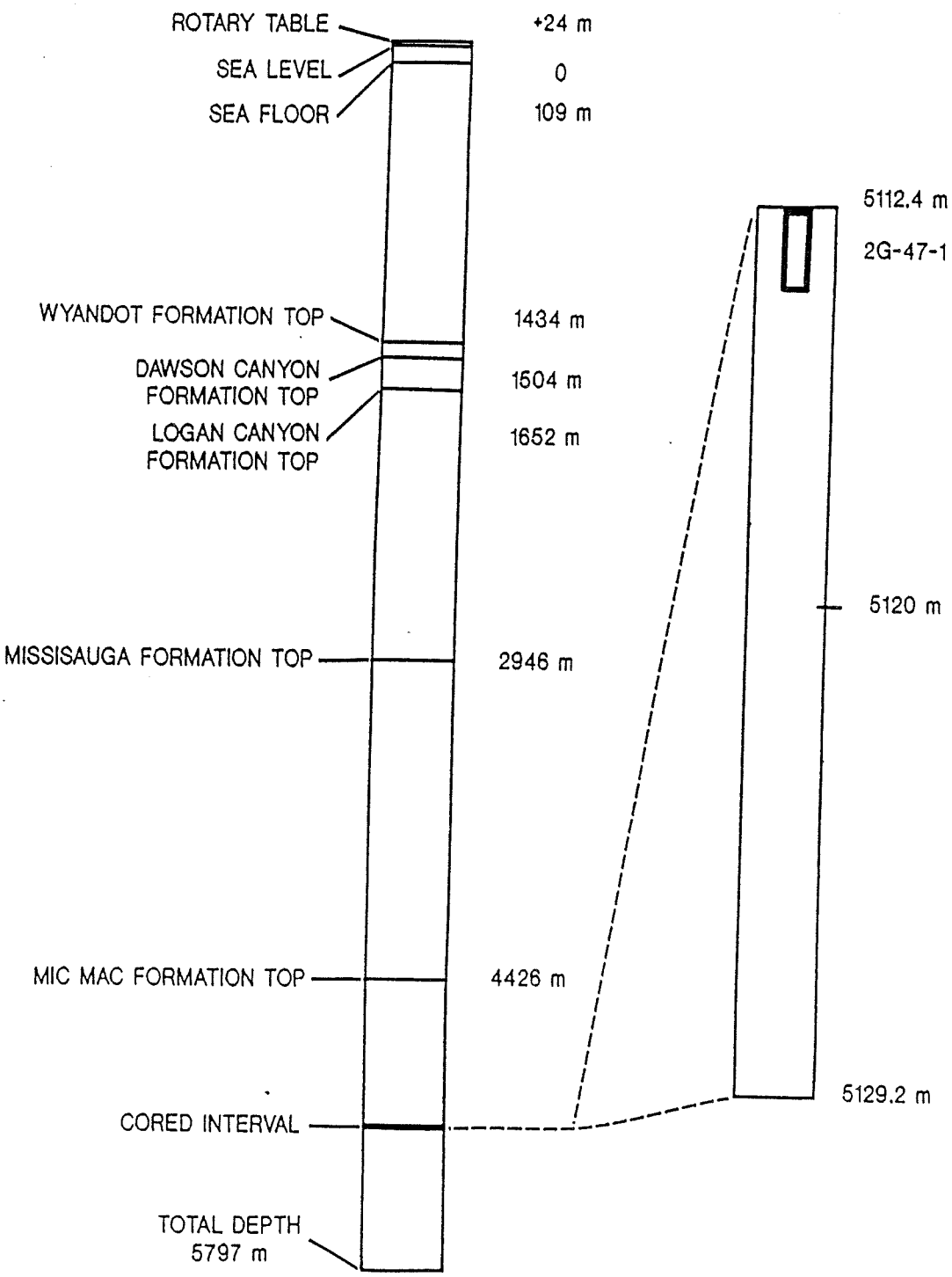

Figure 2.10. Stratigraphy and sample locations (shown with dark rectangles) for the Bluenose 2G-47 well.

2.2 Argon laboratory procedures

The K-feldspar and mica mineral separates prepared for argon analysis were wrapped in high-purity aluminium foil and shaped into dime-sized pieces that were stacked into an aluminium irradiation capsule. Interspersed among the samples were six similarly wrapped aliquots of the MMHb-1 flux monitor mineral. The capsules were irradiated at site 5C in the McMaster Nuclear Reactor for 10 hours. J-values as a function of position in the capsule were determined from analysis of the standards using equation 5 (in Chapter 1); sample values were then obtained by interpolation. Ages of samples were then determined using equation 6. Figure 2.11 is a schematic diagram of the argon gas extraction and measurement system. Once a sample was loaded, the whole system as far as the MS-10 mass spectrometer was evacuated and heated to a temperature of 200°C for 24 hours to drive off any loosely held atmospheric argon. The system vacuum was maintained with conventional oil diffusion pumps.

Standards, placed in a quartz tube set in a Lindberg resistance furnace, were outgassed by heating them to a temperature of 1000°C for 60 minutes. Micas were also heated in the Lindberg furnace, in a stepwise manner over the temperature range 200°C to about 1150°C. Heating times of approximately 50 minutes per step were used (see sample summaries in Appendix 2 for individual sample heating schedules). Several of the K-feldspar samples were also heated in the Lindberg furnace in a stepwise manner over the temperature range 200°C to 1150°C, using heating times of 20 minutes per step (see

Section 3.4.3 for an explanation as to why the reduced step heating times were used). Most of the K-feldspar samples were heated in a tantalum crucible in an internal resistance furnace. This latter furnace is capable of attaining the high temperatures (over 1350°C) that are necessary to completely outgas K-feldspars. These samples were also outgassed in a stepwise manner, over the temperature range 200°C to about 1350°C, using step heating times of approximately 50 minutes (see sample summaries in Appendix 2 for individual sample heating schedules). The Lindberg furnace has the more precise temperature control, and hence is advantageous when the data are to be used in diffusion calculations (see Chapter 1). Temperatures in the Lindberg furnace were monitored with a thermocouple set directly beneath the quartz tube. Temperatures in the internal furnace were monitored with a thermocouple set beneath, and in contact with, the tantalum crucible.

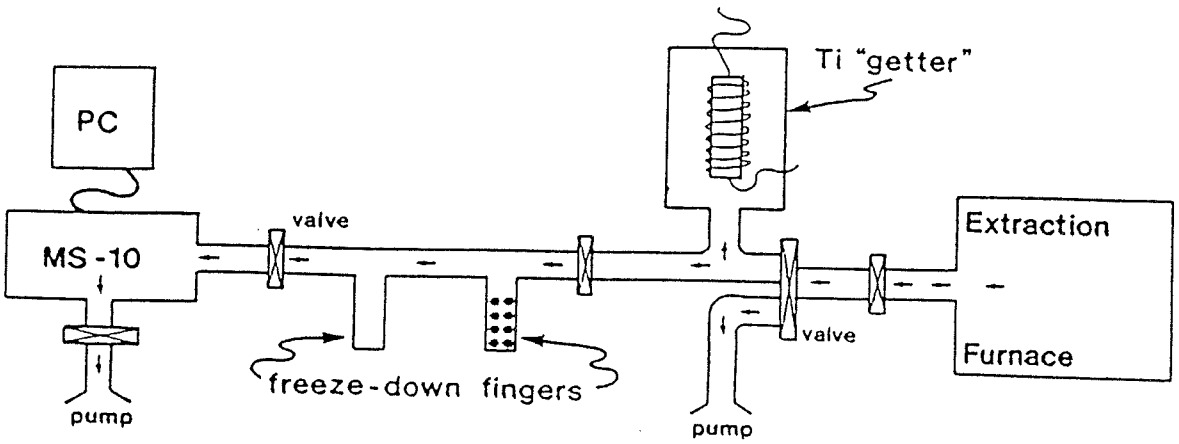

Figure 2.11. Argon gas extraction and data reduction system.

The gases evolved during each heating step were collected in a cold trap containing activated charcoal, that was maintained at a temperature of approximately -196°C by immersion in liquid nitrogen. Extracted gas was cleaned (to remove active gases and other contaminants) by means of a titanium getter held at a temperature of 600°C (by means of a resistance heating coil) for 15 minutes, at 300°C for a further 15 minutes. The purified argon gas was then admitted to the MS-10 mass spectrometer, where it was isotopically analyzed by a fully-automated data acquisition system.

2.3 Fission track laboratory procedures

2.3.1 Grain mount preparation

The procedures employed in the preparation of apatite grain mounts for fission track analysis were suggested by Dr. Randall R. Parrish (in: a short-course on the fission track method, Dalhousie University, October, 1986). The materials used were as follows:

-a 20 X 25 X 0.5 cm sheet of teflon (wiped clean and sprayed with an anti-static spray),

-a marking-pen and a dime,

-a box of glass microscope slides,

-clear epoxy, such as Araldite (the use of 5-minute epoxy is not recommended because it darkens significantly when irradiated).

Evenly spaced circles were traced on the teflon using the marking-pen and dime (one for each grain mount). The diameter of the dime (approximately 1.8 cm) is slightly less than the inside diameter of

the irradiation capsule, and the circles were used to establish a correct size for the grain mounts. In addition, some of the ink from the marking-pen was taken up by the hardening epoxy, forming a thin layer that was used to gauge the correct amount of grinding required to expose the apatite grains without removing them. Two glass slides were placed on the teflon near each circle (one on either side), close enough together that a third slide could be placed on them, forming a bridge over the circle. The two slides were then taped in place. Apatite grains from each sample or standard were then distributed into each circle (not more than 150 to 200 grains per circle) and the circles were labelled (see Figure 2.12).

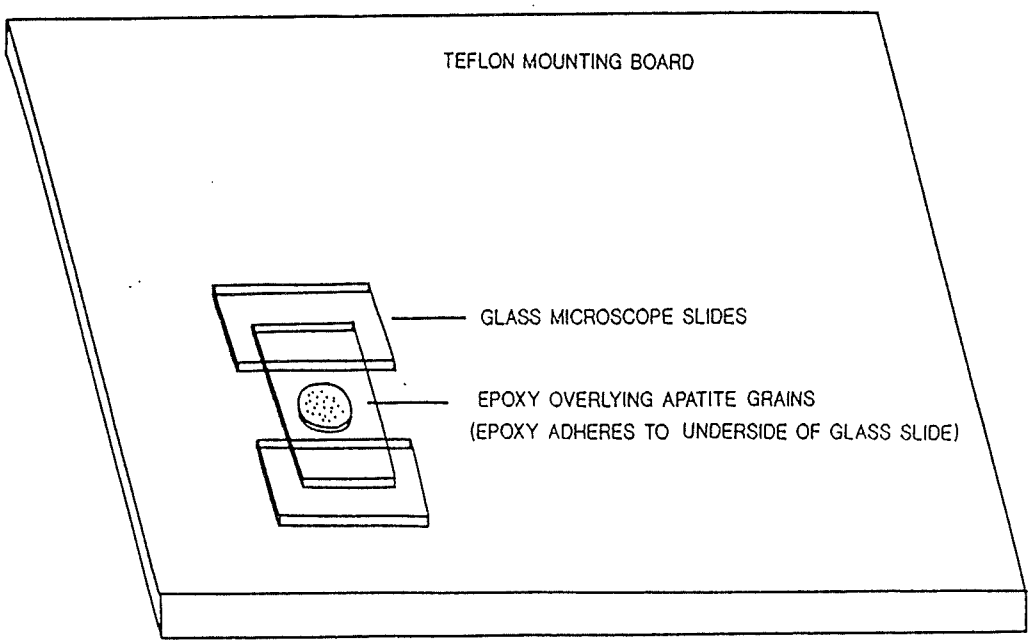

Figure 2.12. Diagram illustrating the creation of an epoxy grain mount (see text for description).

The epoxy and hardener were mixed and stirred gently so as not to create too many air bubbles. Approximately 5 or 6 drops of epoxy were placed into the center of each circle (nearly enough to fill it), and a glass slide was placed on top, forming a bridge. The epoxy adhered to the slide and spread radially to just beyond the edge of the circle. The grain mounts were allowed to harden for 24 to 48 hours, and were then removed from the teflon sheet (still adhering to the glass slide) by bending it slightly. The glass slides holding the grain mounts were then attached to specially machined teflon blocks (used for polishing thin sections) with a few drops of petroleum jelly.

Grinding and polishing of apatite grain mounts were done using a Buehler Polimet polishing machine with interchangeable 20.3 cm (8 inch) polishing wheels. Initial grinding was done on a wheel mounted with Leco 600-grit silicon-carbide sandpaper. The wheel was set to spin at approximately 200 r.p.m. while the grain mount (held in both hands) was slowly revolved in the opposite direction until the marking-pen circle began to appear faint (approximately 25 turns under light to moderate pressure).

The polishing of apatite grain mounts was done using wheels prepared with Leco 15-, 9-, 1-micron microid diamond compound. The wheels were prepared as follows:

-a piece of cloth was stretched tightly over the surface of a cleaned wheel and held in place with a large hose clamp,

-approximately .25 to .5 grams of the appropiate microid diamond

compound was put into a vial containing 10 grams of a light oil, shaken, and then poured evenly over the working surface of the wheel.

The 15-micron wheel was used for the initial polish. The teflon block and grain mount were first washed with soapy water to get rid of any loose 600-grit. Then the mount was turned against the spinning wheel (set at approximately 200 r.p.m.) for about 50 turns. It was then held in one position for approximately 45 seconds to create a set of parallel 15-micron scratches. The mount was then washed again with soapy water, rinsed, and inspected with a reflected-light microscope (at 400 X magnification) to see if any large scratches (from the 600-grit) were present. If so, the mount was then given an additional 50 turns and another set of parallel 15-micron scratches. If not, and the only marks visible were parallel 15-micron scratches, then the mount was washed with soapy water to get rid of any loose 15-micron compound, rinsed, and the procedure was repeated for the 9-micron and 1-micron wheels.

For the final polish a piece of 20.3 cm (8 inch) diameter Leco flocked twill was put on a cleaned wheel. A slurry containing approximately 50 grams of Buehler 0.05-micron gamma alumina in 300 ml of water was made, and about 50 ml of this slurry was spread evenly over the flocked twill. The wheel was set to spin slowly (20 to 30 r.p.m.), and, under very light pressure, the mount was revolved in the opposite direction for 5 or 6 turns (only), following which the mount was washed and rinsed.

Before they were etched, the polished grain mounts were removed from the glass slides. This was done by filling a basin with tepid water and, with a razor blade, sawing at the epoxy-glass contact while holding the mount under water. If this procedure is done in air the mounts tend to break rather than part from the glass. The water tends to propagate the parting, and the entire mount is released quite suddenly. To etch the grain mounts and thereby reveal fossil fission tracks, a solution of 7 percent nitric acid (HNO_3) was used. Mounts were etched for 40 seconds.

After they were etched, the external (mica) detector was attached to each grain mount or glass monitor with Scotch-tape. The mica used was Brazilian Ruby Clear (#5 1/2) muscovite, cleaved into very thin (<0.1 mm) sheets, and then cut with scissors into irregular polygonal shapes. The thickness of each of the grain mounts and glasses was measured using micrometer calipers. The pieces were then placed in an aluminium irradiation capsule (2 cm inside diameter, 4.5 cm total length), with one glass at the top, one at the bottom, and the other two interspersed among the sample and standard grain mounts. The position of each of the pieces in the capsule was recorded so that the reactor flux gradients throughout the capsule could be evaluated using the glasses, and hence the flux at any position in the capsule determined by interpolation.

2.3.2 Sample irradiation

Samples from the Scotian Basin were included in 3 separate irradiation capsules. The first included samples from the Mic Mac J-77, and H-86 wells. The second included the Venture H-22, B-13, and B-43 wells. The third included the Erie D-26, Chebucto K-90, Bluenose 2G-47, and Sable Island C-67 wells, and a re-irradiation of one sample (VB-13-1). (The latter had separated from its detector during an earlier irradiation and produced no induced tracks.) The positions of the various samples, standards, and glasses in each of the three irradiation capsules are shown in Tables 2.2 - 2.4.

Capsules for fission track analysis were irradiated at site 9D in the McMaster University Nuclear Reactor, Hamilton, Ontario, for 555 seconds to obtain a total neutron flux of 5 X 10^{15} n/cm^2. After they were returned, the irradiated capsules were stored under lead for 2 weeks to allow the level of radioactivity to diminish. They were then opened by the Dalhousie Geology Department radiation safety officer K. Taylor, and the level of activity of each mount or glass monitored. Radiation levels of samples were generally less than 2 mr/hr at one centimeter distance. Radioactive grain mounts and glasses were handled with tweezers while wearing gloves, and all material which came in contact with the mounts and glasses was considered contaminated.

Table 2.2. The positions in the irradiation capsule of the Mic Mac J-77, and Mic Mac H-86 samples. The depths of the sampled intervals are shown in Table 2.1.

Sample	Thickness (mm)	Position in capsule (mm)
SRM 614 Glass T (inverted)	2.05	2.05
other sample	1.40	2.05
other sample	0.90	3.45
other sample	1.40	4.35
FCN-4 standard	1.45	5.75
H-86I	1.40	7.20
SRM 614 Glass MT	2.05	8.60
J-77P	1.45	10.65
other sample	1.25	12.10
FCN-8 standard	1.45	13.35
other sample	1.40	14.80
other sample	1.05	16.20
other sample	1.70	17.25
FCN-7 standard	1.45	18.95
J-77I	1.45	20.40
other sample	1.45	21.85
FCN-6 standard	1.65	23.30
other sample	1.10	24.95
other sample	1.85	26.05
other sample	1.45	27.90
other sample	1.30	29.35
FCN-2 standard	1.80	30.65
SRM 614 Glass MB	2.10	32.45
other sample	1.50	34.55
other sample	1.35	36.05
other sample	1.60	37.40
SRM 614 Glass B	2.05	39.00

Table 2.3. The positions in the irradiation capsule of the Venture B-13, B-43, and H-22 samples. The depths of the sampled intervals are shown in Table 2.1.

Sample	Thickness (mm)	Position in capsule (mm)
SRM 614 Glass T (inverted)	2.15	2.15
SRM 614 Glass T2	2.00	2.15
VB-13-1	1.45	4.15
VH-22-1	1.75	5.60
FCN-7 standard	1.45	7.35
SRM 614 Glass MT (inverted)	2.15	10.95
SRM 614 Glass MT2	2.05	10.95
VH-22-9	1.80	13.00
FCN-10 standard	1.45	14.80
VB-43-1a	1.80	16.25
VB-43-1b	1.80	18.05
SRM 614 Glass MB (inverted)	2.15	22.00
SRM 614 Glass MB2	2.10	22.00
VB-13-4	1.80	24.10
FCN-13 standard	1.40	25.90
VB-13-4b	1.50	27.30
VB-43-8	1.75	28.80
other sample	1.55	30.55
FCN-14 standard	1.40	32.10
other sample	1.50	33.50
SRM 614 Glass B (inverted)	2.05	37.05
SRM 614 Glass B2	2.15	37.05

Table 2.4. The positions in the irradiation capsule of the Erie D-26, Sable Island C-67, Chebucto K-90, and Bluenose 2G-47 samples. The depths of the sampled intervals are shown in Table 2.1.

Sample	Thickness (mm)	Position in capsule (mm)
SRM 614 Glass T (inverted)	2.10	2.10
K-90-1	1.60	3.70
other sample	1.50	5.20
FCN-15 standard	1.60	6.80
other sample	1.60	8.40
C-67-1	1.45	9.85
other sample	1.80	11.65
SRM 614 Glass MT	2.10	13.75
D-26-1	1.45	15.20
other sample	1.70	16.90
FCN-17 standard	1.55	18.45
C-67-2	1.45	19.90
other sample	1.80	21.70
2G-47-1	1.35	23.05
other sample	1.60	24.65
SRM 614 Glass MB	2.25	26.90
FCN-11 standard	1.40	28.30
D-26-2	1.45	29.75
other sample	1.55	31.30
other sample	1.80	33.10
FCN-10 standard	1.40	34.50
VB-13-1	1.50	36.00
SRM 614 Glass B	2.35	38.35

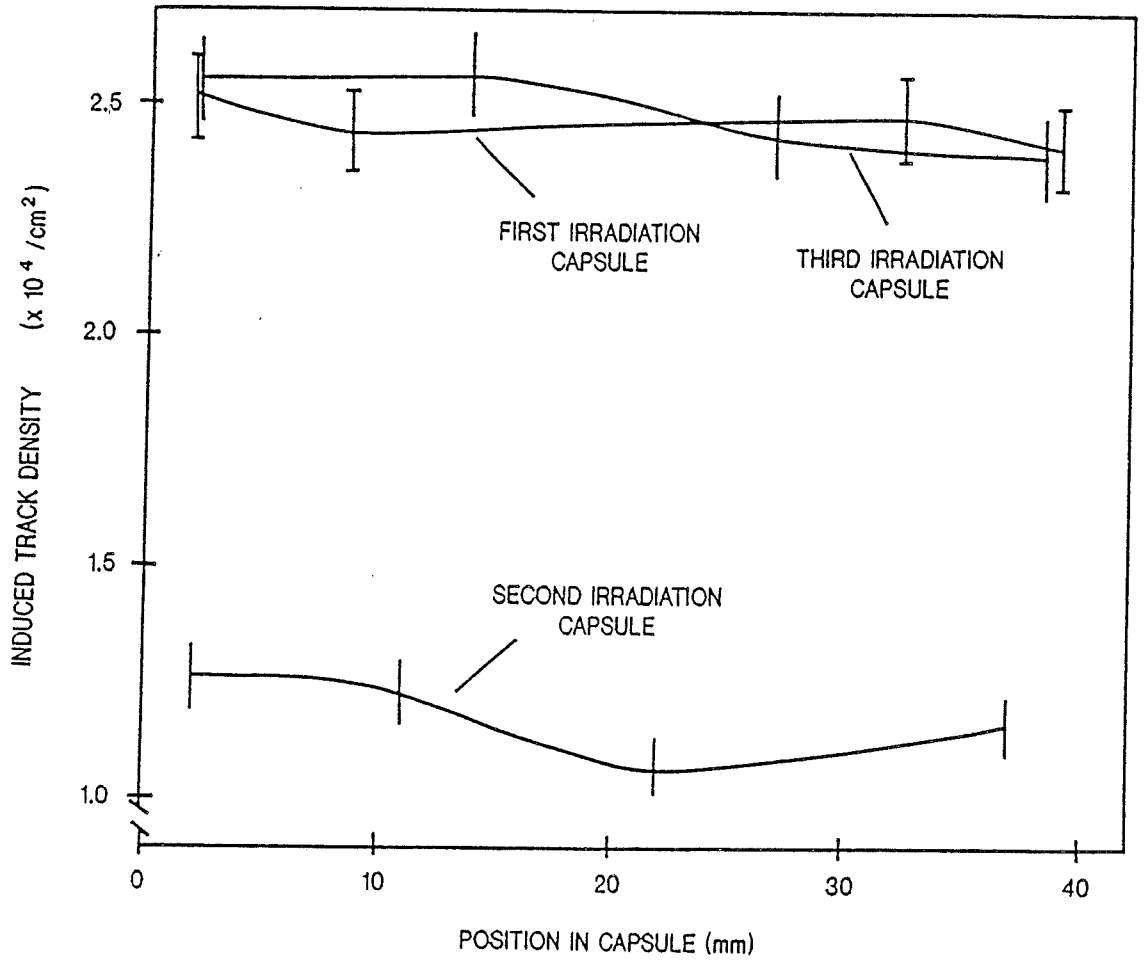

Figure 2.13. A plot of induced track density for the three irradiation packages that contained samples from the Scotian Basin.

2.3.3 Counting and track length measurement conditions

Six holes were punched through the tape and mica into each grain mount using the tip of a razor knife to make a regularly spaced array of triangles (see Figure 2.14). (This was not done to the micas on the glass monitors.) The tape was then removed and discarded. The micas were placed, facing side up, in small teflon beakers in a fume-hood and etched with 48% HF. Micas from standards and samples were etched

for 15 minutes, and micas from glasses for 40 minutes (all at room temperature). They were then rinsed thoroughly with distilled water and dried on a hotplate (on low heat) for 5 minutes to drive off any remaining HF.

Some glass slides were cut in half, and one of the halves and a grain mount were attached side by side to a second glass slide using a few drops of melted wax (see Figure 2.14). The corresponding mica was then placed on the half-slide, facing side up, and its position adjusted until the triangular holes in the mount and mica formed precise mirror images (so that it was possible to translate from a marker-hole in the grain mount to the same marker-hole in the mica, under 100X magnification, using only the X-adjustment of a microscope's mechanical stage). Scotch tape was then used to secure it in this position. Micas from glasses were simply taped face up on glass slides to be counted.

Fission tracks were counted using a Leitz Laborlux D microscope, equipped with a mechanical stage, 100-watt transmitted light source, and an Olympus 5 mm X 5 mm graticule in the right eyepiece. Induced tracks (in mica) from the glass neutron dosimeter were counted at 650X magnification (NPL Fluotar 50X/0.85 (dry) objective, Periplan GF 12.5X/20 oculars). Spontaneous tracks in apatite and induced tracks from the samples and standards were counted at 1250X magnification (NPL Fluotar 100X/0.85 (dry) objective, Periplan GF 12.5X/20 oculars). Track lengths were measured using a Leitz drawing tube and a Houston Instruments HIPAD True Grid 1011 digitizing tablet, equipped

with a cursor with LED and a 9-volt battery. Data reductions (including chi-square, zeta, age and track length statistics, and uranium concentration calculations) were done using a microcomputer software system developed by Donelick (1988).

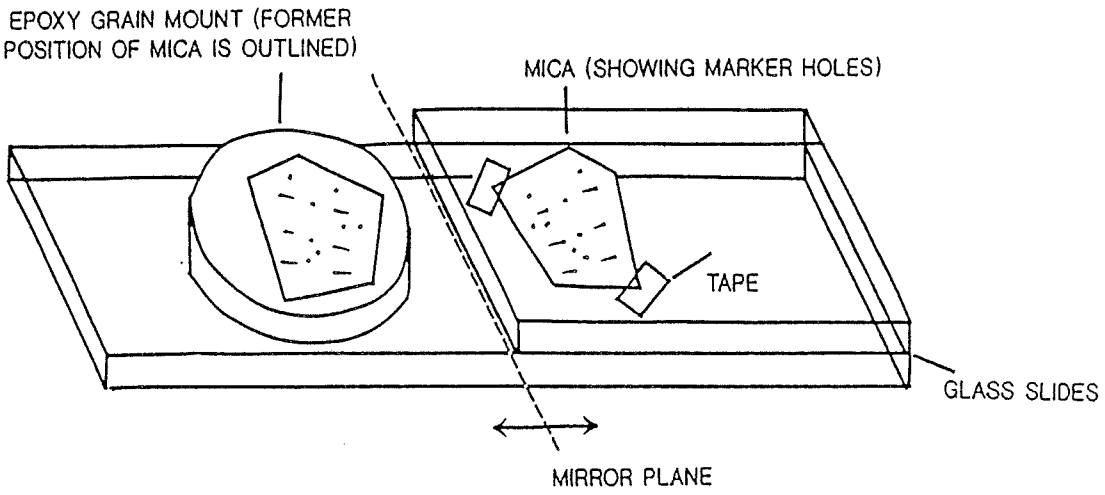

Figure 2.14. Diagram of epoxy grain mount (containing apatite grains) and corresponding external detector (approximately 2x magnification).

3 Argon dating: observations and interpretations

3.1 Argon data

3.1.1 Micas

A total of five mica separates were analyzed (one biotite and four muscovites). A summary of the mica argon ages is given in Table 3.1.

Table 3.1. A summary of mica argon total gas ages determined in this study. Depths are B.R.T. (below rotary table). The total gas age is a weighted average of all the step ages of the analysis (see sample summaries in Appendix 2).

Well Name	Sample Name	Formation	Depth (m)	Mineral	Total Gas Age (Ma)
Mic Mac H-86	H-86 (BT)	Mohican	4714-4725	biotite	195 ± 3
Mic Mac H-86	H-86 (MU)	Mohican	4714-4725	muscovite	329 ± 3
Mic Mac J-77	J-77 (MU)	Missisauga	2814-2823	muscovite	508 ± 5
Venture B-13	B-13-2 (MU)	Missisauga	4723	muscovite	372 ± 4
Venture B-13	B-13-5 (MU)	Missisauga	4955	muscovite	337 ± 3

The single biotite spectrum obtained is shown in Figure 3.1. The sample was obtained from the Mohican Formation, at a depth of 4715 - 4725 m in the Mic Mac H-86 well. The initial seven heating steps (representing 80 percent of the total ^{39}Ar) produced a gradient of step ages that increase from 140 Ma to 240 Ma. The final three heating steps produced a negative gradient of ages that decrease from 250 Ma

to 230 Ma. Approximately 70 percent of the argon in the sample was released during the first four heating steps (up to 650°C) indicating that the gas was situated in low-activation energy sites. The mean age of the released gas is 195 Ma.

The four muscovite spectra that were determined are shown in Figures 3.2 to 3.5. The H-86 (MU) spectrum (Figure 3.2) represents the same sampled interval as H-86 (BT) in the Mic Mac H-86 well. H-86 (MU) also contains a gradient of step ages, that increase from 140 Ma to 340 Ma over the first 30 percent of ^{39}Ar release. The final six heating steps (representing 70 percent of the total ^{39}Ar) produced a well-defined plateau at an age of 360 Ma. Approximately 70 percent of the argon in the sample was released during the four heating steps between 750°C and 900°C, indicating that most of the sample argon was situated in high-activation energy sites. The mean age of the released gas is 329 Ma.

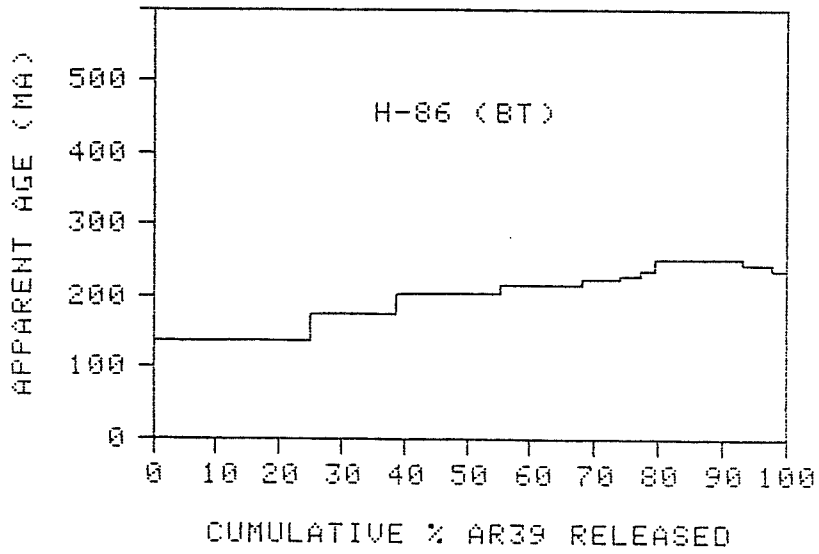

Figure 3.1. Biotite argon spectrum for H-86I (Mohican Fm.), obtained at a depth of 4715 - 4725 m (B.R.T.) in the Mic Mac H-86 well.

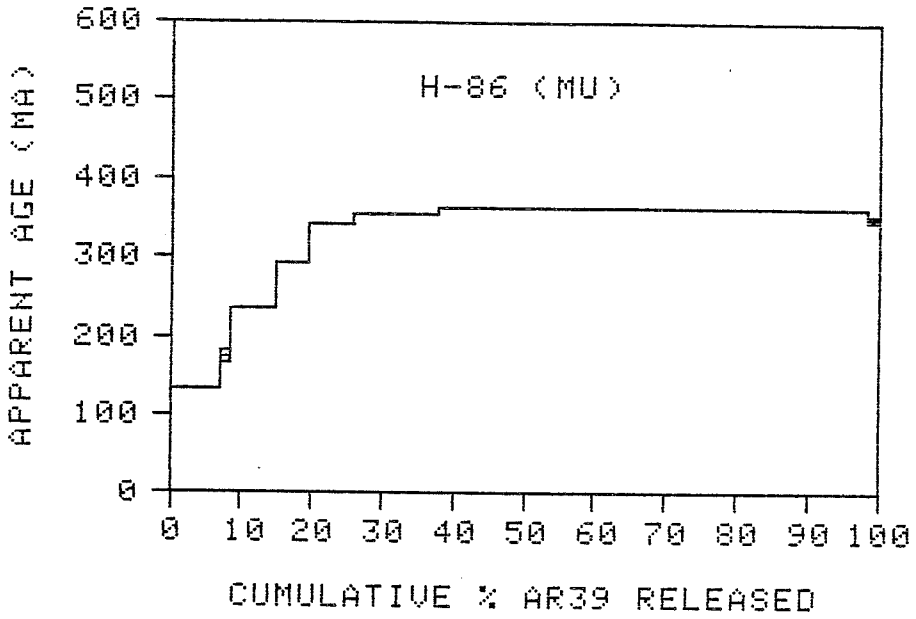

Figure 3.2. Muscovite argon spectrum for H-86I (Mohican Fm.), obtained at a depth of 4715 - 4725 m (B.R.T.) in the Mic Mac H-86 well.

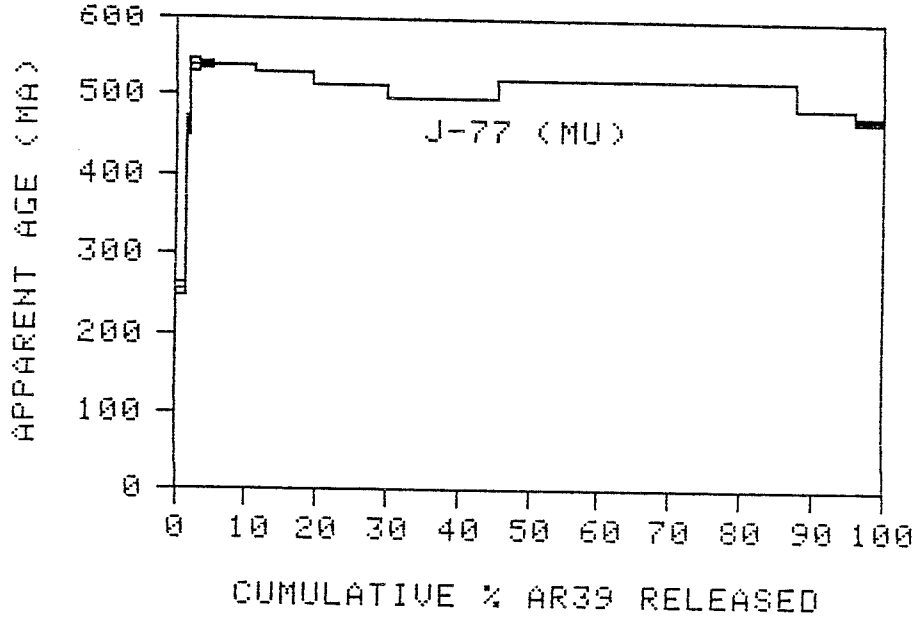

Figure 3.3. Muscovite argon spectrum for J-77I (Missisauga Fm.), obtained at a depth of 2814 - 2823 m (B.R.T.) in the Mic Mac J-77 well.

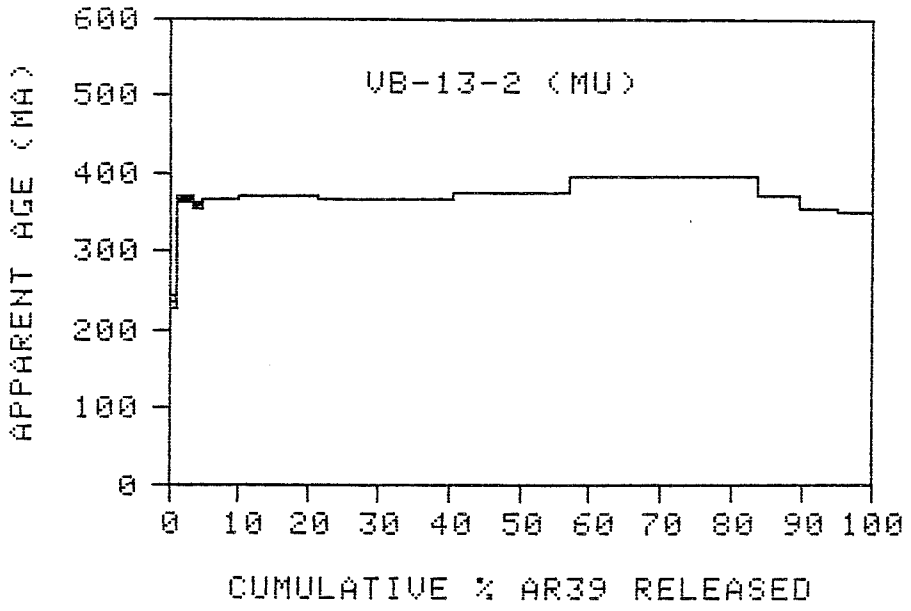

Figure 3.4. Muscovite argon spectrum for VB-13-2 (Missisuaga Fm.), obtained at a depth of 4723 m (B.R.T.) in the Venture B-13 well.

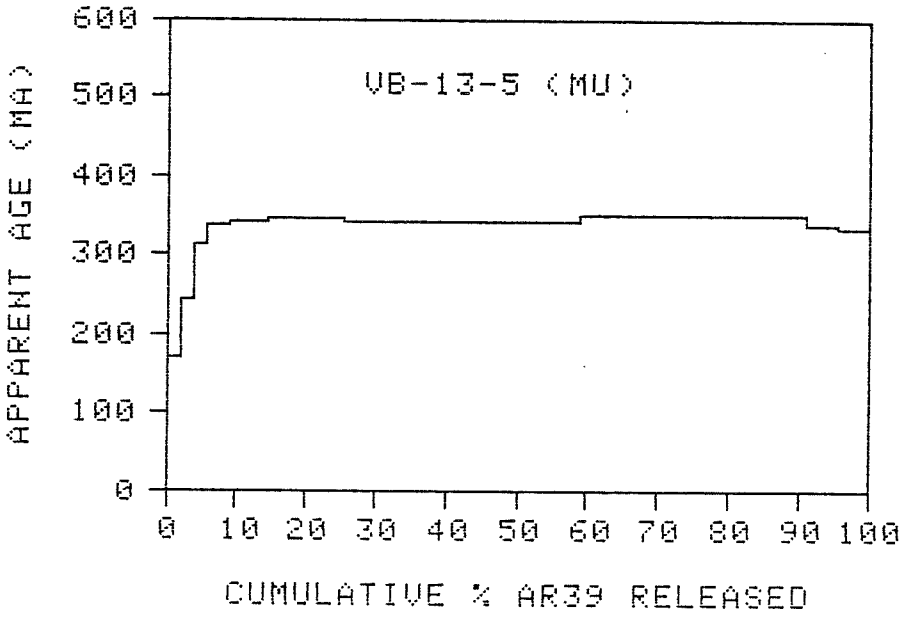

Figure 3.5. Muscovite argon spectrum for VB-13-5 (Missisauga Fm.), obtained at a depth of 4955 m (B.R.T.) in the Venture B-13 well.

The J-77 (MU) spectrum (Figure 3.3) is from a sample that was obtained from the Missisauga Formation, at a depth of 2814 - 2824 m in the Mic Mac J-77 well. This spectrum contains several step age gradients. The initial three heating steps (representing 3 percent of the total ^{39}Ar) produced increasing ages, which range from 250 Ma to 540 Ma. The third through eighth steps (representing 40 percent of the total ^{39}Ar) produced a negative gradient of step ages, which decrease to about 500 Ma. The ninth step makes up 40 percent of the total argon, and is slightly older than the preceding step. The final three steps produced a second negative gradient, with ages that decrease to 450 Ma. The mean age of the released gas is 508 Ma.

The VB-13-2 and VB-13-5 spectra (Figures 3.4 and 3.5) are also from samples that were obtained from the Missisauga Formation, from the Venture B-13 well, at depths of 4723, and 4955 m respectively. The initial two heating steps of the VB-13-2 sample (representing 2 percent of the total ^{39}Ar) produced ages that increased from 240 Ma to 300 Ma. The third through eighth steps (representing 55 percent of the total ^{39}Ar) produced a plateau at an age of 370 Ma. The final four heating steps produced a negative gradient, with ages that decrease from 400 Ma to 350 Ma. The total gas age of the sample is 370 Ma. The initial three heating steps of the VB-13-5 spectrum (representing 6 percent of the total ^{39}Ar) produced a gradient of increasing step ages that range from 170 Ma to 320 Ma. The fourth through eighth steps (representing 84 percent of the total ^{39}Ar) produced a plateau at 340 Ma. The final

10 percent of ^{39}Ar released (two steps) produced a slight negative age gradient. Two of the heating steps (800°C, and 850°C) accounted for 65 percent of the total ^{39}Ar. The mean age of the released gas is 337 Ma.

3.1.2 K-feldspars

A total of thirteen K-feldspar argon spectra were determined from seven of the nine wells sampled. Mineral separates from the other two wells, Bluenose 2G-47 and Venture H-22, contained little or no potassium feldspar. Eight of the spectra are from the Missisauga Formation, two each are from the Mohican and Logan Canyon Formations, and one is from the Mic Mac Formation. A summary of the feldspar argon total gas ages for the various formations and depths is given in Table 3.2.

Table 3.2. A summary of the K-feldspar argon total gas ages determined in this study. Depths are B.R.T. (below rotary table).

Well name	Sample Name	Formation	Depth (m)	Total gas age (Ma)
Venture B-13	VB-13-1	Missisauga	4718	761 ± 8
Venture B-13	VB-13-2	Missisauga	4723	790 ± 8
Venture B-43	VB-43-1	Missisauga	4430	969 ± 10
Venture B-43	VB-43-4	Missisauga	4673	772 ± 8
Chebucto K-90	K-90-2	Missisauga	4286	829 ± 8
Sable Island C-67	C-67-2	Missisauga	3377	867 ± 9
Mic Mac J-77	J-77I	Missisauga	2814 - 2823	841 ± 8
Mic Mac J-77	J-77P	Missisauga	2817	934 ± 9
Sable Island C-67	C-67-1A	Logan Canyon	2471 - 2481	829 ± 8
Sable Island C-67	C-67-1B	Logan Canyon	2471 - 2481	944 ± 9
Erie D-26	D-26-1	Mic Mac	1955 - 1959	535 ± 5
Mic Mac H-86	H-86I	Mohican	4715 - 4725	214 ± 2
Mic Mac H-86	H-86P	Mohican	4720	234 ± 2

The total gas ages of the eight samples from the Missisauga Formation range from 761 Ma to 969 Ma, and they are much older than corresponding mica argon ages (Table 3.1). The samples from the Logan Canyon Formation have similar total gas ages to those of the Missisauga Formation, but the Mic Mac and Mohican Formations are much younger. The total gas ages of the K-feldspar samples from the Mohican Formation are intermediate between the corresponding biotite and muscovite argon ages (Table 3.1).

The thirteen K-feldspar argon spectra that were determined in this study are shown in Figures 3.6 - 3.18. The C-67-2 spectrum (Figure 3.6) is from a sample that was obtained from the Missisauga Formation, at a depth of 3377 m in the Sable Island C-67 well. The initial heating step of this sample (representing 2 percent of the total ^{39}Ar) produced an age of 840 Ma. The second through fifth steps (representing 8 percent of the total ^{39}Ar) produced a steep gradient of step ages that increase form 680 Ma to 780 Ma. The final ten heating steps (representing 90 percent of the total ^{39}Ar) produced a shallow gradient of step ages that increase from 800 Ma to 930 Ma. The heating of the C-67-2 sample was done using the quartz tube furnace, and the sample is likely to have retained a fraction of its ^{39}Ar. Therefore, the spectrum shows the sample as having released an estimated 90 percent of its total argon. The mean age of the released gas is 867 Ma.

The K-90-2 spectrum (Figure 3.7) is from a K-feldspar sample that

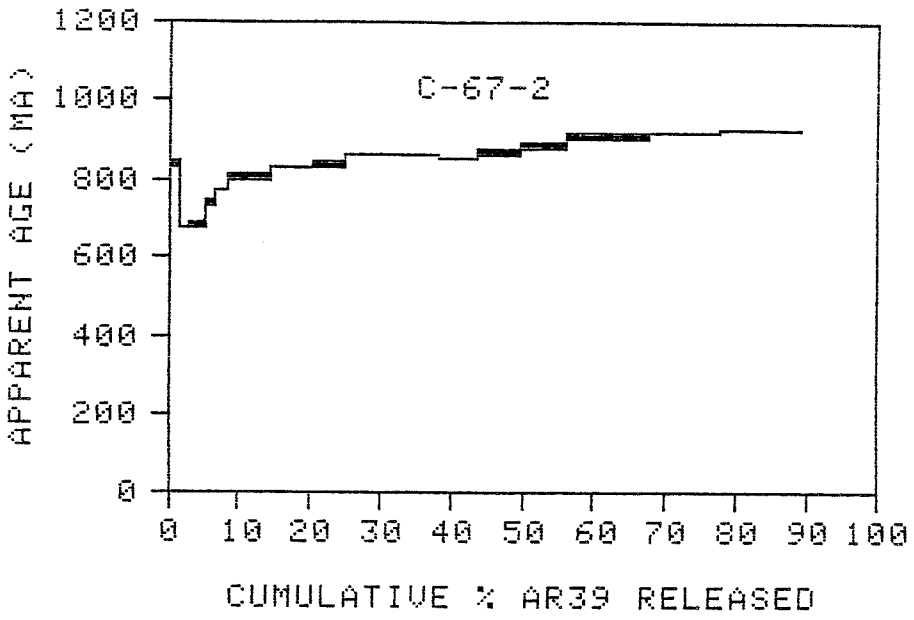

Figure 3.6. K-feldspar argon spectrum for C-67-2 (Missisauga Fm.), obtained at a depth of 3377 m (B.R.T.) in the Sable Island C-67 well. Sample extraction heating was done using a Lindberg furnace.

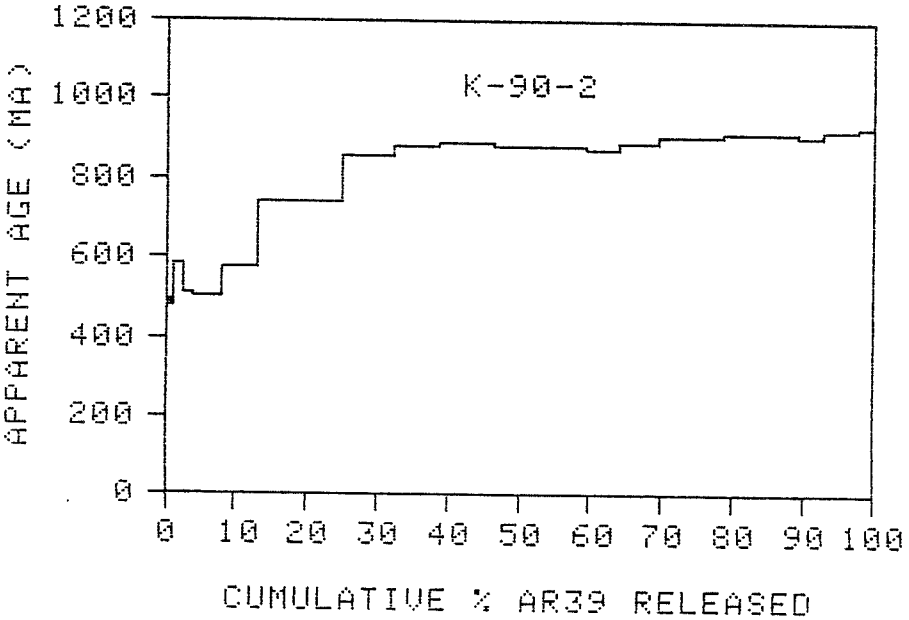

Figure 3.7. K-feldspar argon spectrum for K-90-2 (Missisauga Fm.), obtained at a depth of 4286 m (B.R.T.) in the Chebucto K-90 well.

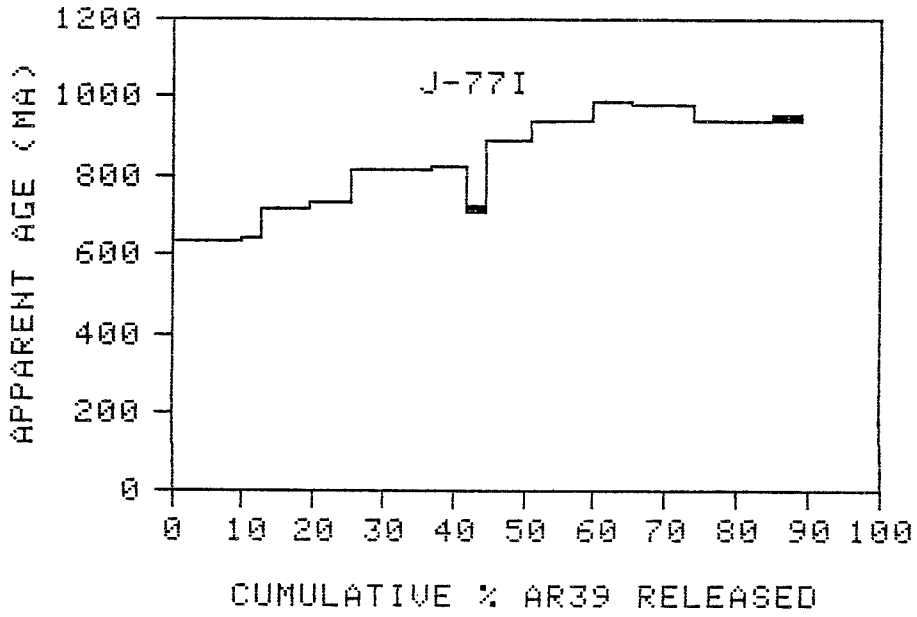

Figure 3.8. K-feldspar argon spectrum for J-77I (Missisauga Fm.), obtained at a depth of 2814 - 2823 m (B.R.T.) in the Mic Mac J-77 well.

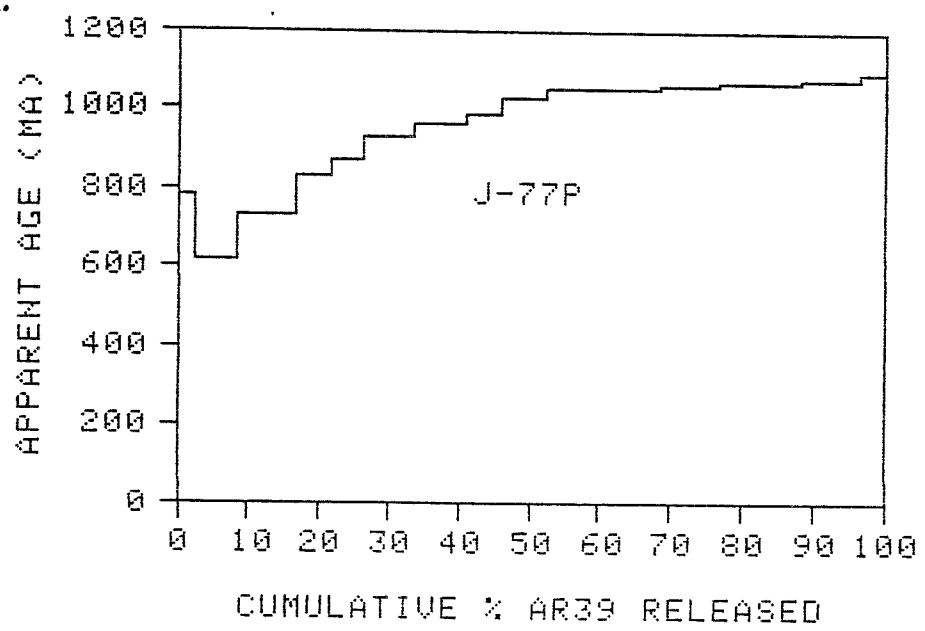

Figure 3.9. K-feldspar argon spectrum for J-77P (Missisauga Fm.), obtained at a depth of 2817 m (B.R.T.) in the Mic Mac J-77 well. Sample extraction heating was done using a Lindberg furnace.

was obtained from the Missisauga Formation, at a depth of 4286 m (B.R.T.) in the Chebucto K-90 well. The initial three heating steps of this sample (representing 5 percent of the total ^{39}Ar) produced ages that range from 490 Ma to 590 Ma. The fourth through seventh steps (representing 30 percent of the total ^{39}Ar) produced a steep gradient of step ages that increase from 500 Ma to 860 Ma. The final ten heating steps produced a shallow gradient of step ages that increase from 870 Ma to 910 Ma. The mean age of the released gas is 829 Ma.

The J-77I spectrum (Figure 3.8) is from a K-feldspar sample that was obtained from the Missisauga Formation, at a depth of 2814 - 2823 m (B.R.T.), in the Mic Mac J-77 well. The initial six heating steps of this sample (representing 40 percent of the total ^{39}Ar) produced a gradient of step ages that increase from 620 Ma to 810 Ma. The seventh heating step (representing 3 percent of the total ^{39}Ar) produced an age of 700 Ma. The eighth through tenth steps (representing 20 percent of the total ^{39}Ar) produced a gradient of step ages (similar to the gradient over the initial six steps) that increase from 880 Ma to 980 Ma. The final three heating steps (representing 25 percent of the total ^{39}Ar) produced a slight negative gradient of step ages that decrease from 970 Ma to 920 Ma. Because the heating of the J-77I sample was also done in a quartz tube furnace, the spectrum shows the sample as having released an estimated 90 percent of its total argon. The mean age of the released gas is 841 Ma.

The J-77P spectrum (Figure 3.9) is from a sample that was obtained from the Missisauga Formation, at a depth of 2817 m (B.R.T.)

in the Mic Mac J-77 well. The initial heating step of the sample (representing 3 percent of the total ^{39}Ar) produced an age of 760 Ma. The second through ninth heating steps (representing 52 percent of the total ^{39}Ar) produced a gradient of ages that increase from 600 Ma to 990 Ma. The gradient becomes less steep at high extraction temperatures. The final seven heating steps (representing 45 percent of the total ^{39}Ar) produced a very shallow gradient of step ages that increase from 1000 Ma to 1050 Ma. The mean age of the released gas is 934 Ma.

The VB-13-1 spectrum (Figure 3.10) is from a K-feldspar sample that was obtained from the Missisauga Formation, at a depth of 4718 m (B.R.T.) in the Venture B-13 well. The initial heating step of this sample (representing 4 percent of the total ^{39}Ar) produced an age of 460 Ma. The second and all subsequent heating steps (representing 96 percent of the total ^{39}Ar) produced a steep gradient of step ages that increase from 310 Ma to 1050 Ma. The gradient is less steep at high extraction temperatures. The mean age of the released gas is 761 Ma.

The VB-13-2 spectrum (Figure 3.11) is from a K-feldspar sample that was obtained from the Missisauga Formation, at a depth of 4723 m (B.R.T.) in the Venture B-13 well. The initial heating step of this sample (representing 6 percent of the total ^{39}Ar) produced a step age of 570 Ma. The second through fourteenth steps (representing 78 percent of the total ^{39}Ar) produced a steep gradient of step ages that increase from 330 Ma to 1000 Ma. The fifteenth step (representing 7 percent of the total ^{39}Ar) produced a slightly younger age (980 Ma).

The final three steps (representing 9 percent of the total ^{39}Ar) produced a shallow gradient of step ages that increase from 1000 Ma to 1020 Ma. The mean age of the released gas is 790 Ma.

The VB-43-1 spectrum (Figure 3.12) is from a K-feldspar sample that was obtained from the Missisauga Formation, at a depth of 4430 m (B.R.T.) in the Venture B-43 well. The initial heating step of this sample (representing 1 percent of the total ^{39}Ar) produced an age of 1420 Ma. The second and third steps (representing 2 percent of the total ^{39}Ar) produced ages of 730 Ma and 805 Ma, respectively. The third through twenty-first steps (representing 97 percent of the total ^{39}Ar) produced a steep gradient of step ages that increase from 545 Ma to 1145 Ma. The gradient is less steep at high extraction temperatures. The mean age of the released gas is 969 Ma. The VB-43-4 spectrum (Figure 3.13) is from a K-feldspar sample that was obtained from the Missisauga Formation, at a depth of 4673 m (B.R.T.) from the Venture B-43 well. The initial heating step of this sample (representing 3 percent of the total ^{39}Ar) produced a step age of 650 Ma. The second and all subsequent heating steps (representing 97 percent of the total ^{39}Ar) produced a gradient of step ages that increase from 295 Ma to 980 Ma. The gradient is quite steep from the second to the seventh steps, becomes quite shallow between the eighth and fourteenth steps, and then becomes steeper again over the final two steps. The mean age of the released gas is 772 Ma.

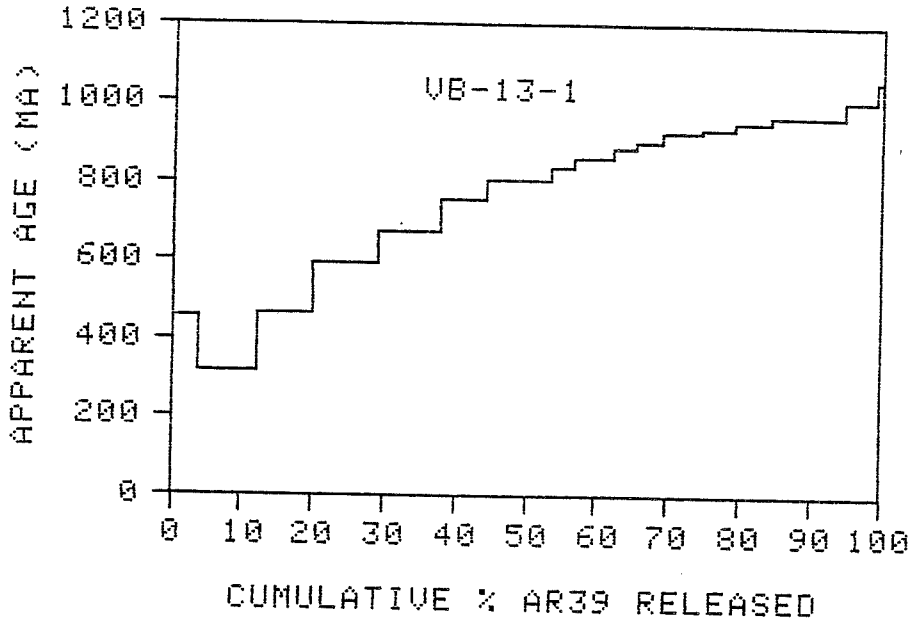

Figure 3.10. K-feldspar argon spectrum for VB-13-1 (Missisauga Fm.), obtained at a depth of 4718 m (B.R.T.) in the Venture B-13 well.

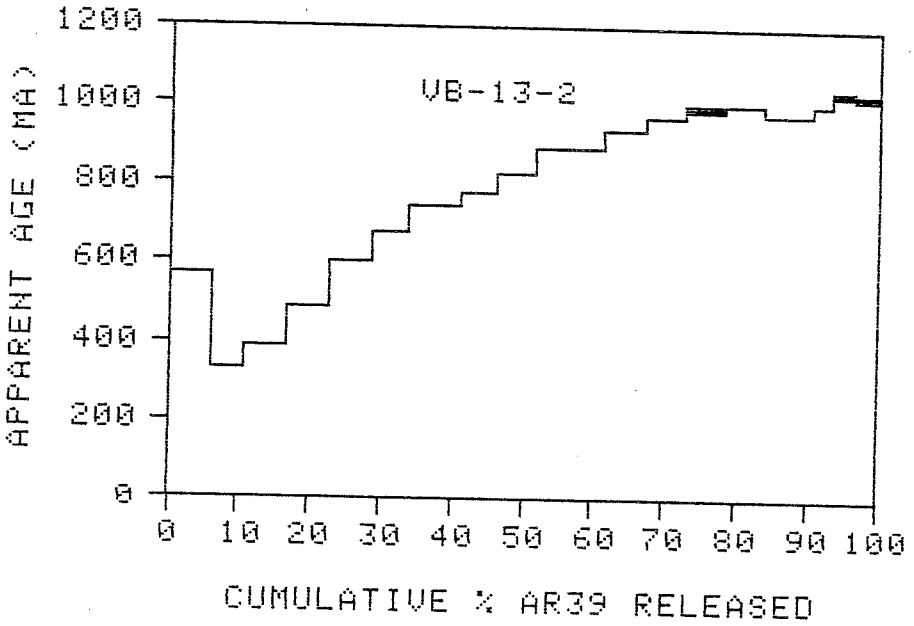

Figure 3.11. K-feldspar argon spectrum for VB-13-2 (Missisauga Fm.), obtained at a depth of 4723 m (B.R.T.) in the Venture B-13 well (note the similarity to Figure 3.10).

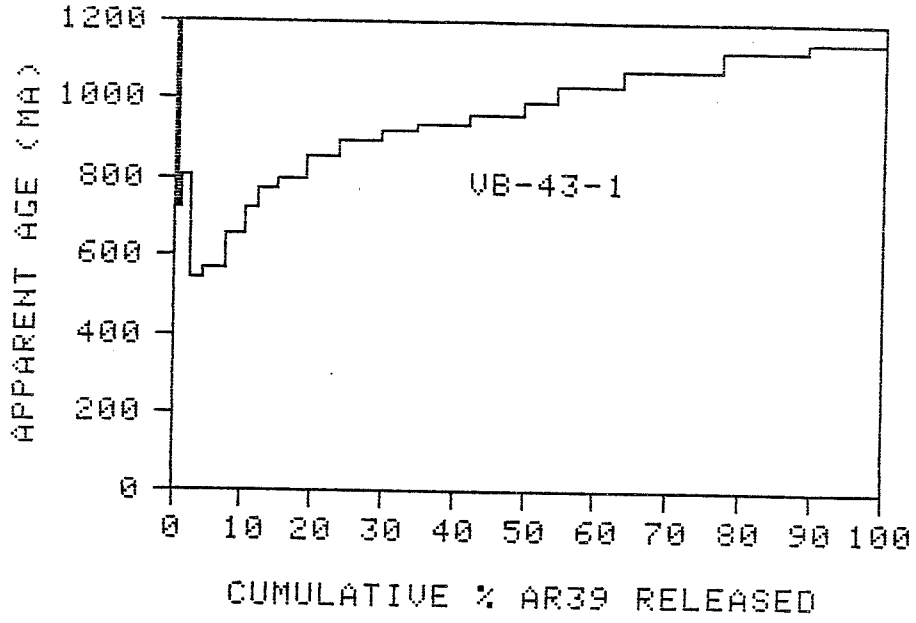

Figure 3.12. K-feldspar argon spectrum for VB-43-1 (Missisauga Fm.), obtained at a depth of 4430 m (B.R.T.) in the Venture B-43 well.

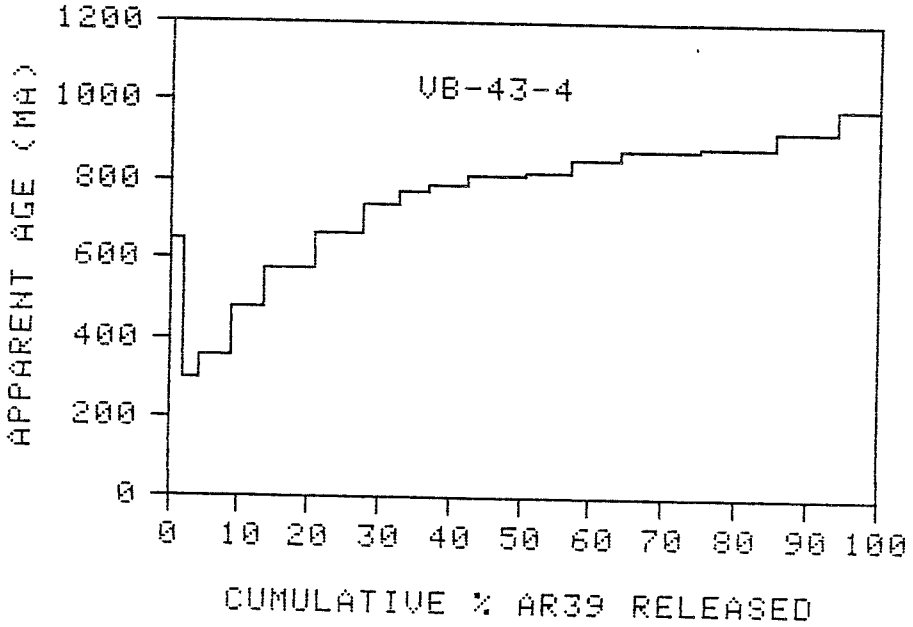

Figure 3.13. K-feldspar argon spectrum for VB-43-4 (Missisauga Fm.), obtained at a depth of 4673 m (B.R.T.) in the Venture B-43 well.

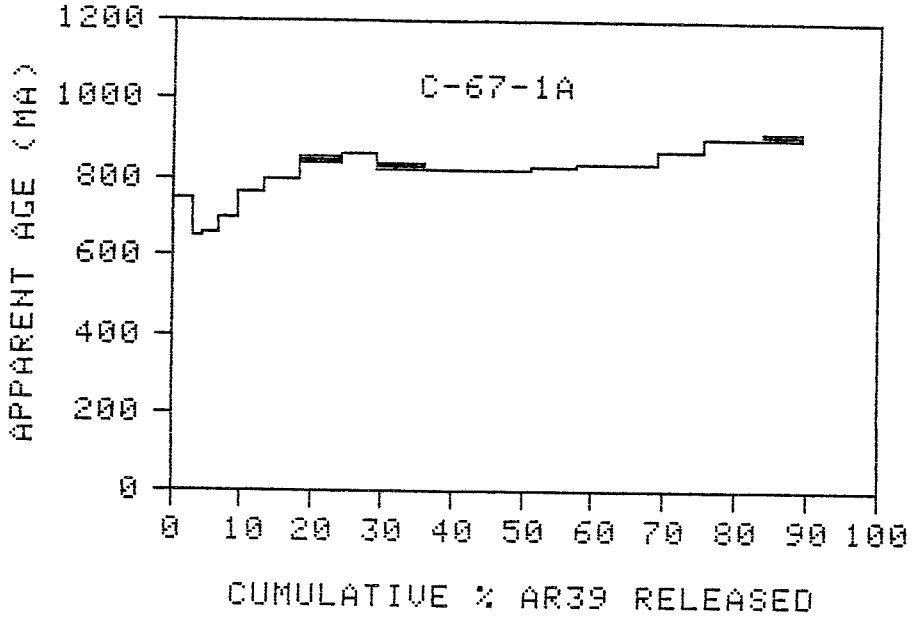

Figure 3.14. K-feldspar argon spectrum for C-67-1A (Logan Canyon Fm.), obtained at a depth of 2471 - 2481 m (B.R.T.) in the Sable Island C-67 well.

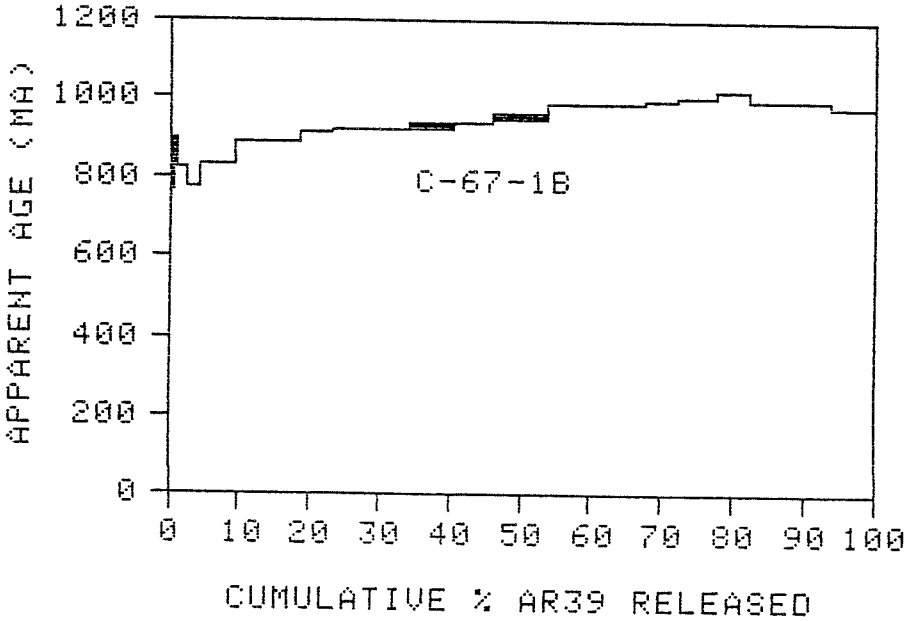

Figure 3.15. K-feldspar argon spectrum for C-67-1B (Logan Canyon Fm.), obtained at a depth of 2471 - 2481 m (B.R.T.) in the Sable Island C-67 well.

The C-67-1A spectrum (Figure 3.14) is from a K-feldspar sample that was obtained from the Logan Canyon Formation, at a depth of 2471-2481 m (B.R.T) in the Sable Island C-67 well. This spectrum contains several step age gradients. The initial heating step (representing 4 percent of the total ^{39}Ar) produced an age of 750 Ma. The second through seventh steps (representing 20 percent of the total ^{39}Ar) produced a steep gradient of step ages that increase from 640 Ma to 850 Ma. The eighth and ninth steps (representing 10 percent of the total ^{39}Ar) produced a slight negative gradient, with ages that decrease to 810 Ma. The final six steps (representing 56 percent of the total ^{39}Ar) produced a slight gradient of step ages that increase from 810 Ma to 900 Ma. Because the heating of the C-67-1A sample was also done in a quartz tube furnace, the spectrum of the sample is shown as having released an estimated 90 percent of its total argon. The mean age of the released gas is 829 Ma.

The C-67-1B spectrum (Figure 3.15) is from a K-feldspar sample that was also obtained from the Logan Canyon Formation, at a depth of 2471-2481 m (B.R.T) in the Sable Island C-67 well. This sample was a subsample of C-67-1A, that consisted of a selection of clear to pale blue, euhedral, perthitic grains. The initial three heating steps of this sample (representing 4 percent of the total ^{39}Ar) produced a negative gradient of ages that decrease from 850 Ma to 780 Ma. The fourth through fifteenth steps (representing 80 percent of the total ^{39}Ar) produced a gradient of step ages that increase from 850 Ma to 1010 Ma.

The final two steps (representing 16 percent of the total ^{39}Ar) produced a negative gradient, with ages that decrease to 990 Ma. The mean age of the released gas is 944 Ma.

The D-26-1 spectrum (Figure 3.16) is from a highly-altered K-feldspar sample that was obtained from the Mic Mac Formation, at a depth of 1955-1959 m (B.R.T.) in the Erie D-26 well. The initial heating step of this sample (representing 4 percent of the total ^{39}Ar) produced an age of 400 Ma. The second through twelfth steps (representing 70 percent of the total ^{39}Ar) produced a gradient of step ages that increase from 340 Ma to 680 Ma. The gradient is steeper at high extraction temperatures. The final three heating steps (representing 26 percent of the total ^{39}Ar) produced a negative gradient of step ages that decrease from 700 Ma to 640 Ma. The mean age of the released gas is 535 Ma.

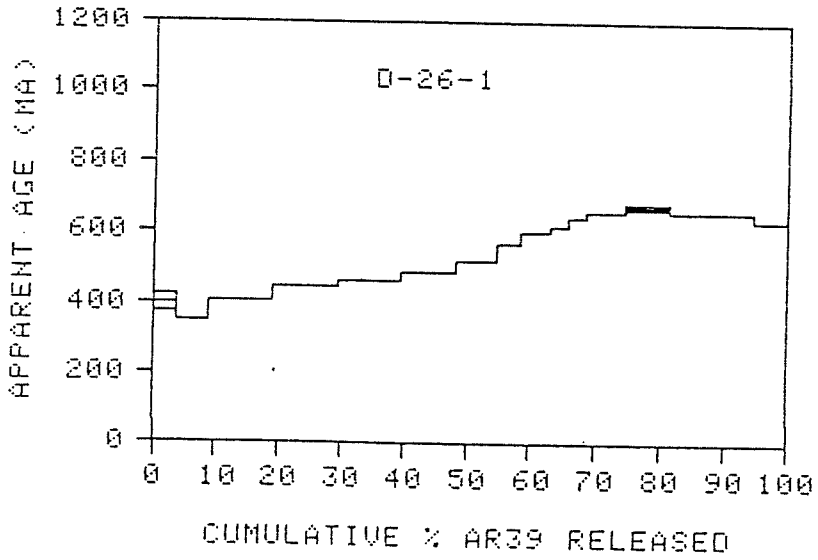

Figure 3.16. K-feldspar argon spectrum for D-26-1 (Mic Mac Fm.), obtained at a depth of 1955 - 1959 m (B.R.T.) in the Erie D-26 well.

The H-86P spectrum (Figure 3.17) is from a K-feldspar sample that was obtained from the Mohican Formation, at a depth of 4720 m (B.R.T.) in the Mic Mac H-86 well. The initial three heating steps of this sample (representing 40 percent of the total ^{39}Ar) produced a gradient of ages that increase from 130 Ma to 290 Ma. The final twelve heating steps (representing 60 percent of the total ^{39}Ar) produced a plateau at an age of 280 Ma. Approximately 30 percent of the total ^{39}Ar was released by the initial heating step, indicating that the gas was situated in low-activation energy sites. The mean age of the released gas is 242 Ma.

The H-86I spectrum (Figure 3.18) is from a K-feldspar sample that was obtained from the Mohican Formation, at a depth of 4715 - 4725 m (B.R.T.) in the Mic Mac H-86 well. The initial four heating steps of this sample (representing 42 percent of the total ^{39}Ar) produced a gradient of step ages that increase from 65 Ma to 280 Ma. The final eight heating steps (representing 48 percent of the total ^{39}Ar) produced a negative gradient of step ages that decrease from 280 Ma to 235 Ma. Over 40 percent of the total ^{39}Ar was released by the initial four heating steps, indicating that the gas was situated in low-activation energy sites. Because the heating of the H-86I sample was done using a quartz tube furnace, the spectrum shows the sample as having released an estimated 90 percent of its total argon. The mean age of the released gas is 221 Ma.

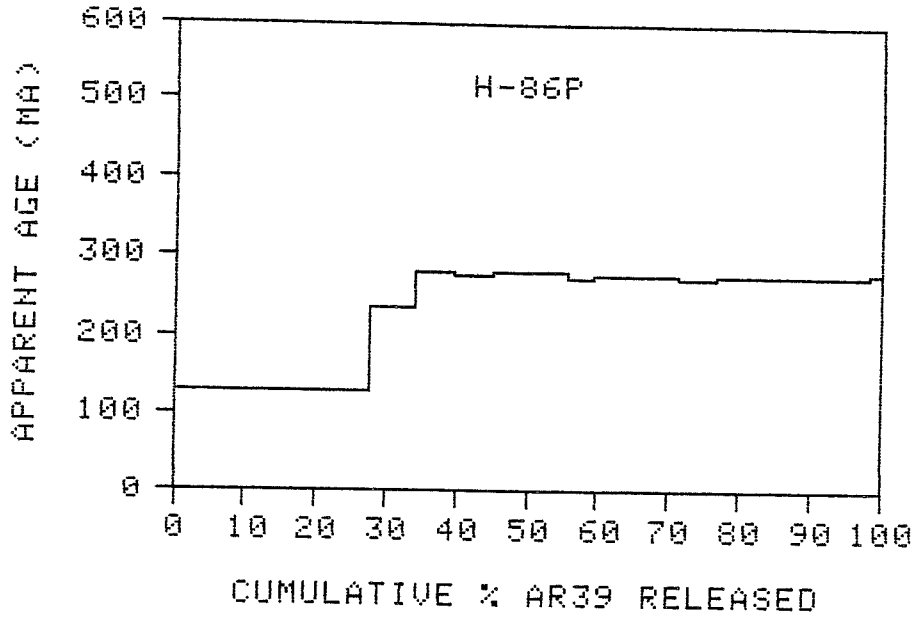

Figure 3.17. K-feldspar argon spectrum for H-86P (Mohican Fm.), obtained at a depth of 4720 m (B.R.T.) in the Mic Mac H-86 well.

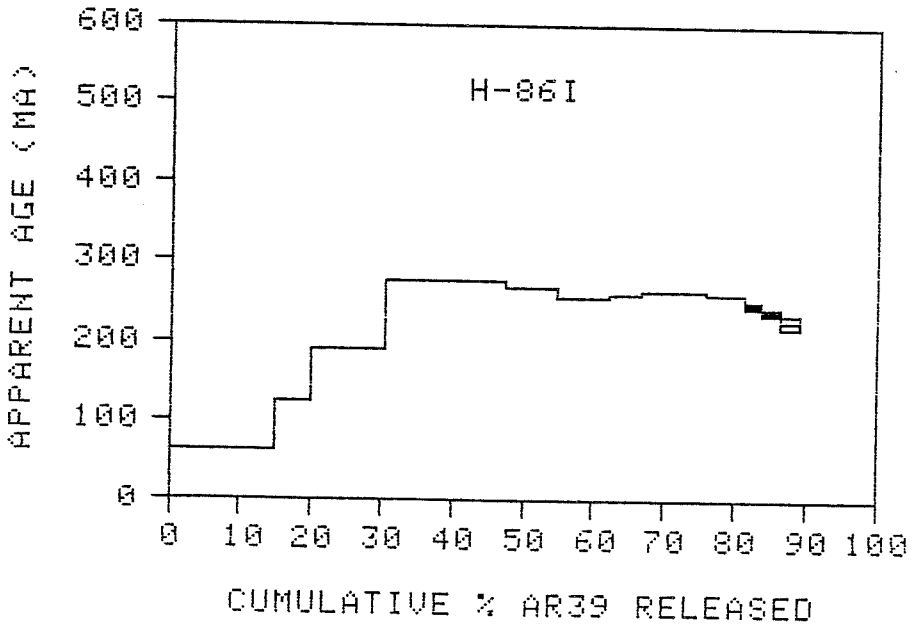

Figure 3.18. K-feldspar argon spectrum for H-86I (Mohican Fm.), obtained at a depth of 4715 - 4725 m (B.R.T.) in the Mic Mac H-86 well. Sample extraction heating was done using a Lindberg furnace.

3.2 Interpretation of argon data

3.2.1 Micas

The biotite argon spectrum from the Mic Mac H-86 sample (Figure 3.1) appears to be partially outgassed. Although the estimated interval temperature (approximately 138°C) is too low to cause thermal diffusive loss of radiogenic argon ($^{40}Ar^{*}$) from biotite, the staircase-shape pattern of gas release is atypical of an undisturbed biotite spectrum (Harrison et al., 1985). Similar staircase-shape patterns were obtained by Ozima et al. (1979) for biotite that was heated in air, and subsequently irradiated and analyzed by the $^{40}Ar/^{39}Ar$ technique. The H-86 sample grains were quite altered, and had opaque patches and rims, and were probably chemically unstable in the basin. This instablity may have caused a partial outgassing of radiogenic argon and a reduction in the argon age. Therefore, the total gas age of 195 Ma cannot be considered to have geologic significance.

The step age gradient in the muscovite sample from the Mic Mac H-86 well (Figure 3.2) is thought to have resulted from the outgassing of authigenic sericite, which is ubiquitous in thin-section. The sericite would totally outgas at low extraction temperatures because of its fine grain size, resulting in a reduction of the step ages over the initial 30 percent of ^{39}Ar release. The sericite also reduces the total gas age slightly, and because of this the plateau at 360 Ma probably represents a better estimate of the age of the source of the detrital grains than does the total gas age. The age gradients over the initial 2 to 6

percent of ^{39}Ar release in the muscovite spectra from the Mic Mac J-77, and Venture B-13 wells (Figures 3.3 - 3.5) are also thought to be a result of the outgassing of authigenic sericite.

The significance of the negative age gradients in the muscovite spectrum from the Mic Mac J-77 sample (Figure 3.3) is unclear. They may indicate a degree of mixing of source rocks that have different thermal histories or a single, thermally disturbed source. The muscovite spectra obtained from the Venture B-13 well (Figures 3.4 and 3.5) are reasonably flat and do not appear to be significantly affected by present-day burial heating. The differences between the total gas ages of the muscovite samples from Venture B-13 and Mic Mac J-77 wells can likely be attributed to variations in the age and thermal history of the source rocks.

3.2.2 K-feldspars

The initial heating steps of most of the K-feldspar argon spectra (Figures 3.6 - 3.18) appear to be affected by recoil ^{39}Ar loss (as explained in Section 1.4), resulting in an elevated step age (with respect to the second step age). This effect is not visible in the spectra from the Mohican Formation (Figures 3.17 and 3.18) but this is probably because of the large size of the initial gas fractions released during extraction heating.

The shape of the C-67-2 spectrum (Figure 3.6) is typical of that produced by simple slow-cooling (Harrison and McDougall, 1982; Hanes et al., 1988); over 90 percent of the ^{39}Ar produced ages between 800

and 900 Ma. The small amount of ^{39}Ar that produced ages between 700 and 800 Ma may be a result of slight thermal overprinting, or of a limited amount of mixing with a younger-age K-feldspar. The shape of the K-90-2 spectrum (Figure 3.7) is similar to that of the C-67-2 spectrum (Figure 3.6), except for the steep gradient of ages from the fourth to the seventh steps (representing 30 percent of the total ^{39}Ar). The range in ages of these steps (approximately 360 Ma) is too large to be a result of simple slow-cooling, without invoking unreasonably slow cooling rates. More reasonably this may be interpreted as having resulted from an episode of partial thermal resetting. The age of the event (as indicated by the initial ^{39}Ar released) is approximately 500 Ma.

The step age gradients in the J-77I and J-77P spectra (Figures 3.8 and 3.9) occur over a larger fraction of ^{39}Ar release, and span a greater range of ages (approximately 400 Ma) than does the gradient in the K-90-2 spectrum (Figure 3.7). The gradients in J-77I and J-77P spectra are also too steep to be a result of simple slow-cooling (without invoking unreasonably slow cooling rates), and should also be interpreted as having resulted from a combination of slow-cooling followed by an episode of partial resetting. Obviously, the same argument may be made for the K-feldspar spectra from the Venture B-13, and Venture B-43 wells (Figures 3.10 - 3.13), in which the range in the step ages is 600 Ma to 700 Ma. The steep gradients and lack of plateaus suggest a substantial ougassing event (Harrison, 1983).

The shapes of the C-67-1A, and C-67-1B spectra (Figures 3.14 and 3.15) are very similar to that of the C-67-2 spectrum (Figure 3.6), and may also be interpreted to result from simple slow-cooling. The D-26-1 spectrum (Figure 3.16) appears to have been thermally overprinted. This interpretation is consistent with the highly altered state of this feldspar. Also, in this case, the substantial range in the step ages makes slow-cooling an unlikely interpretation.

The two spectra from the Mohican Formation (Figures 3.17 and 3.18) are the only ones that contain step ages that are younger than the stratigraphic age of the formation from which they were obtained. This observation may be interpreted as definite evidence of a partial resetting associated with present day burial heating. The presence of plateaus in these spectra is interpreted to mean that the source rocks of the detrital grains cooled quite rapidly through the range of temperatures associated with argon closure in K-feldspars.

3.3 Discussion of provenance

The argon spectra presented in the previous sections provide information about the thermal histories experienced by the samples. The thermal histories consist of two phases. The first is the pre-depositional (or pre-Scotian Basin), or provenance phase. Considerable variation in provenance may exist between adjacent mineral grains in a sample, as well as between adjacent formations in the basin. The second part of the thermal history is the post-depositional phase. All of the samples have had similar

post-depositional thermal histories, that consist simply of a gradual heating by burial subsidence and/or heating by convecting fluids. The effect of this second phase is to cause a reduction in the amount of radiogenic argon in the samples. In the argon spectra, burial heating results in the overprinting of pre-existing (provenance related) gradients by gradients related to the partial outgassing of radiogenic argon. Estimates of gas loss related to thermal maturity are discussed in the next section. The remainder of this section is devoted to a discussion of the provenance of the detrital grains, as revealed by the argon spectra.

Although the argon spectra do provide information about the thermal history of the source rocks of the formations sampled, they do not give any information about where these sources were located. Neither do they provide information about whether or not the grains have been reworked or recycled prior to deposition in the Scotian Basin. In this thesis, the regions that are invoked as the sources of the detrital grains are those that have thermal histories that are consistent with the argon spectra, and that are also consistent with the inferred directions of sediment transport (based on facies distributions) as discussed in Section 1.2. Although the provenance of the grains may actually be quite complex, and involve distant and/or reworked sources, these possibilities will not be considered.

There are certain similarities in all of the K-feldspar spectra from the Missisauga Formation. The simplest of these, the C-67-2 spectrum (based on the interpretation that it resulted from simple slow-cooling)

is similar in shape and age to spectra from the Grenville Province in the Canadian Shield. Figure 3.19 is a map of the Grenville Province which shows the locations of two rock bodies for which K-feldspar argon spectra have been determined. Four spectra from the Elzevir Batholith (located in the Central Metasedimentary Belt, S.W. Grenville Province), reported by Hanes et al., (1988) are shown in Figures 3.20 and 3.21. Figures 3.22 and 3.23 show four K-feldspar argon spectra from the Britt Domain in the Central Gneiss Belt, S.W Grenville Province (Check, 1989). The Grenvillian Orogeny has been assigned an age of approximately 1000 to 1200 Ma (Moore, 1986). The K-feldspar spectra shown in Figures 3.20 - 3.23 give slightly younger ages (possibly because of protracted cooling?). All of the K-feldspar spectra from the Missisauga Formation obtained in this study are consistent with a Grenvillian-age source.

The observation that the mica argon ages from Missisauga Formation samples (Figures 3.3 - 3.5) are different from the corresponding K-feldspar argon ages indicates that the micas and feldspars must have had different pre-basin thermal histories. The total gas ages of the mica from the Mic Mac J-77 well indicates a thermal history dominated by a 500 Ma event. The thermal history of the micas from the Venture B-13 well appear to have been dominated by the Acadian Orogeny. These micas also have similar argon ages to that of the muscovite from the Mic Mac H-86 well, which may indicate a similar provenance.

Consideration must also be given to the possibility that the K-feldspar grains in each of the Missisauga Formation samples are not derived from a single population, but are instead mixtures, and that each argon spectrum represents an average of two (or more) sources which have had quite different thermal histories. (eg. A mixture of 500 Ma and 1500 Ma grains could result in an argon age of 1000 Ma.) Although it is almost certain that the samples are mixtures, it is unlikely that they contain significant proportions of very-old and very-young grains, but instead are mixtures that contain only Grenvillian-aged feldspars. There are two observations which support this assertion. Firstly, the spectra are all very similar, both in age and in the pattern of gas release. If the samples from widely separated parts of the basin did not have a uniform thermal history, then the spectra would not be similar, and the step ages of the spectra would be more erratic, and not increase in such a uniform manner. Secondly, the location of the proposed older sources is much more distant. Rocks which preserve a record of pre-Grenville orogenic events are located in the Grenville Front Tectonic Zone, in the northwestern part of the Grenville Province.

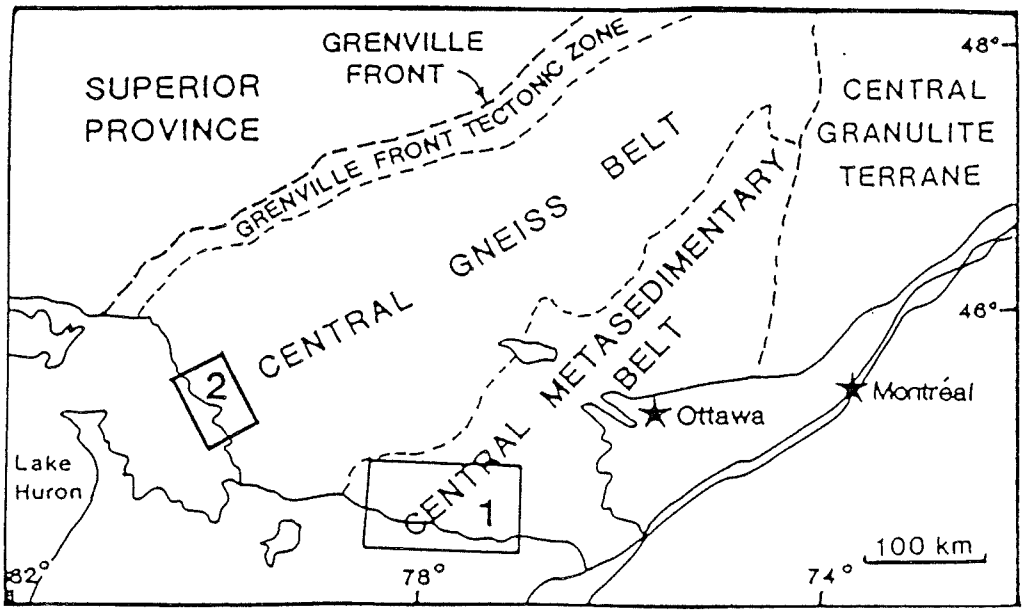

Figure 3.19. Map showing the locations of samples whose spectra are shown in Figures 3.20 - 3.23 (1 = Hanes et al., 1988; 2 = Check, 1989; modified from Hanes et al. (1988)).

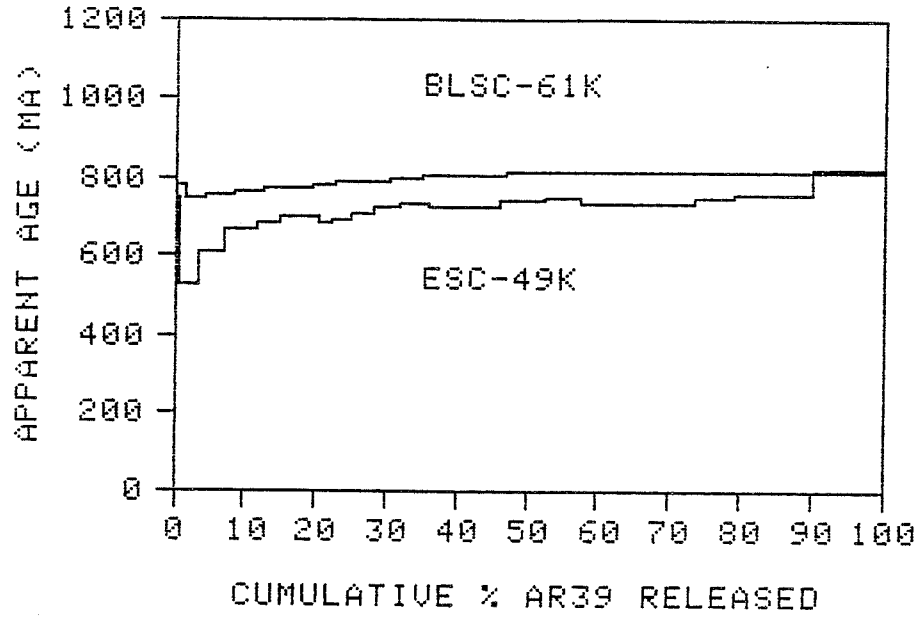

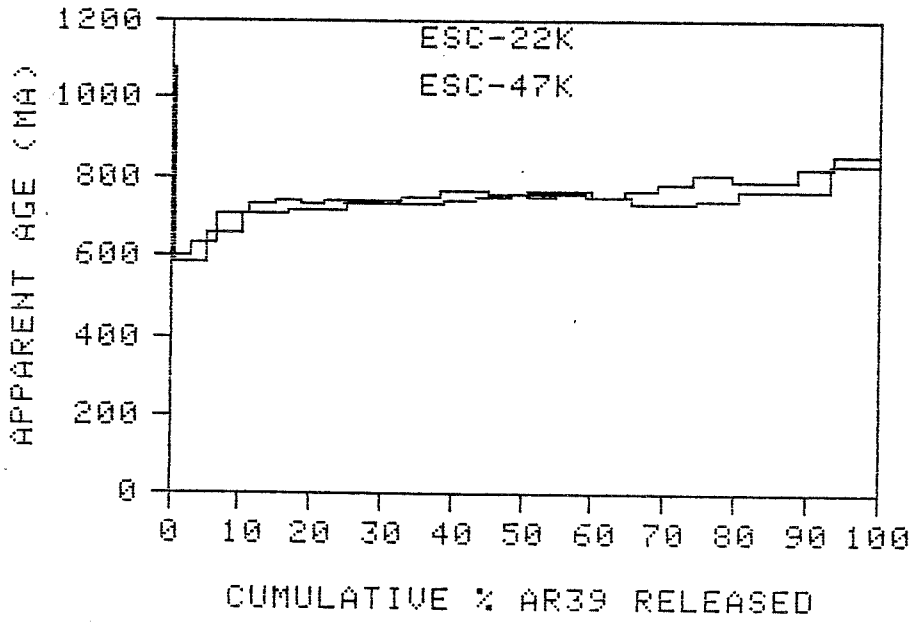

Figures 3.20 and 3.21. Four K-feldspar argon spectra from the Elzevir Batholith, Central Metasedimentary Belt, S.W. Grenville Province, (modified from Hanes et al. (1988)). The BLSC-61K spectrum gives a total gas age of 804 Ma. The ESC-49K spectrum gives a total gas age of 724 Ma. The ESC-47K spectrum gives a total gas age of 754 Ma. The ESC-22K spectrum gives a total gas age of 739 Ma.

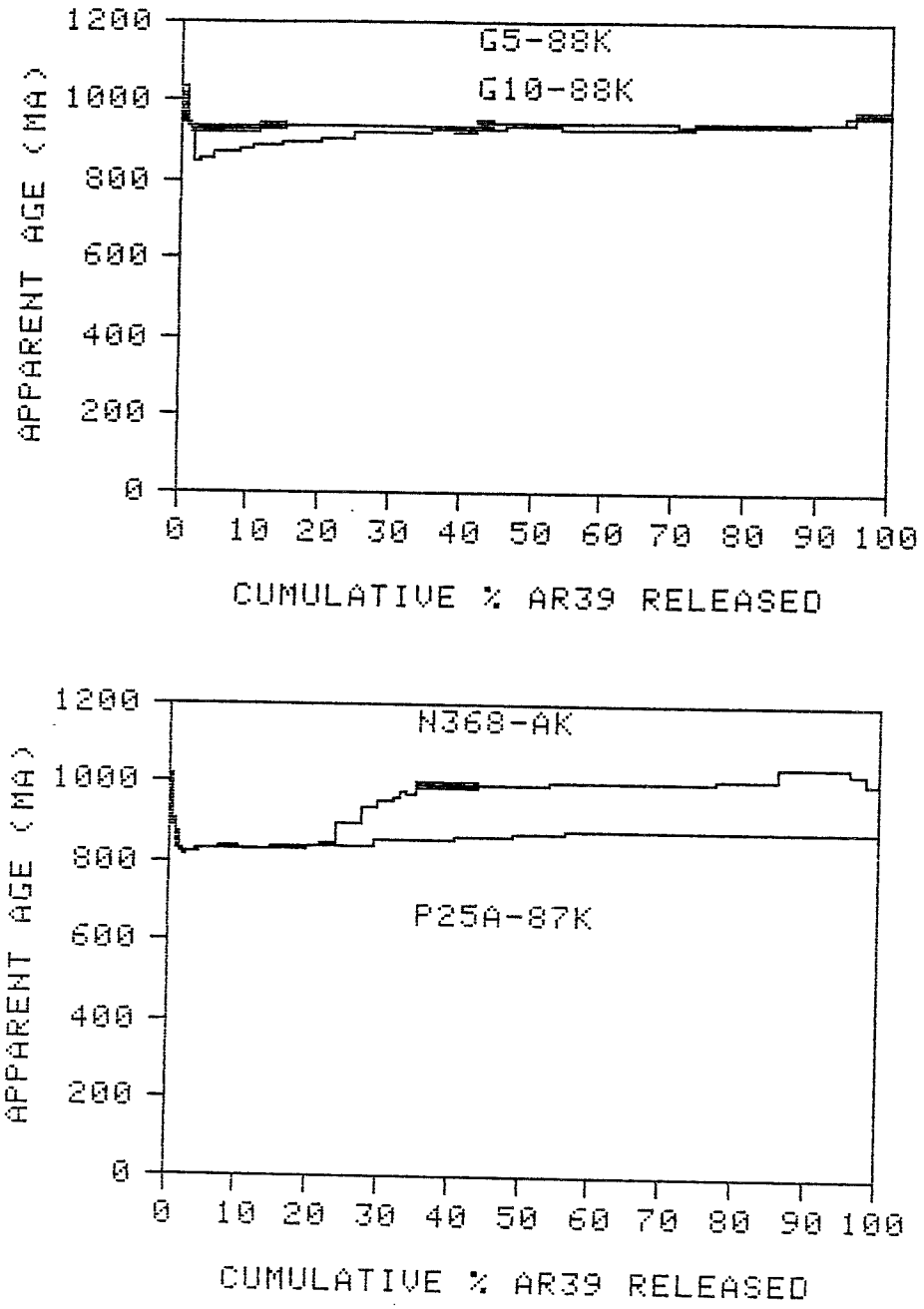

Figure 3.22 and 3.23. Four K-feldspar argon spectra from the Britt Domain, Central Gneiss Belt, S.W. Grenville Province, (modified from Check (1989)). The G5-88K spectrum gives a total gas age of 936 Ma. The G10-88K spectrum gives a total gas age of 925 Ma. The N368-AK spectrum gives a total gas age of 970 Ma. The P25A-87K spectrum gives a total gas age of 862 Ma.

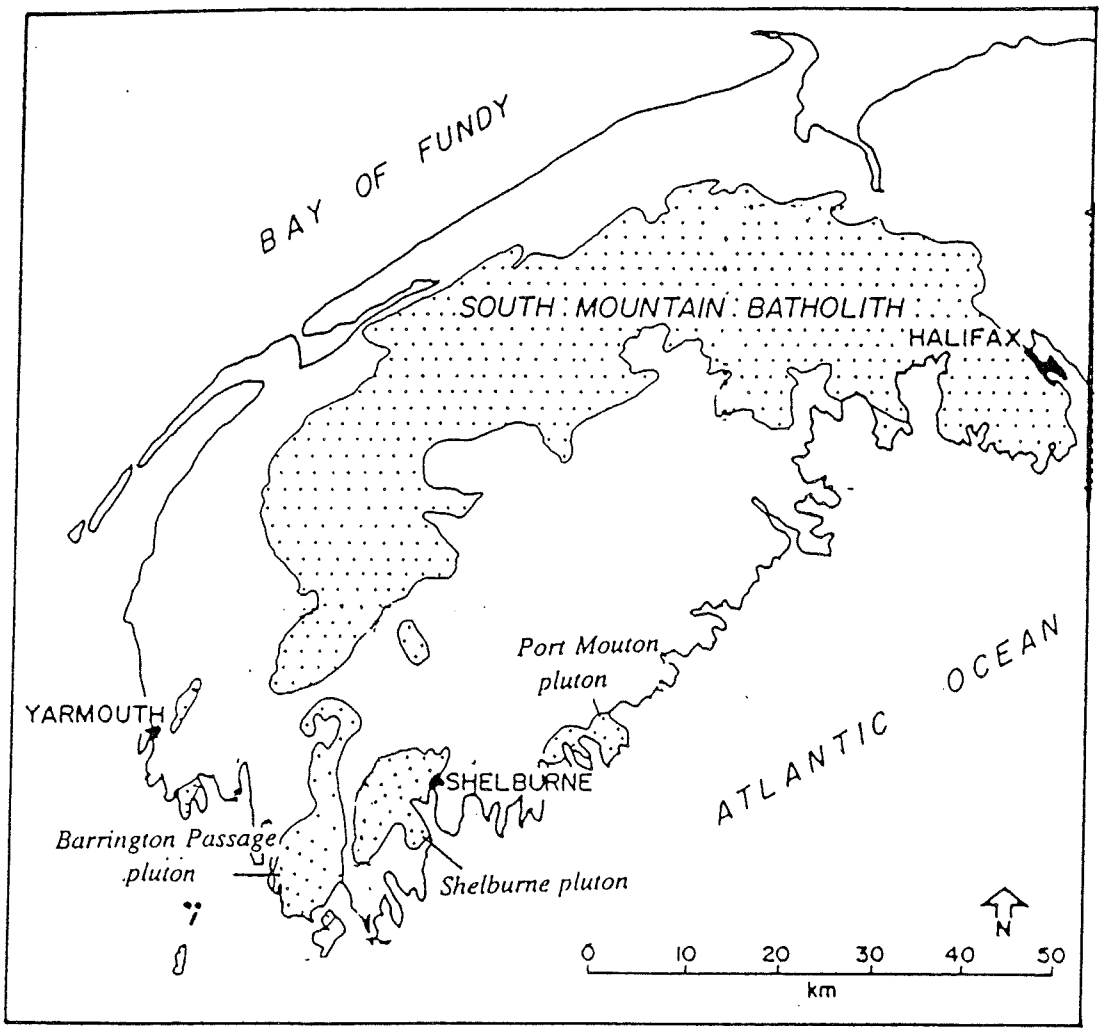

Figure 3.24. Map showing the locations of sampled formations on the Nova Scotian mainland (modified from Reynolds et al. (1987)).

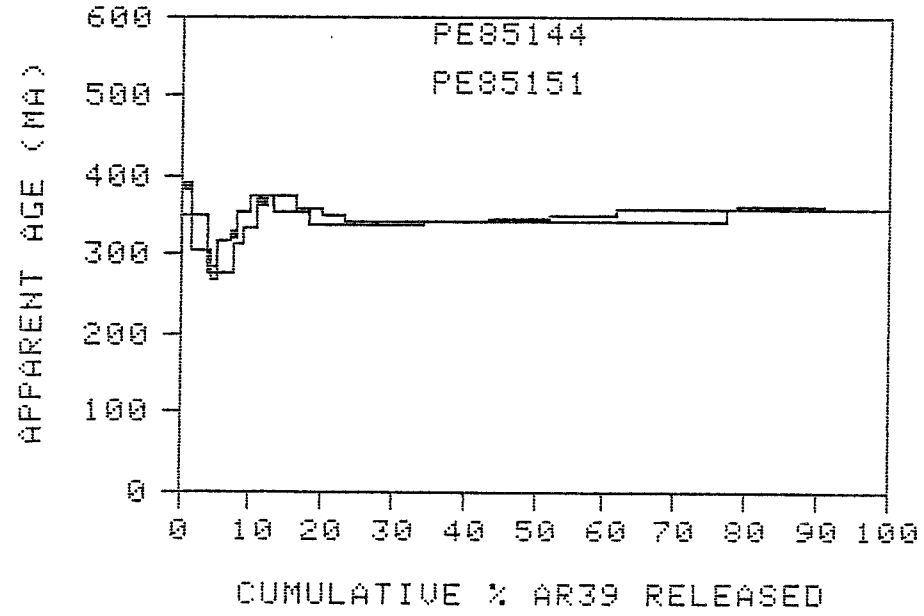

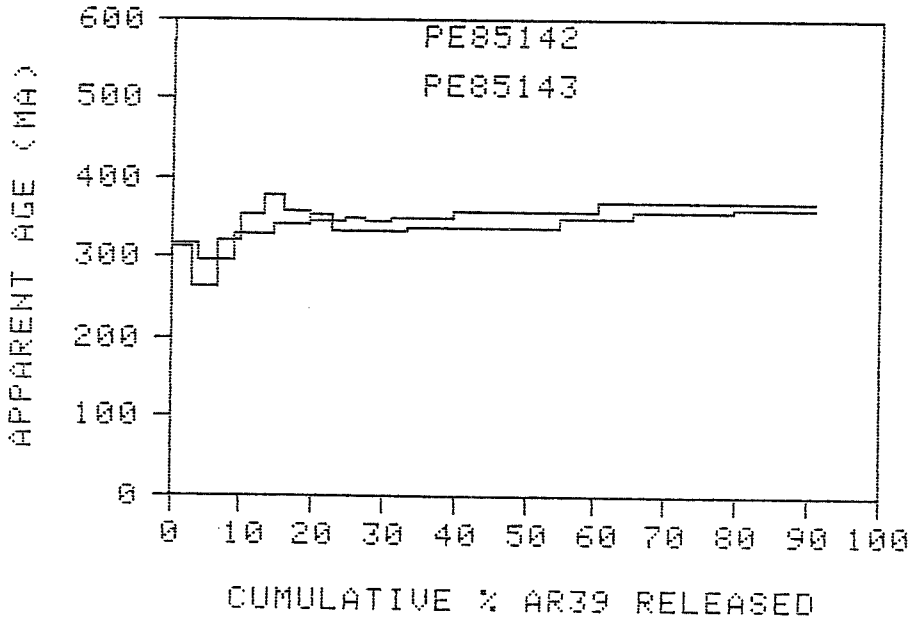

Figures 3.25 and 3.26. Four K-feldspar argon spectra from the South Mountain Batholith, Nova Scotia, (modified from Reynolds et al. (1987)). The location of the South Mountain Batholith is shown in Figure 3.24.

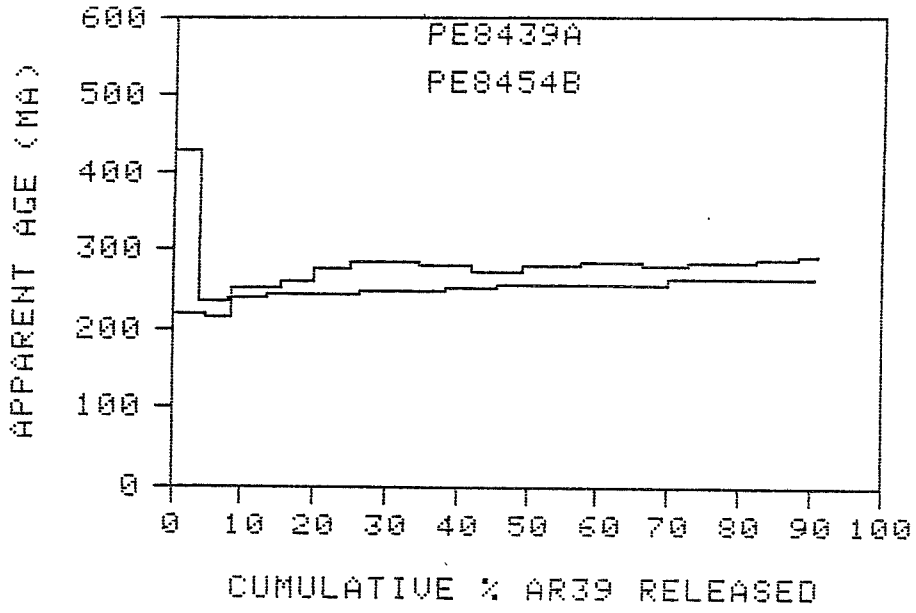

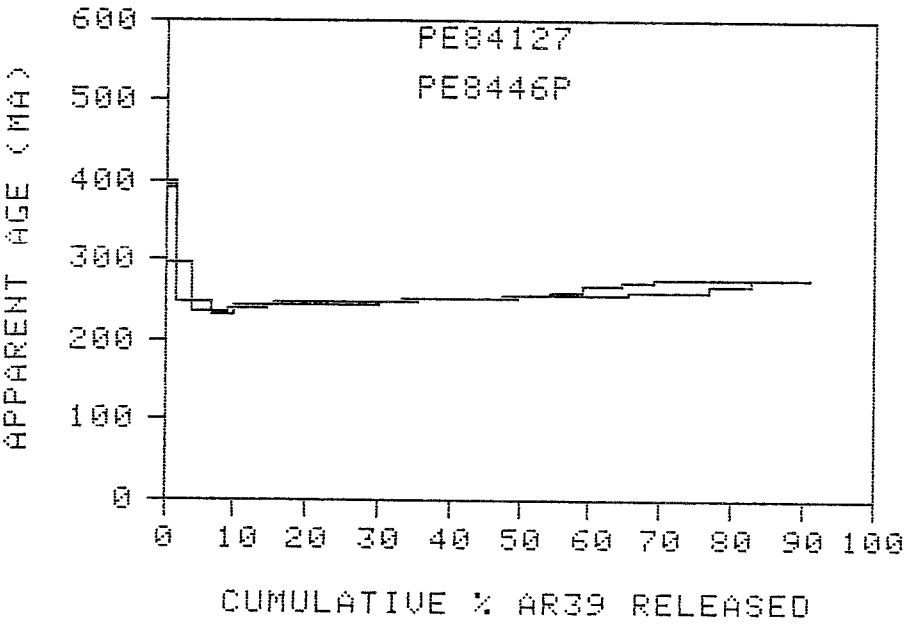

Figures 3.27 and 3.28. Four K-feldspar argon spectra from southern satellite plutons, Nova Scotia, (modified from Reynolds et al. (1987)). The locations of the plutons is shown in Figure 3.24.

According to Jansa and Wade (1975), Given (1977), and others, the Mohican Formation sediments originated from the northwest, in the direction of the LaHave Platform, and mainland Nova Scotia. The Mohican Formation K-feldspar and mica argon spectra (Figures 3.17, 3.18, 3.1, and 3.2) are similar to K-feldspar and mica argon spectra from igneous intrusions located on the Nova Scotian mainland. Figure 3.24 is a map of southwestern Nova Scotia, that shows the locations of several igneous rock bodies for which K-feldspar argon spectra have been determined. Figures 3.25 and 3.26 are four spectra from the South Mountain Batholith, reported by Reynolds et al. (1987). Figures 3.27 and 3.28 show four spectra from three intrusions in southwestern Nova Scotia (two from the Shelburne Pluton, one each from the Port Mouton and Barrington Passage Plutons), also from Reynolds et al. (1987). The latter four spectra are quite similar to the K-feldspar spectra in Figures 3.17 and 3.18.

Although all of the above named intrusions are probably located too far to the southwest to have been the actual sources for the Mohican Formation sediments in the Mic Mac H-86 well, the spectra from these intrusions, especially Figures 3.27 and 3.28, may represent the appearance of the Mohican Formation spectra without any superimposed loss of radiogenic argon that has resulted from present-day burial heating (that is, undisturbed counterparts to the spectra in Figures 3.17 and 3.18). Given (1977) reported K-Ar radiometric ages of from 300 $\pm$ 19 Ma to 329 $\pm$ 14 Ma for samples from four wells that reached basement beneath the LaHave Platform. The depths at which these

basement samples were obtained are 2 - 3 km, and therefore it is unlikely that the present-day interval temperatures would be sufficient to cause any reduction in the K-Ar ages. The similarity of the $^{40}Ar/^{39}Ar$ ages of the samples from the Mic Mac H-86 well to $^{40}Ar/^{39}Ar$ ages from plutons in southwestern Nova Scotia, as well as to K-Ar ages of basement rocks from the LaHave Platform is consistent with the proposal that the Mohcan Formation feldspars and micas were derived from rocks from the Nova Scotian mainland, or from equivalent areas that are now submerged offshore.

The provenance of the samples from the Logan Canyon Formation (Figures 3.14 and 3.15) appears to be similar to that of the Missisauga Formation (based on the similarity of the respective spectra). The spectra from the Logan Canyon Formation may also demonstrate the effect caused by the mixing of altered and unaltered source rocks. The differences in the shapes of these spectra are interpreted to be a result of the larger proportion of altered grains in the C-67-1A sample. The spectrum of the latter is somewhat saddle-shaped, and appears to be more disturbed than does the C-67-1B spectrum. C-67-1B has a less steep age gradient and a greater total gas age, and is interpreted to be the result of simple slow-cooling of a Grenvillian-age source. The single argon spectrum from the Mic Mac Formation (Figure 3.16) is strongly overprinted, but at high extraction temperatures the step ages exceed 600 Ma. The spectrum may indicate an older source that has been strongly overprinted by an Acadian-age event.

3.4 Estimates of $^{40}Ar^*$ loss using K-feldspar argon spectra

According to Harrison and Burke (1988) a temperature of 110°C to 120°C over geologic periods of time is sufficient to cause a measurable diffusive loss of radiogenic argon ($^{40}Ar^*$) from K-feldspars. Using the corrected down-hole well temperatures and geothermal gradient map for the Scotian Basin calculated by Issler (1983), one can obtain the following interval temperatures: 126 $\pm$ 8°C for K-90-2; 137 $\pm$ 4°C for VB-13-1 and VB-13-2; 129 $\pm$ 4°C for VB-43-1; 136 $\pm$ 4°C for VB-43-4; and 138°C for H-86I and H-86P. It was expected therefore that the K-feldspar argon spectra of these (deep) samples would show measurable $^{40}Ar^*$ loss.

Because the initial step ages are younger than the stratigraphic age of the Mohican Formation, it is apparent from the Mic Mac H-86 argon spectra (Figures 3.1, 3.2, 3.17 and 3.18) that significant diffusive loss of $^{40}Ar^*$ has occurred. The other deep samples are all from the Missisauga Formation, and the step ages of the spectra from these samples all exceed the formation stratigraphic age. However, the step age gradients present in the spectra of the deep samples are quite steep, and were interpreted in the previous section as having resulted from a partial thermal resetting. It is likely that these samples have also experienced fractional argon loss as a result of recent burial heating; but that the timing of the loss has not been preserved in the spectra because of ^{39}Ar recoil loss (see Section 1.4).

If the K-feldspar argon spectra from mainland Nova Scotia represent undisturbed counterparts of the spectra from the Mohican Formation, then the fraction of radiogenic argon lost due to present-day burial heating is proportional to the difference in the areas under the respective age spectral curves. These areas can be estimated by counting squares. If the spectra from the South Mountain Batholith (Figure 3.25) are used as the basis of comparison, the estimated fractional loss is 33 percent. If the spectra from plutons in southwestern Nova Scotia, (Figure 3.26) are used the estimated fractional loss is 15 percent.

If one assumes that the spectra of samples from the Missisauga Formation from relatively shallow intervals where the interval temperature is less than the minimum required to initiate argon diffusion, such as for the Mic Mac J-77, ($T = 84 \pm 4^{o}C$) or Sable Island C-67-2 ($T = 97 \pm 4^{o}C$) samples, represent the undisturbed counterparts of the deeper (and potentially partially outgassed) samples, such as VB-13-1, VB-13-2, VB-43-1, and VB-43-4, then it is possible to estimate the fractional argon loss as above. If the C-67-2 (Figure 3.6) spectrum is used as the basis of comparison, the estimates of argon loss range from 5 to 12 percent. If the slightly older but more disturbed J-77P spectrum (Figure 3.9) is used, the estimates of argon loss range from 12 to 19 percent. A summary of the estimated argon losses from the deep Missisauga Formation samples is given in Table 3.3.

Table 3.3. Argon estimates from Missisauga Formation K-feldspars. The estimates are equal to 1 - (area under the age spectrum of the deep sample divided by the area under the age spectrum of the shallow sample). The deep samples are those in left column. The shallow samples are those in the top row. The VB-43 1 spectrum has the oldest total gas age, resulting in an apparent argon gain (which is probably not real, see below).

	C-67-2	J-77P
VB-13-1	-.12	-.19
VB-13-2	-.09	-.16
VB-43-1	+.12	+.04
VB-43-4	-.11	-.17

The reason why the VB-43-1 sample produced the greatest total gas age remains uncertain. It may simply be that this sample contained some relatively old grains. Another possible explanation is that the increased total gas age is a grain size effect. This particular sample contained the largest grains of any that were analyzed, as well as the greatest range of grain sizes. According to Zeitler (1987) the analysis of such samples results in spectra with diminished plateaus, and increased total gas ages. Figure 3.29 is a histogram of percent ^{39}Ar release versus extraction temperature for the VB-43-1, and VB-13-1 samples. From the figure it can be seen that the VB-43-1 sample did not outgas significantly at low extraction temperatures, and released only 7 percent of its argon below 600°C. By comparison, the

VB-13-1 sample has a more uniform grain size that is typical of most of the samples. In these samples substantial argon diffusion occurred over a wider range of extraction temperatures.

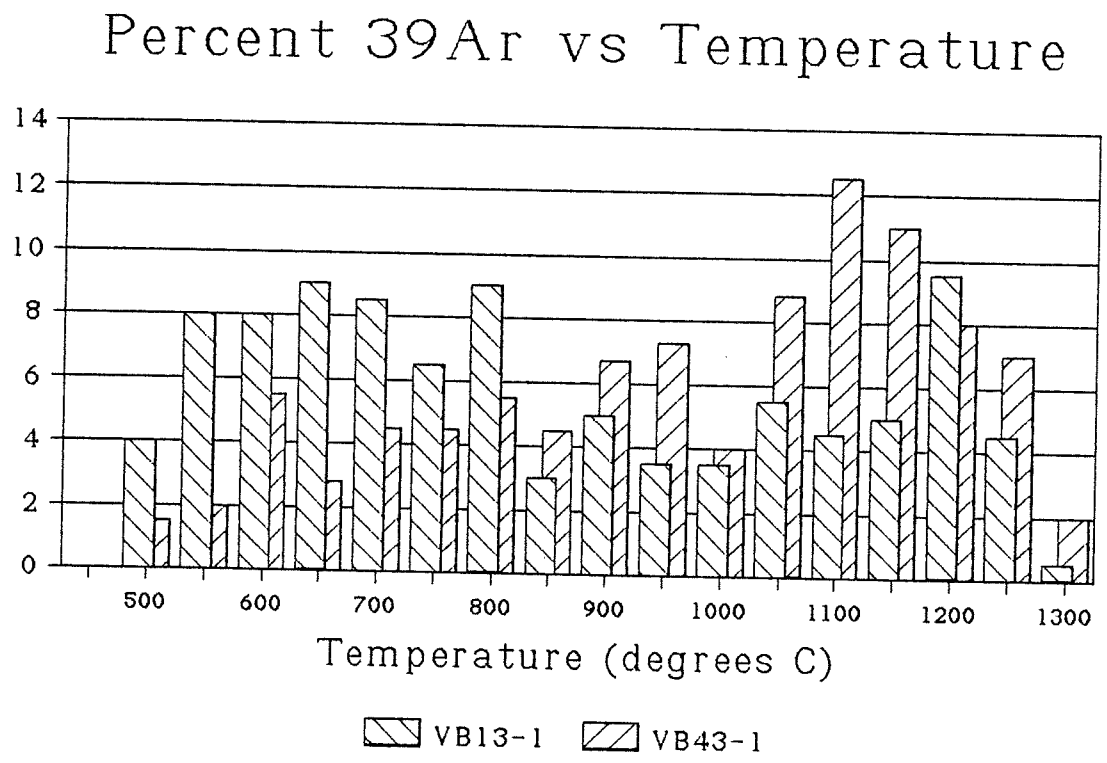

Figure 3.29. Histogram of percent ^{39}Ar released versus temperature for the Venture B-13-1 and B-43-1 samples (see text for description).

3.5 Estimates of $^{40}Ar^*$ loss using single-site diffusion models

Three of the K-feldspar argon analyses (C-67-1B, C-67-2, and VB-13-2) were conducted as controlled diffusion experiments. The laboratory heating of these samples was done in a quartz tube in the Lindberg furnace (for precise temperature control). In addition, 30 degree temperature steps and heating times of only 20 minutes/step were used. (The other analyses were carried out using 50 degree steps and heating times of 40 to 60 minutes/step.) The smaller temperature steps were used to increase the number of data points. The brief heating times were used because the samples were thought to contain a range of effective diffusion grain sizes (because they were detrital). As pointed out by Zeitler (1987), longer heating times tend to deplete the smaller diffusion domains, resulting in an increase in the effective diffusion radius with increasing temperature, thereby severely restricting the linear portions of the Arrhenius plot. By keeping the heating times as brief as possible, one minimizes this effect. The Berger and York method (see Section 1.3.2) has been applied to five of the sample analyses, the three above (C-67-1B, C-67-2, and VB-13-2), and two others (VB 43-1 and VB 43-4). The resulting Arrhenius diagrams are shown in Figures 3.30 to 3.34.

Even at extraction temperatures below 750°C, all of the data point arrays contain non-linear portions. This may result from the presence of a range of K-feldspar compositions, and/or effective diffusion radii, causing variation in D_o/a^2, E_a, or both. The latter in turn may be partly a result of the detrital (mixed) origin of the

samples. Weighted least-squares regression lines (see York, 1969) have been fitted to portions of the Arrhenius plots to determine values for E_a, and D_o/a^2. The calculated values are given in Table 3.4.

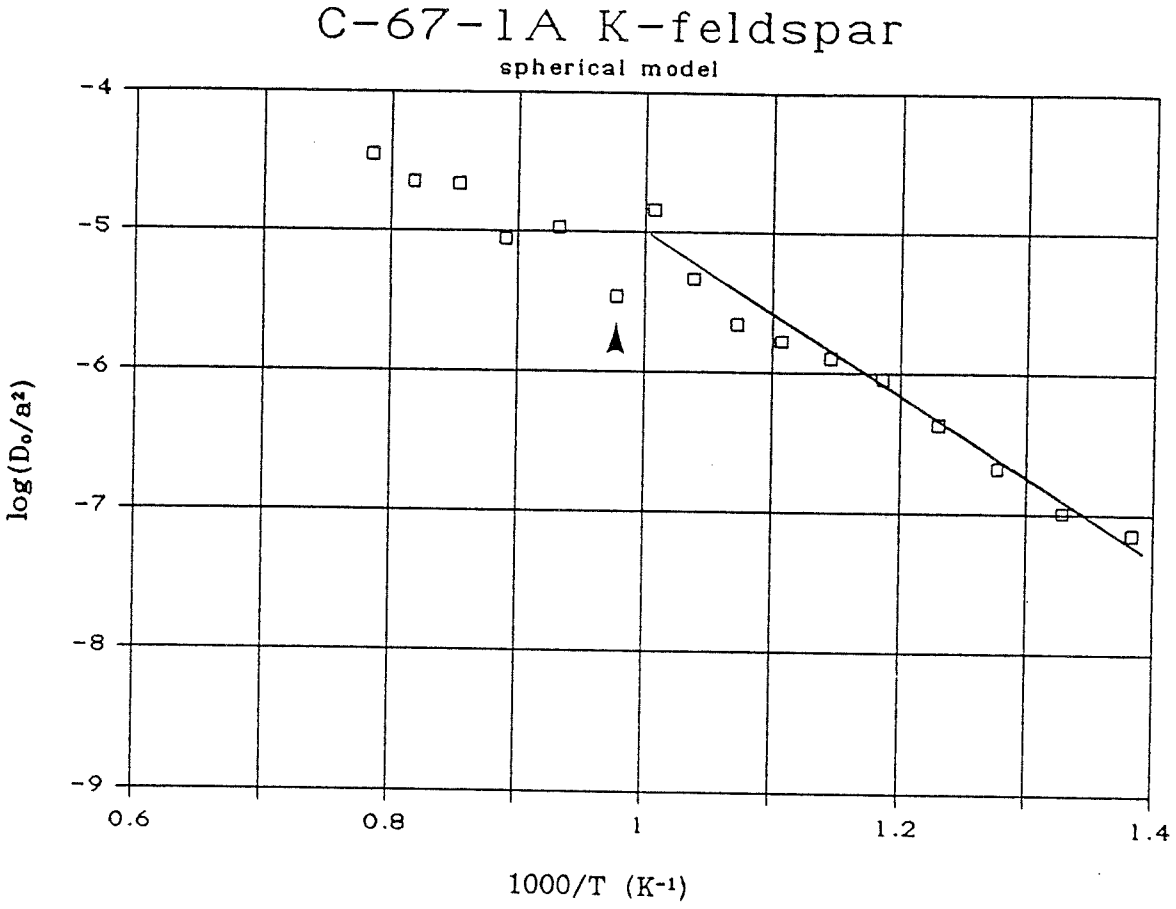

Figure 3.30. Arrhenius diagram for sample C-67-1A (spherical model). The arrow indicates a temperature of 750°C. The line segment indicates the points that were used to calculate the diffusion parameters in Table 3.4.

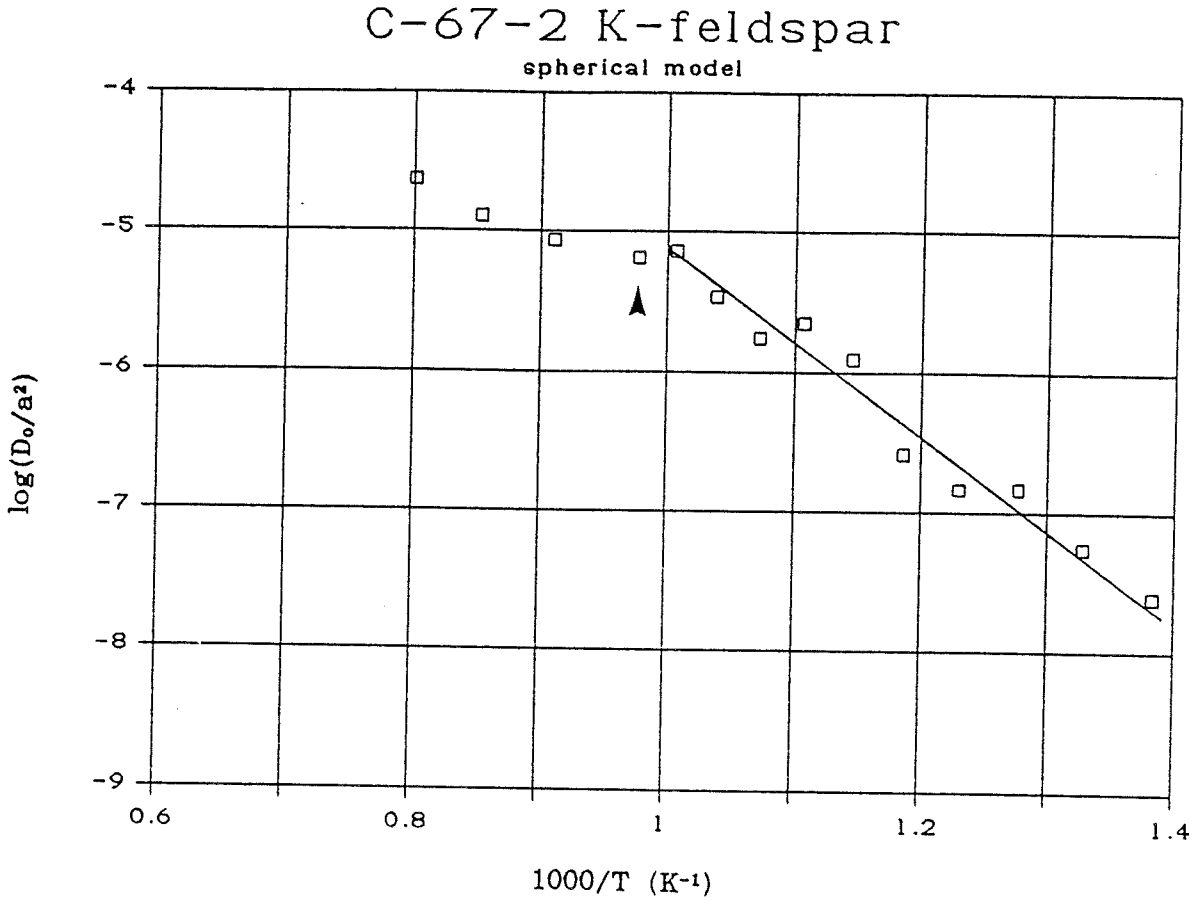

Figure 3.31. Arrhenius diagram for sample C-67-2 (spherical model). The arrow indicates a temperature of 750°C. The line segment indicates the points that were used to calculate the diffusion parameters in Table 3.4.

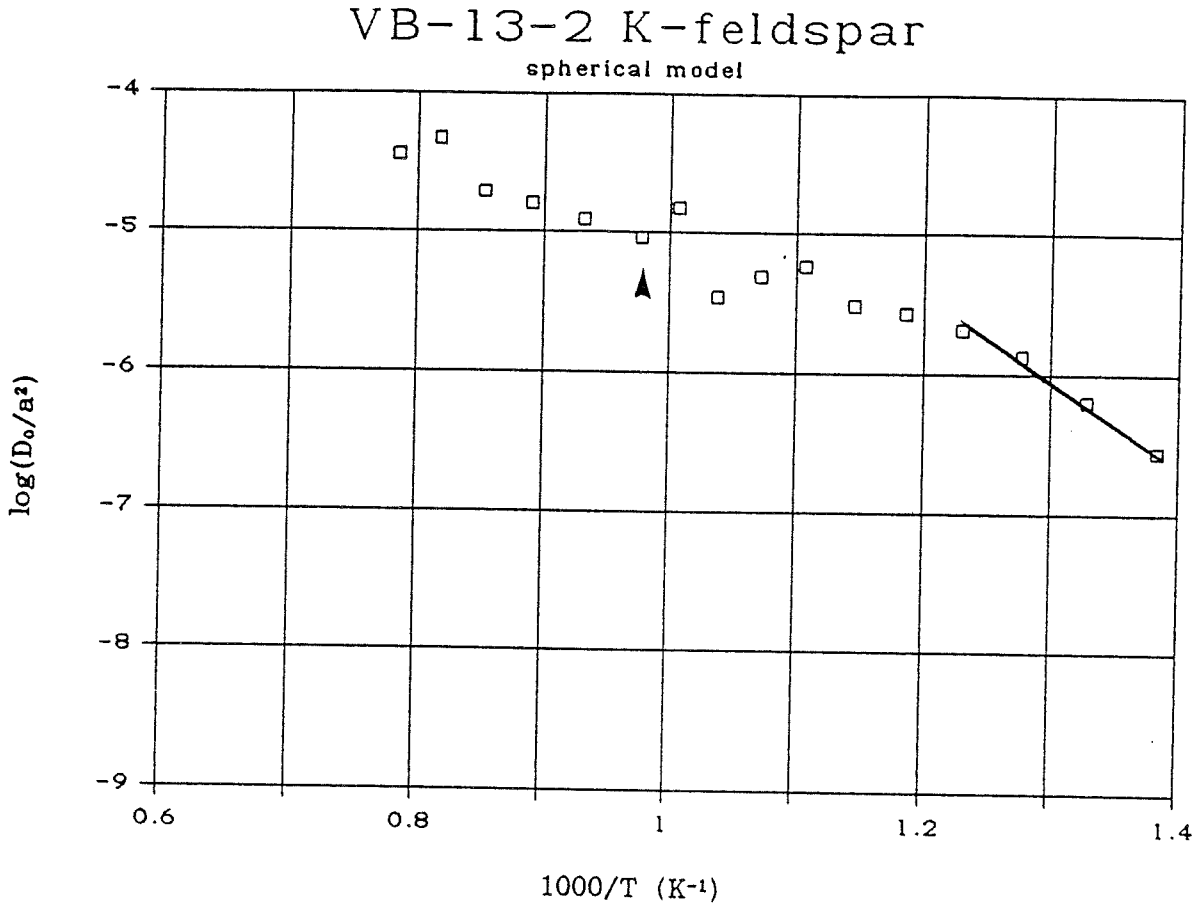

Figure 3.32. Arrhenius diagram for sample VB-13-2 (spherical model). The arrow indicates a temperature of 750°C. The line segment indicates the points that were used to calculate the diffusion parameters in Table 3.4.

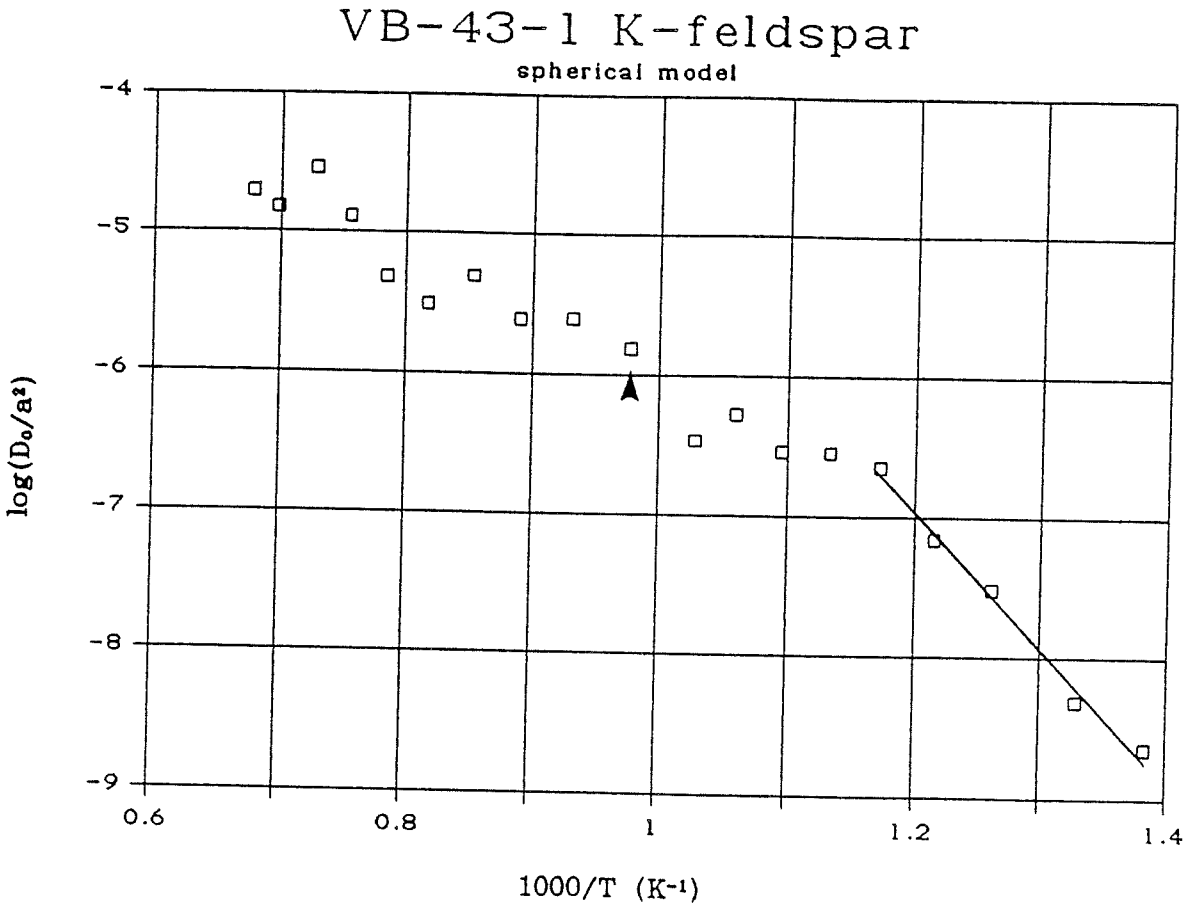

Figure 3.33. Arrhenius diagram for sample VB-43-1 (spherical model). The arrow indicates a temperature of 750°C. The line segment indicates the points that were used to calculate the diffusion parameters in Table 3.4.

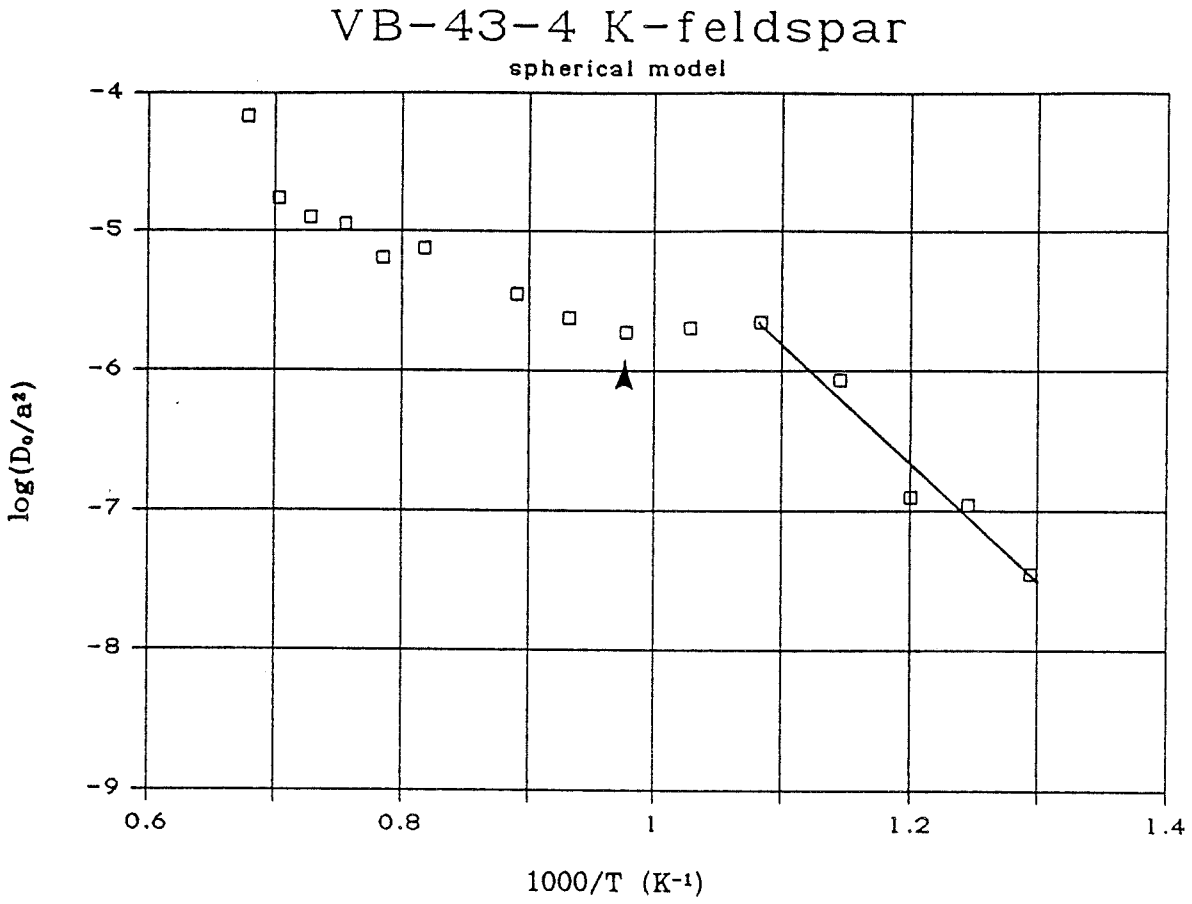

Figure 3.34. Arrhenius diagram for sample VB-43-4 (spherical model). The arrow indicates a temperature of 750°C. The line segment indicates the points that were used to calculate the diffusion parameters in Table 3.4.

Table 3.4. Calculated values of the diffusion parameters.

Sample	Points	E_a (kcal/mol)	D_0/a^2 (s^{-1})
C-67-1A	2 to 7	26 ± 2	5 (+8 -3)
C-67-2	1 to 3	34 ± 2	300 (± 300)
VB-13-2	1 to 4	27 ± 2	37 (+88 -26)
VB-43-1	1 to 5	45 ± 2	(60 (+210 -47)) x10^3
VB-43-4	1 to 4	43 ± 10	(3 (+1740 -3)) x10^4

Using the diffusion parameters in Table 3.4, one can calculate the expected fractional argon loss for each of the samples, provided that the effective temperature and heating time in the basin environment can be estimated. The burial subsidence curve for the Venture Gas Field (from Grant et al., 1986) is used here to make a first-order approximation of recent burial heating of the Venture samples. If a time of 40 Ma (9.167 x 10^{14} seconds), and a temperature of 129°C (402 K) are used, substitution into the Arrhenius equation (equation 7 in Section 1.3.2) gives for VB-43-1:

$$\frac{D}{a^2} = 60{,}000\left(\exp\left(\frac{45}{(1.987\times10^{-3})(402)}\right)\right)^{-1}$$

= 2.05 x 10^{-20} s^{-1}

Substituting this value into the equation for fractional loss from a sphere (equation 8 in Section 1.3.2) gives:

$$f = 3.385\left(\left(1.16\times10^{-20}\right)\left(9.167\times10^{14}\right)\right)^{1/2} - 3\left(1.16\times10^{-20}\right)\left(9.167\times10^{14}\right)$$

= .01, or a 1 percent argon loss. Repeating the calculations for VB-43-4 (using a time of 40 Ma, and a temperature of 136°C (409 K) to approximate the subsidence heating) gives a value of 3.15 x 10^{-19} s^{-1} for D/a^2, and an estimated argon loss of 6 percent for this sample.

However, using the same values of T and t, and repeating the calculations for the VB-13-2 sample, a 100 percent outgassing is predicted (due to the low calculated E_a for this sample) (Table 3.4). Similarly, the low calculated E_a values of the C-67-1 and C-67-2 samples predict 100 percent outgassing at a temperature as low as 50°C.

Because they predict 100 percent outgassing, the calculated E_a values of the VB-13-2, C-67-1, and C-67-2 samples are clearly too low to be realistic. The calculated E_a values of samples VB-43-1 and VB-43-4 predict fractional argon losses that are much more reasonable, and are consistent with the estimates made in Section 3.4. Reported values of E_a for perthitic microclines range from 35 - 45 kcal/mol (McDougall and Harrison, 1988).

If an average value of E_a (ie. 40 kcal/mol), and an estimated D_0/a^2 of 15,000 are assumed for the K-feldspar from the Mohican Formation in the Mic Mac H-86 well, then an expected fractional argon loss can be calculated for the H-86 samples. Using a time of 50 Ma (1.578×10^{15} seconds), and a temperature of 138°C (411 K) as first-order approximations of the intensity and duration of subsidence heating one obtains a value of 8.02×10^{-18} s^{-1} for D/a^2. Substitution of this number into equation 8 gives an estimated argon loss of 38 percent for these samples. If a slightly lower E_a (39 kcal/mol) is used, the expected argon loss becomes much greater (approximately 70 percent). If a slightly greater E_a (41 kcal/mol) is used, the expected argon loss is

less (approximately 21 percent). These estimates are consistent with the observation made in the previous section that the spectra of the H-86I, and H-86P samples appear to be moderately outgassed.

3.6 Summary and conclusions

The following conclusions are made based on the argon spectra presented in this chapter.

1. The muscovite and feldspar argon spectra from the Mic Mac H-86 well reveal that the source rocks of the Mohican Formation were Early Carboniferous to Permian in age. The spectra are similar to those of intrusive rocks from mainland Nova Scotia (Reynolds et al., 1987), and this region (extending beyond the present east coast onto the LaHave Platform) is interpreted to have been the source area for the Mohican Formation sediments.

2. The muscovite argon spectra from the Mic Mac J-77 and Venture B-13 wells range from Early Ordovician to Early Carboniferous in age, and indicate that the sources of muscovite for the Missisauga Formation in these two wells had quite different thermal histories.

3. The K-feldspar argon spectra from the Missisauga Formation in the Mic Mac J-77, Venture B-13, Venture B-43, Chebucto K-90, and Sable Island C-67 wells all indicate that the source rocks of the formation have dominantly Grenvillian ages (early Late Proterozoic). The sample from the Sable Island C-67 well has a spectrum that is characteristic of simple slow-cooling, but those from the Mic Mac J-77

(and possibly the Chebucto K-90) well(s) have spectra which display limited thermal overprinting that occurred prior to deposition in the Scotian Basin (Avalonian to Acadian in age).

4. The K-feldspar argon spectra from the Logan Canyon Formation in the Sable Island C-67 well also indicate source rocks that have Grenvillian ages.

5. The feldspar argon spectra from the Mic Mac Formation in the Erie D-26 well indicates an Avalonian source rock that was strongly overprinted by an Acadian event.

6. The K-feldspar argon spectra of the H-86I, VB-13-1, VB-13-2, and VB-43-4 (and possibly the K-90-2, and VB-43-1) samples all appear to contain a limited degree of thermal overprinting that can be attributed to recent burial heating within the Scotian Basin. From a comparison with the J-77 and C-67-2 spectra, the amount of radiogenic argon lost from the Venture samples is estimated to be between 10 and 20 percent. Diffusion calculations for these samples predict an outgassing of 6 percent or less. Comparison of the H-86 feldspar spectra with feldspar spectra from Nova Scotia results in an estimated argon loss of between 15 and 33 percent for this sample. Diffusion calculations for this same sample predict an argon loss of approximately 40 percent.

4 Apatite fission track analysis; observations and interpretations

4.1 Observations

The five fission track temperature-sensitive parameters that were listed in Section 1.3.1 (apparent fission track age, variation in apparent age with depth, distribution of single grain ages, distribution of confined track lengths, and variation in mean confined track length with depth) are here evaluated with regard to the samples from the Scotian Basin. A total of 17 fission track ages were calculated, 4 of which were from duplicate[1] samples. The accuracy of the age determinations is not uniform, however. At depths greater than four kilometers severe annealing of the samples made track identification difficult. In addition, many of the etched sample grains (especially in the Venture, Erie, and Bluenose wells) contained numerous dislocations. Because the number of tracks-per-grain present in most of the deep samples is very low (approximately 1) the inadvertent inclusion of a few dislocations in the count data can greatly affect the age calculation. Table 4.1 gives a summary of the count data. The calculated fission track ages range from approximately 2 to 200 Ma. However, only one sample (C-67-1) has a fission track age that exceeds

---

1 The Venture B-43-1A and B, and B-13-4A and B are true duplicates in that the mineral separate was split and 2 grain mounts of each were made. The Erie D-26-1 and D-26-2 samples were obtained from a single sandstone unit (only 2 m apart), and therefore have had identical subsidence histories. The Mic Mac J-77I and J-77P samples have also had identical subsidence histories. J-77P was a single 100 gram piece of core obtained at a depth of 2816 m (B.R.T.). J-77I consisted of several smaller pieces that were taken over the entire cored interval 2813 - 2822 m (B.R.T.).

Table 4.1. A summary of the fission track count data. Ns and Ni are the numbers of spontaneous tracks (in apatite) and induced tracks (in muscovite detector) that were counted. The ρ_s and ρ_i columns give the spontaneous and induced track densities (tracks/cm^2). Fission track age error estimates are at the 2 sigma confidence level. Samples marked with an asterisk (*) failed the chi-squared test at the 95 percent confidence level. A weighted mean value of 10594 ± 439 was used for the ζ parameter (based on six determinations) for all of the age calculations. The age calculations summary sheets are given in Appendix 3.

Well Name	Depth (m)	Formation	Sample Name	Grains Counted	Ns	Ni	ρ_s	ρ_i	Fission Track Age (Ma)	U (ppm)
Sable Is. C-67	2471-2481	Logan Canyon	C-67-1	16	773	480	1.2 E6	7.9 E5	199 ± 15	11
Erie D-26	1955-1959	Mic Mac	D-26-1	10	304	437	7.8 E5	1.1 E6	91 ± 8	15
Erie D-26	1955-1959	Mic Mac	D-26-2	9	334	509	9.5 E5	1.5 E6	85 ± 7	20
Mic Mac J-77	2814-2823	Missisauga	J-77I	35	348	564	1.7 E7	2.7 E5	64 ± 6	5
Mic Mac J-77	2817	Missisauga	J-77P	13	143	238	2.8 E5	4.7 E5	62 ± 7	8
Sable Is. C-67	3377	Missisauga	C-67-2*	16	63	296	1.0 E5	4.7 E5	42 ± 5	6
Venture B-43	4430	Missisauga	VB-43-1A	18	18	82	3.3 E5	1.5 E5	13 ± 4	5
Venture B-43	4430	Missisauga	VB-43-1B	8	12	44	3.8 E5	1.4 E5	17 ± 6	4
Venture B-43	4954	Missisauga	VB-43-8	23	21	245	2.3 E4	2.7 E5	5 ± 1	8
Venture H-22	4717	Missisauga	VH-22-1	16	14	98	2.2 E4	1.7 E5	9 ± 3	4
Venture H-22	5394	Mic Mac	VH-22-9	21	31	407	3.8 E4	5.0 E5	5 ± 1	14
Venture B-13	4718	Missisauga	VB-13-1	17	17	111	2.6 E4	1.7 E5	20 ± 5	2
Venture B-13	4954	Missisauga	VB-13-4A	30	32	328	2.7 E4	2.8 E5	6 ± 1	8
Venture B-13	4954	Missisauga	VB-13-4B	20	12	140	1.5 E4	1.8 E5	5 ± 2	5
Bluenose 2G-47	5112-5129	Mic Mac	2G-47-1*	30	68	633	5.9 E4	5.5 E5	16 ± 4	7
Chebucto K-90	4286	Missisauga	K-90-1	9	6	238	1.7 E4	6.8 E5	3 ± 1	9
Mic Mac H-86	4715-4725	Mohican	H-86I*	10	14	1146	3.6 E4	2.9 E5	2 ± 1	49

the stratigraphic age of the formation sampled. All of the other samples have fission track ages that are younger than the respective formation stratigraphic ages.

Figure 4.1 is a plot of corrected present-day interval temperature versus apatite fission track age for the seventeen samples in Table 4.1. The interval temperature estimates were obtained from Issler (1983). Temperature error estimates are $\pm$ 8°C. Fission track age error estimates are the statistical 2 sigma estimates shown in Table 4.1. Also shown in the figure is the trend of volcanogenic apatites from the Otway Basin (simplified from Green et al. (1989)). Whereas the volcanic sources of the Otway Basin samples have a uniform age of 125 Ma, the detrital sources of the Scotian Basin samples have ages that are likely in excess of 200 Ma. In addition, unannealed samples from the Scotian Basin have a basement-type distribution of confined track lengths (see Figure 4.23), but unannealed Otway Basin samples have a volcanic-type confined track length distribution. Highly annealed samples from the two areas are directly comparable, but unannealed samples are not expected to be similar, and are compared for reference purposes only.

The Scotian Basin samples that were obtained at depths greater than 4 km plot near the Otway Basin trend and indicate a similar zero age intercept at a temperature of approximately 120°C to 140°C. The D-26-1 and D-26-2, and to a lesser extent, the J-77I and J-77P, and C-67-2 samples all plot below (or to the left of) the annealing curve, that is, they appear to be more annealed than would be predicted from

the present-day temperatures of the sampled intervals. The C-67-1 sample, because it contained abundant (detrital) fossil tracks, plots far above the Otway Basin trend.

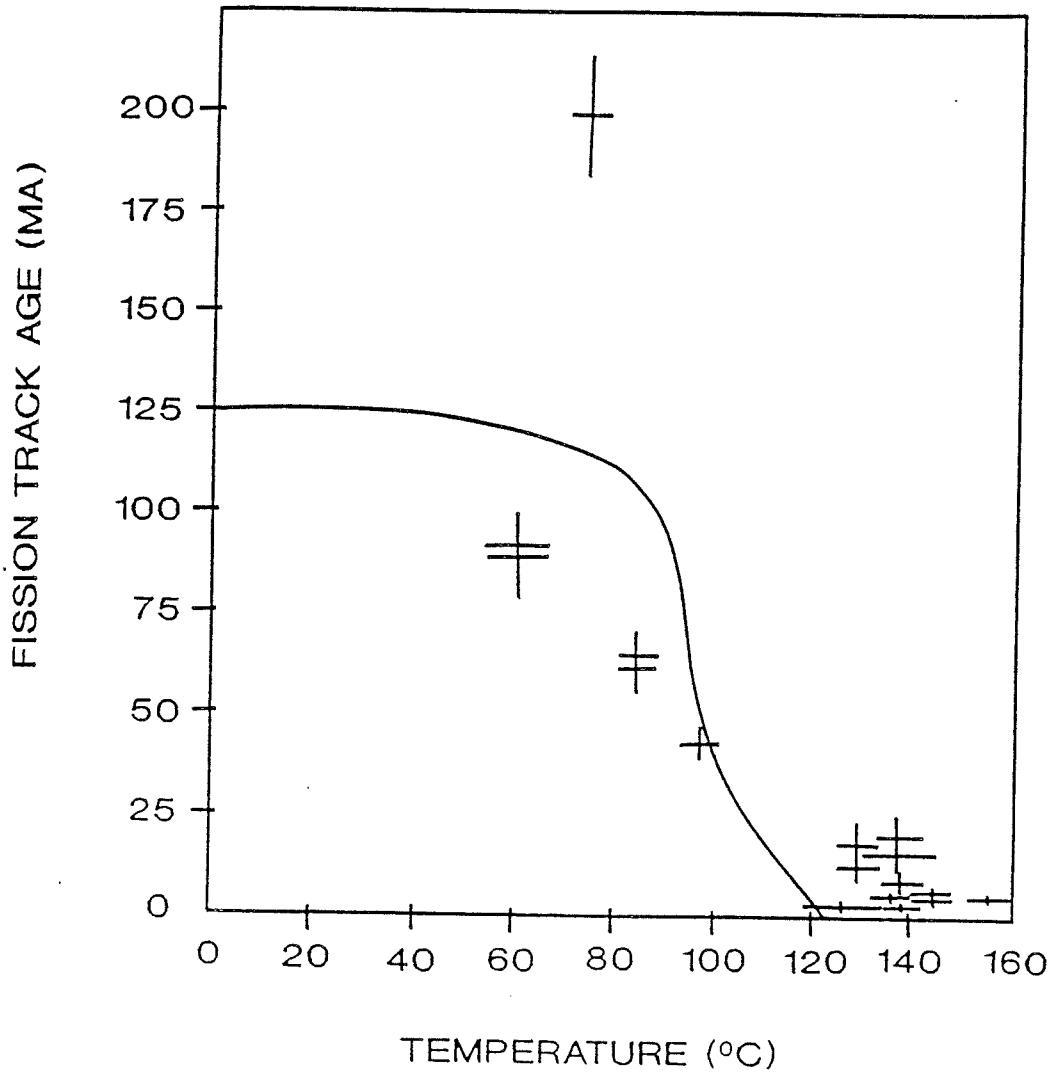

Figure 4.1. Apparent fission track age versus interval temperature for the seventeen apatite samples from the Scotian Basin. Also shown in the figure is the annealing trend for volcanogenic apatites from the Otway Basin (modified from Green et al. (1989)).

Thirteen single grain age histograms have been constructed for the Scotian Basin samples. (The four samples with duplicate analyses have been combined to give four rather than eight histograms.) The single grain age histograms are shown in Figures 4.2 to 4.14. Figure 4.15 shows six single grain age histograms for samples from the Otway Basin. All of the Scotian Basin samples that were obtained from depths greater than 4 km (Figures 4.2 to 4.10) have histograms similar to Figure 4.15 f. The distribution of single grain ages in the histogram of the C-67-2 sample (Figure 4.11) is similar to that of the Otway Basin sample shown in Figure 4.15 e. The corresponding interval temperatures are also similar (97°C for C-67-2, and 92°C for Figure 4.15 e). The C-67-1 single grain age histogram (Figure 4.12) is not directly comparable to any of the Otway Basin samples. This is because the fission track age of this sample far exceeds that of Otway Basin volcanism (approximately 120 Ma, Green et al. (1989)), and hence the maximum fission track age of any of the (volcanogenic) Otway Basin apatites. Moreover, the shape of the single grain age distribution of the Otway Basin sample that has a comparable interval temperature (Figure 4.15 c; 73°C) is narrow and peaked, whereas that of the C-67-1 histogram (Figure 4.12; 73°C) is broad and does not exhibit a strong peak.

The estimated present-day temperature of the interval sampled in the Mic Mac J-77 well is 84°C, and the single grain age histogram of the J-77I and J-77P samples (Figure 4.13) is quite broad and moderately peaked. This is quite similar to the distribution of single

grain ages for the Otway Basin sample from an interval with a similar present-day temperature (Figure 4.15 d; 86°C). The distribution of single grain ages in the histogram of the D-26-1 and D-26-2 samples (Figure 4.14) is also broad and moderately peaked. The estimated present-day temperature of the interval sampled is only 60°C, and the corresponding single grain age histogram for the Otway Basin is either Figure 4.15 b (45°C) or c (73°C). However, the form of the distribution of the Erie D-26 single grain age histogram (like the J-77 histogram) appears to be more like that of Figure 4.15 d, corresponding to an interval temperature of 86°C.

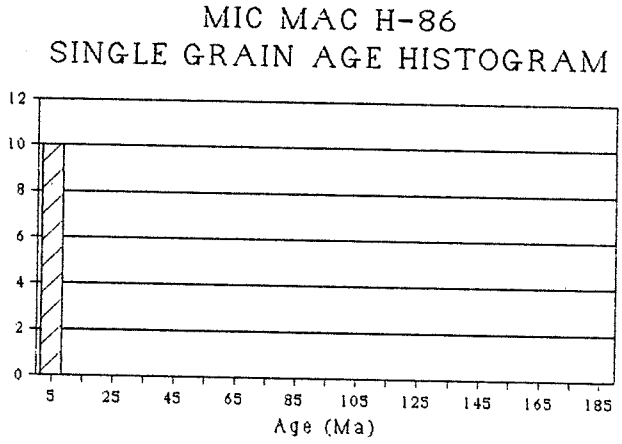

Figure 4.2. Single grain age histogram for H-86I (n = 10 single grain ages).

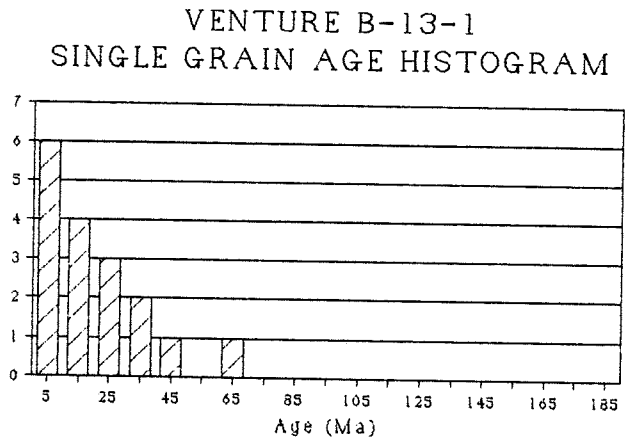

Figure 4.3. Single grain age histogram for VB-13-1 (n = 17 single grain ages).

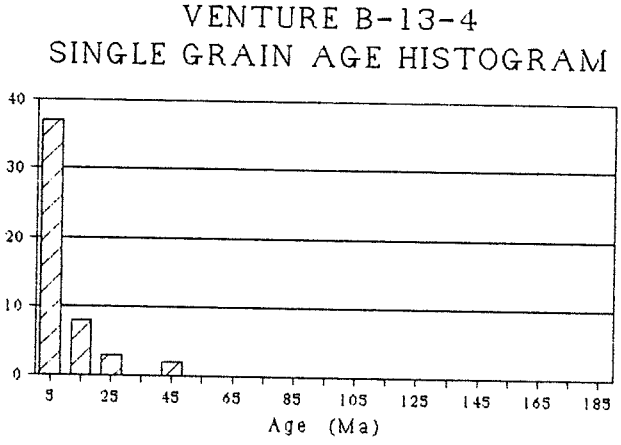

Figure 4.4. Single grain age histogram for VB-13-4A and VB-13-4B (n = 50 single grain ages).

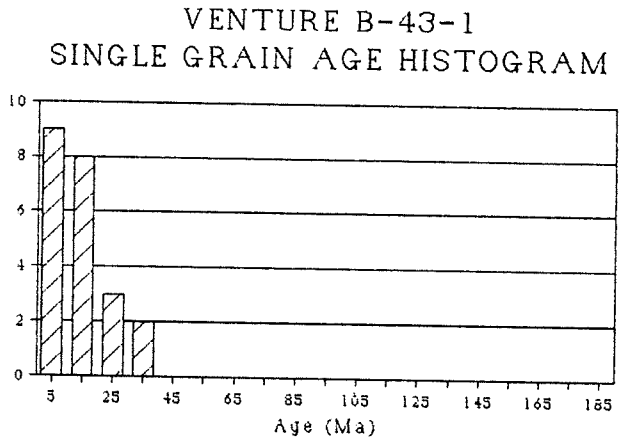

Figure 4.5. Single grain age histogram for VB-43-1A and VB-43-1B (n = 22 single grain ages).

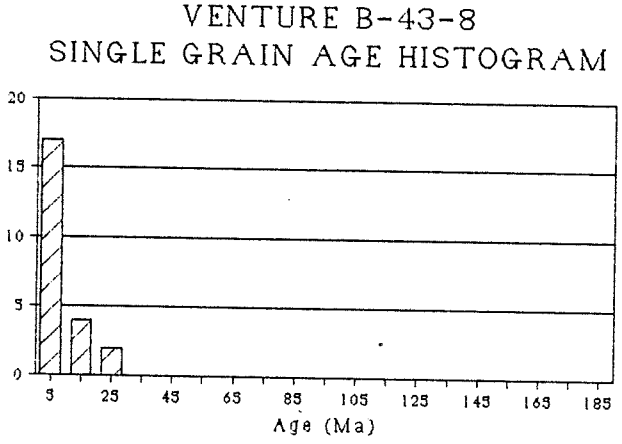

Figure 4.6. Single grain age histogram for VB-43-8 (n = 23 single grain ages).

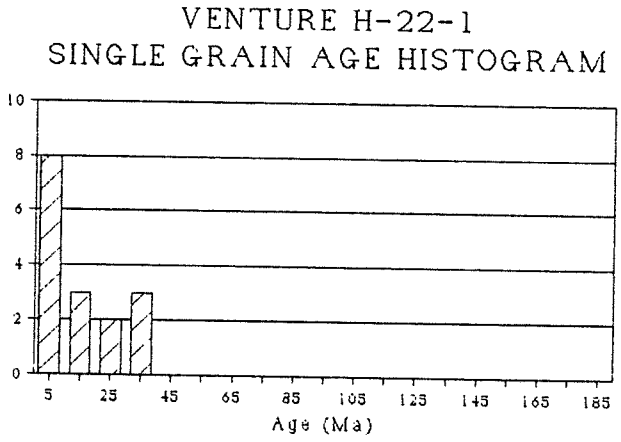

Figure 4.7. Single grain age histogram for VH-22-1 (n = 16 single grain ages).

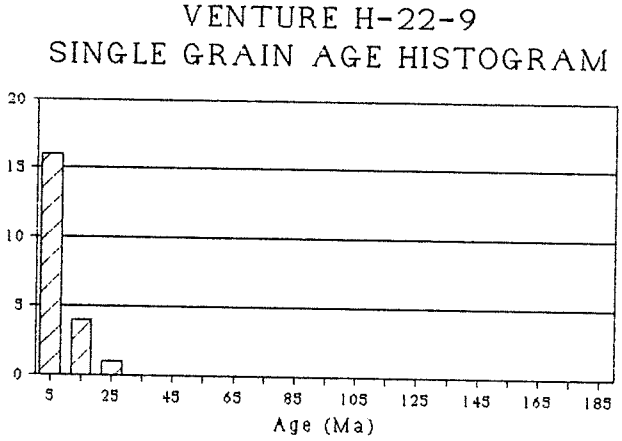

Figure 4.8. Single grain age histogram for VH-22-9 (n = 21 single grain ages).

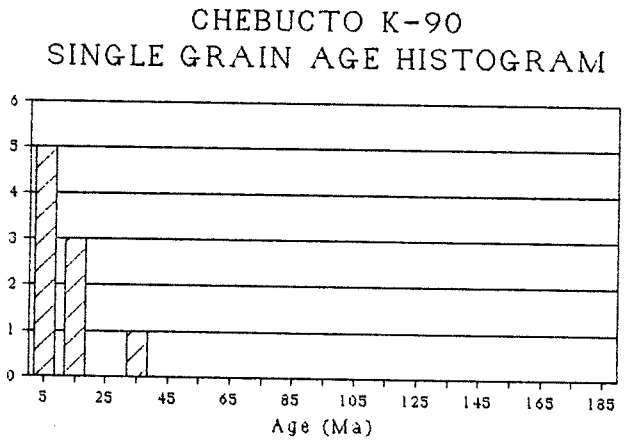

Figure 4.9. Single grain age histogram for K-90-1 (n = 9 single grain ages).

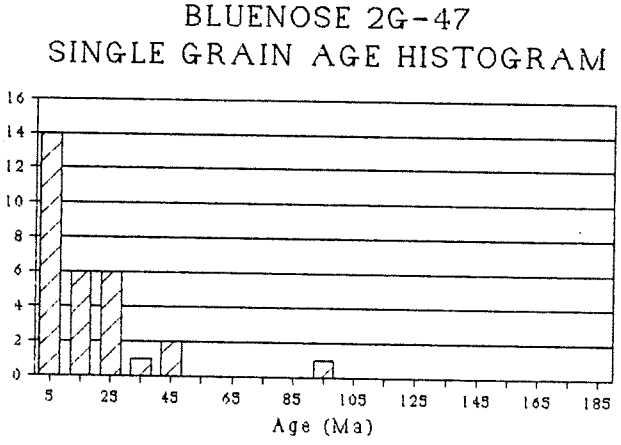

Figure 4.10. Single grain age histogram for 2G-47-1(n = 30 single grain ages).

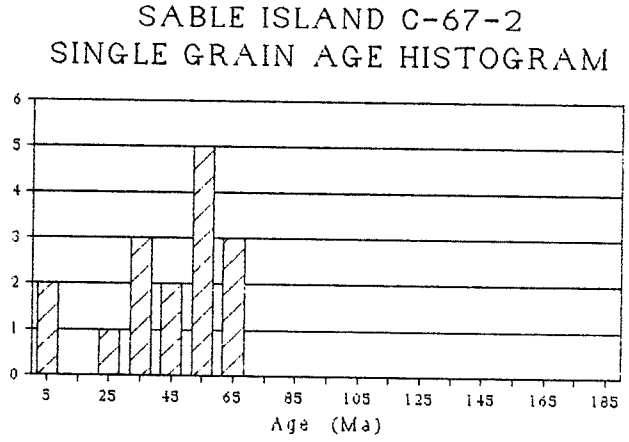

Figure 4.11. Single grain age histogram for C-67-2 (n = 16 single grain ages).

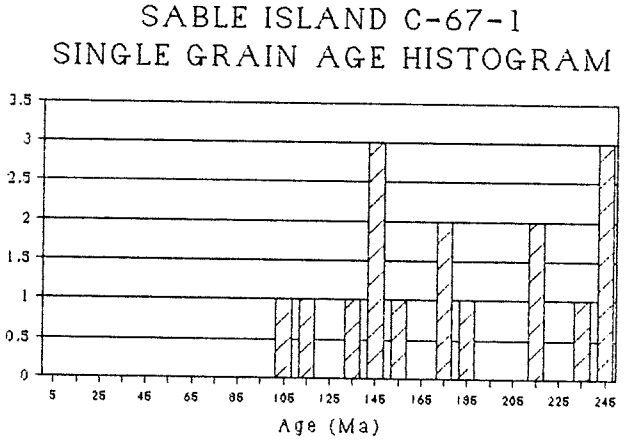

Figure 4.12. Single grain age histogram for C-67-1 (n = 16 single grain ages).

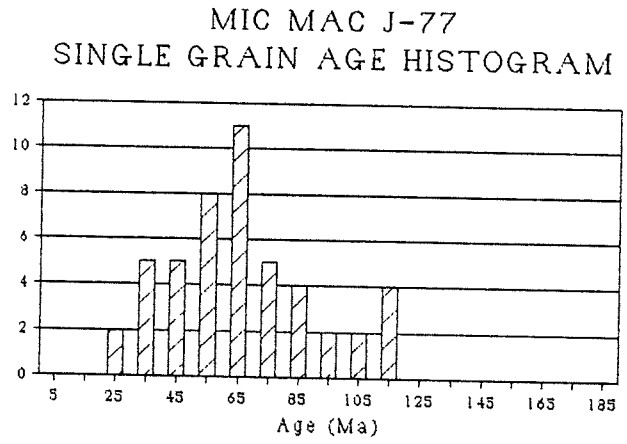

Figure 4.13. Single grain age histogram for J-77I and J-77P (n = 48 single grain ages).

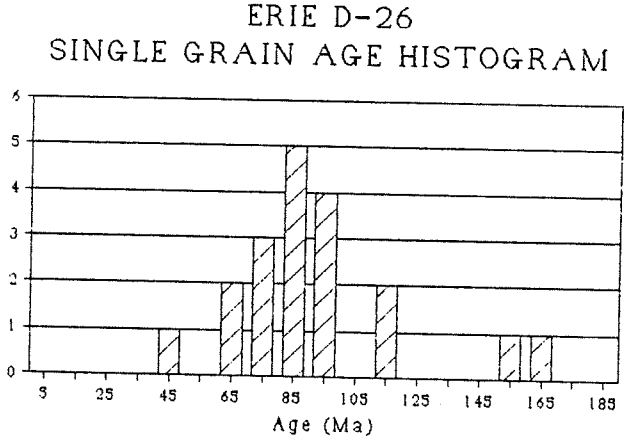

Figure 4.14. Single grain age histogram for D-26-1 and D-26-2 (n = 19 single grain ages).

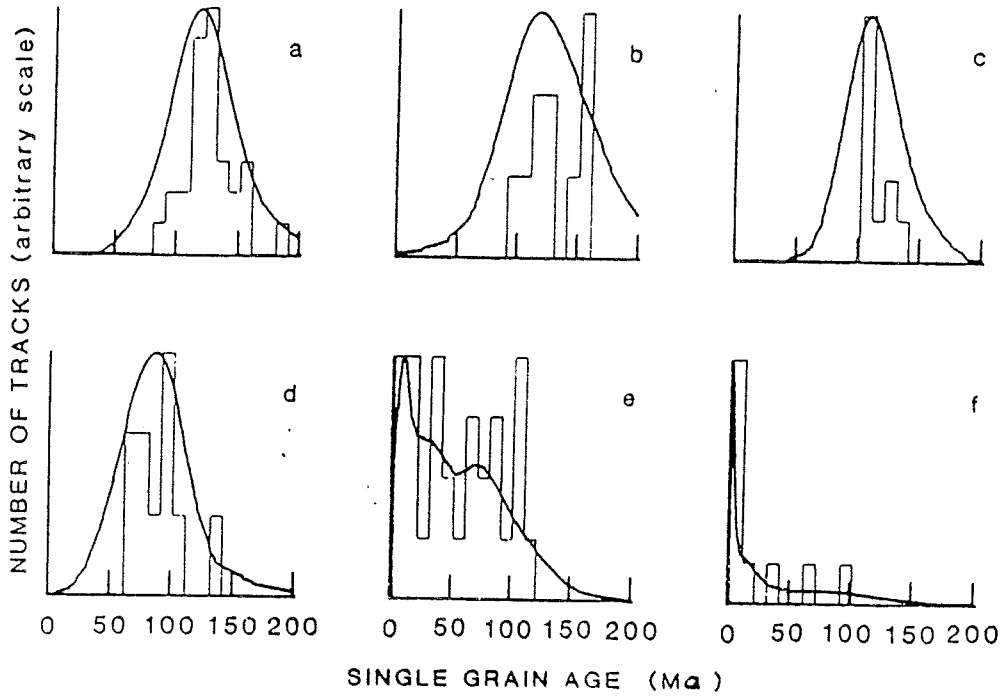

Figure 4.15. Six single grain age histograms for Otway Basin samples (from Green et al. (1989)). Interval temperatures are as follows: a = outcrop; b = 45°C; c = 73°C; d = 86°C; e = 92°C; f = 109°C. (The curves are smoothed probability functions obtained by the addition of Gaussian distributions representing each single grain age and its error.)

The apatite samples from the Scotian Basin that were obtained at depths greater than 4 km contained very few confined fission tracks. Therefore, only five distributions of confined track lengths were measured. These histograms are shown in Figures 4.16 to 4.20. Figure 4.21 shows six composite confined track length histograms for apatite samples from the Otway Basin (from Green et al. (1989). Figure 4.16 is a composite histogram of confined track lengths from the VB-13-1, VB-13-4, and VH-22-1 samples. These samples, which are from intervals that have estimated present-day temperatures of 137°C to 144°C, have a mean confined track length of only 4.9 $\pm$ .5 microns (standard deviation = 1.8 microns). This length is much less than the minimum mean confined track length of 9 microns reported by Green et al. (1989) for Otway Basin apatites from intervals with present-day temperatures of 102°C to 110°C (Figure 4.21 f). Also, the distribution of confined track lengths in Figure 4.16 is not as broad as that of Figure 4.21 f.

The C-67-2 sample, which is from an interval that has an estimated present-day temperature of 97°C, has a mean confined track length of 9.7 $\pm$ .5 microns (standard deviation = 1.9 microns). The mean confined track length for Otway Basin samples from intervals that have similar present-day temperatures (Figure 4.21 e; T = 90°C to 101°C) is approximately 11.3 microns, which is significantly greater than the C-67-2 value above. The confined track length histogram for the C-67-2 sample is shown in Figure 4.17. The broad form of the distribution is like that of the Otway Basin samples from intervals with similar present-day temperatures (Figure 4.21 e).

The C-67-1 sample, which is from an interval that has an estimated present-day temperature of 73°C, has a mean confined track length of 10.8 ± .2 microns (standard deviation = 1.6 microns). The mean confined track length for Otway Basin samples from intervals that have similar present-day temperatures (Figure 4.21 c; T = 60°C to 70°C) is approximately 12.8 microns, which is significantly greater than the C-67-1 value above. The confined track length histogram of the C-67-1 sample is shown in Figure 4.18. The broad form of the distribution of confined track lengths in this sample is like that of Otway Basin samples from intervals with similar present-day temperatures (Figure 4.21 c).

The J-77I and J-77P samples, which are from an interval that has an estimated present-day temperature of 84°C, has a mean confined track length of 10.9 ± .2 microns (standard deviation = 1.8 microns). The mean confined track length for Otway Basin samples from intervals with similar present-day temperatures (Figure 4.21 d; T = 80°C to 90°C) is 12.4 microns, which again is significantly greater than the J-77 value above. The confined track length histogram of the J-77I and J-77P samples is shown in Figure 4.19. The broad form of this histogram is also similar to those of Otway Basin samples from, intervals that have similar present-day temperatures (Figure 4.21 d). However, both the C-67-1 and J-77 confined track length histograms (Figures 4.18 and 4.19) contain a component of shorter tracks (5 to 7 microns) that are not present in the Otway Basin samples (Figures 4.21 c and d). It is also worth noting that the C-67-1 and J-77 confined

track histograms (Figures 4.18 and 4.19) are virtually identical, despite the fact that the calculated fission track ages differ by 135 Ma (199 Ma and 64 Ma, respectively).

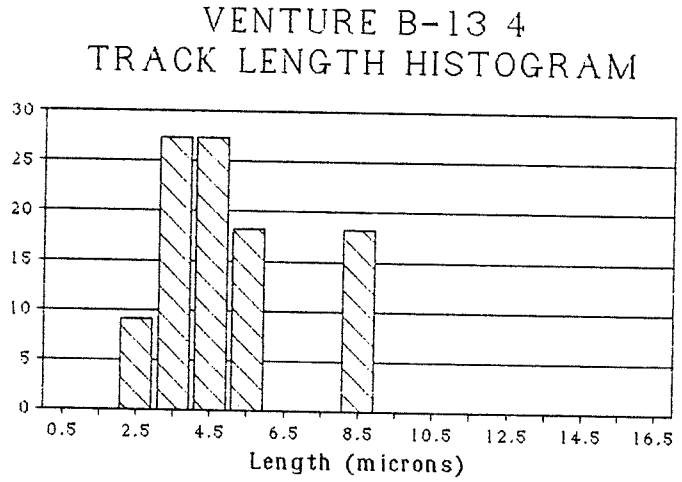

Figure 4.16. Composite normalized confined track length histogram for VB-13-4, VB-13-1, and VH-22-1 (n = 11 lengths (9 from 13-4, 1 from 13-1 and 22-1); mean = 4.9 ± .5 microns; standard deviation = 1.8 microns).

The D-26-1 and D-26-2 samples, which are from an interval that has an estimated present-day temperature of 60°C, has a mean confined track length of 12.6 microns (standard deviation = 1.3 microns). The mean confined track lengths for Otway Basin samples from intervals that have similar present-day temperatures (Figure 4.21 c; T = 60°C to 70°C) is 12.8 microns, which is not significantly different from the D-26 value above. The confined track length histogram of the D-26 samples is shown in Figure 4.20. The form of the distribution of confined track lengths in Figure 4.20 is narrower and more peaked than those

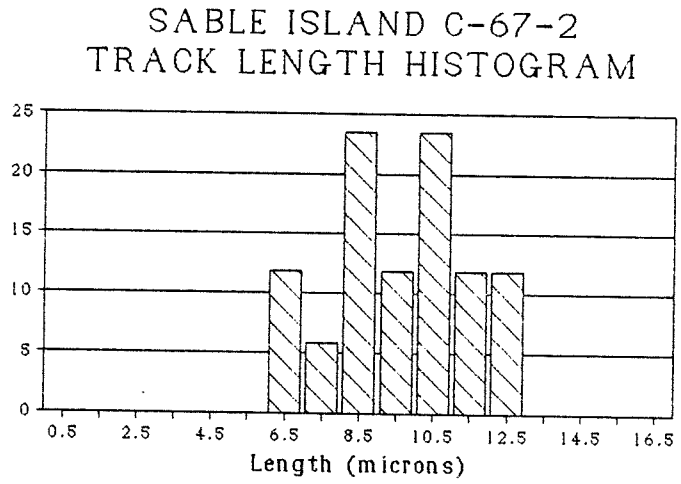

Figure 4.17. Normalized confined track length histogram for C-67-2 (n = 17 lengths; mean = 9.7 ± .5 microns; standard deviation = 1.9 microns).

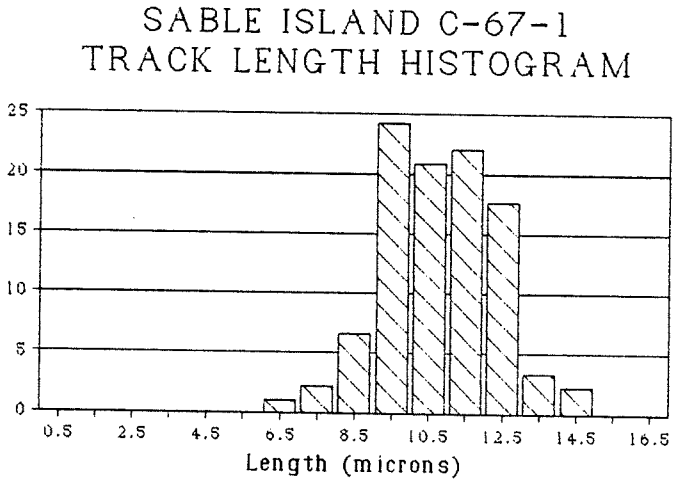

Figure 4.18. Normalized confined track length histogram for C-67-1 (n = 91 lengths; mean = 10.8 ± .2 microns; standard deviation = 1.6 microns)

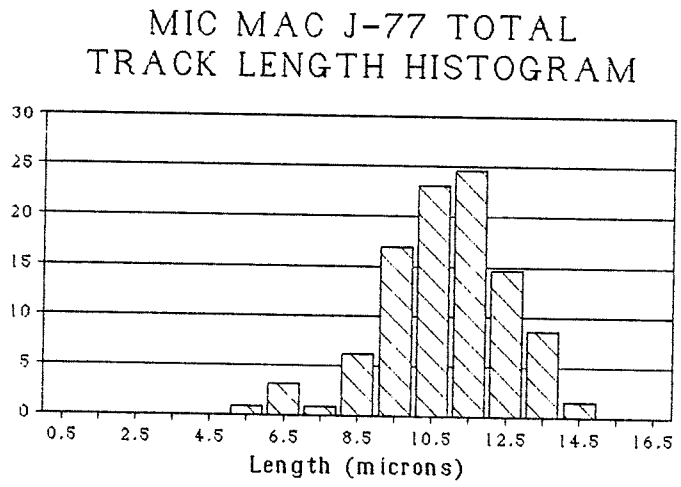

Figure 4.19. Normalized confined track length histogram for J-77I and J-77P (n = 131 lengths; mean = 10.9 ± .2 microns; standard deviation = 1.8 microns).

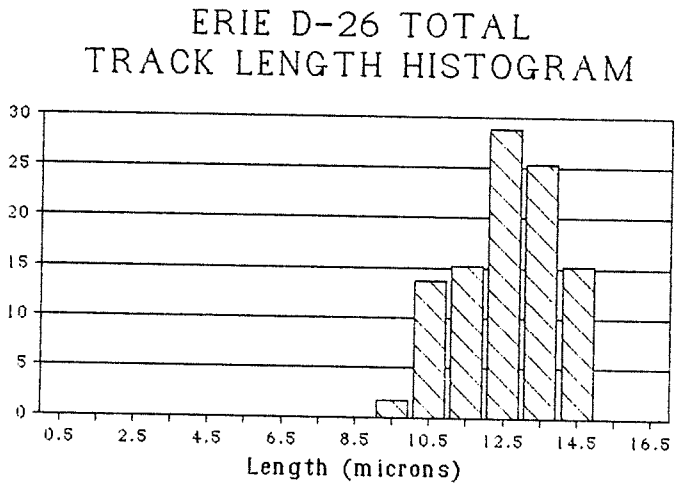

Figure 4.20. Composite normalized confined track length histogram for D-26-1 and D-26-2 (n = 59 lengths; mean = 12.6 ± .2 microns; standard deviation = 1.3 microns).

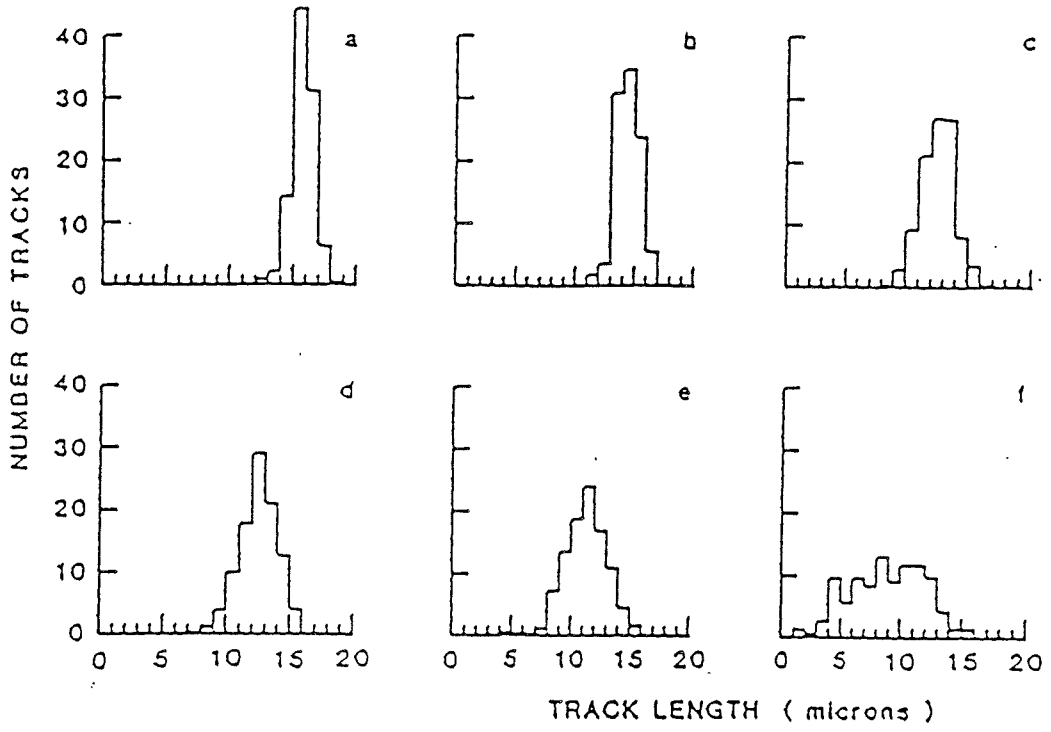

Figure 4.21. Composite normalized confined track length histograms for volcanogenic apatite samples from the Otway Basin (from Green et al. (1989)). Corresponding interval temperatures are as follows: a = outcrop; b = 40° - 50°C; c = 60° - 70°C; d = 80° - 90°C; e = 90° - 100°C; f = 102° - 110°C. The corresponding mean confined track lengths are: a = 16 microns; b = 14.3 microns; c = 12.8 microns; d = 12.4 microns; e = 11.3 microns; f = 9 microns.

of Figures 4.18 and 4.19, and is like those of the Otway Basin samples from intervals that have similar present-day temperatures (Figure 4.21 c).

4.2 Interpretation of fission track data

Because the apparent fission track ages of all of the samples from the Mohican, Mic Mac, and Missisauga Formations are younger than the corresponding formation stratigraphic ages, it is apparent that the predepositional fission tracks in these samples have been partially to completely annealed. For interpretative purposes these samples may be divided into two groups.

The first group includes all of the samples that were obtained from depths of greater than 4 km, and which have fission track ages of 20 Ma or less (see Table 4.1). These samples are all essentially completely annealed. The small differences among the calculated ages of these samples probably do not reflect differences in the degree of thermal maturity of the sampled intervals, but are more likely a result of the necessarily few spontaneous tracks counted, and the difficulties in track identification. Within this group of samples the distributions of single grain ages are also quite similar, with strong peaks at zero age, as only a few grains retained any tracks at all. The one confined track length histogram from this group (Figure 4.16) also reflects the essentially totally annealed character of these samples. The mean confined track length of less than 5 microns indicates that the annealing is sufficiently advanced that track length reduction no longer occurs by progressive shortening, but rather that the tracks are now broken into discontinuous portions separated by unetchable gaps (Gleadow et al., 1986).

The second group of samples includes: D-26-1, D-26-2, J-77I, J-77P, C-67-1, and C-67-2. The fission tracks in these samples are interpreted to be partially annealed. The fission track ages here are less than the depositional ages and decrease with increasing temperature. Fission track data on each of these is interpreted below.

The C-67-2 sample is interpreted to be at or near its maximum temperature. The apparent fission track age of 42 $\pm$ 5 Ma probably results from a substantial reduction in the original detrital age by progressive heating of the sampled interval to the present-day temperature of 97°C. Because of the high degree of annealing in this sample, the single grain age histogram (Figure 4.11) is very similar to Otway Basin samples that are at approximately the same present-day temperature (Figure 4.15 e) even though the Otway Basin samples are volcanogenic and the Scotian Basin samples are detrital. Similarly, the mean confined track length for Otway Basin samples with comparable present-day interval temperatures is the same as that of the C-67-2 sample.

The J-77I and J-77P samples are anomalously annealed. The apparent fission track ages of these samples, 64 $\pm$ 6 Ma, and 62 $\pm$ 7 Ma, respectively, are about one-half the Missisauga Formation stratigraphic age (approximately 130 Ma). However, the estimated present-day temperature of the sampled interval (approximately 84°C) is too low to account for such a substantial reduction in the fission track age. The Mic Mac J-77 well is located on the flank of a salt diapir (L. F. Jansa, 1989, pers. comm.). The presence of this salt diapir can be used to

explain the high degree of annealing of the J-77 samples. Because it has a higher thermal conductivity than the surrounding sediments, the salt may conduct heat into the overlying sediments. Alternatively, the salt may act as a channel for warm fluids from more deeply buried strata.

Figure 4.22 shows the variation in apatite fission track age with present-day down-hole temperature for wells in the Otway Basin (from Green et al., 1989). (The samples in Figure 4.22 have a volcanogenic age of approximately 120 Ma, and are interpreted to be presently at their maximum temperature.) From Figure 4.22 it can be seen that a temperature of approximately 90°C to 100°C is required to account for the high degree of annealing observed in the J-77I and J-77P samples. The confined track length histogram for the J-77 samples (Figure 4.19) is consistent with the proposed thermal event. The presence of some very short tracks in these samples supports the assertion that the temperature of the interval sampled must have been higher at some time in the past than it is at present. There are also some longer tracks (13 - 15 microns) that would not be present if the present-day temperature of the sampled interval was substantially greater than 84°C (compare the J-77 histogram with the one for C-67-2 (Figure 4.17); T= 97°C).

The D-26-1 and D-26-2 samples are also believed to have experienced a thermal event at some time subsequent to deposition. The apparent fission track ages of these samples, 91 $\pm$ 8 Ma, and 85 $\pm$ 7 Ma, respectively, are about one-half that of the stratigraphic age of

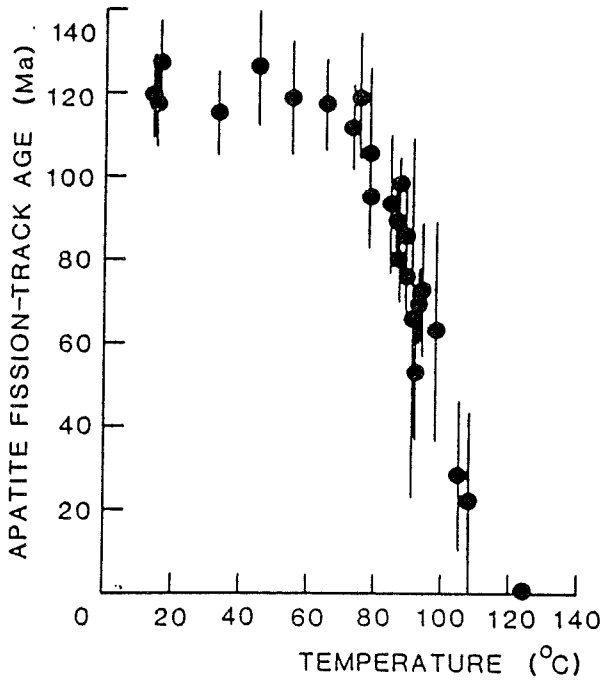

Figure 4.22. Variation of apatite fission track age with present-day down-hole temperature for wells in the Otway Basin (from Green et al. (1989)).

the Mic Mac Formation (approximately 180 Ma), but the estimated present-day temperature of the sampled interval (approximately 60°C) is far too low to cause such a substantial age reduction. However, the long mean confined track lengths are consistent with the present-day interval temperature. The combination of these two observations places certain constraints on the nature of the thermal event. Firstly, the event must have been hot enough to totally anneal all existing fission tracks (to explain the absence of any short tracks), and secondly, the event must have been relatively short-lived, to allow for the subsequent accumulation of slightly-annealed to unannealed fission

tracks that are present in the apatite grains. A temperature of at least 110 - 120°C would be required to totally anneal the preexisting fission tracks.

The fission track age of the D-26-1 and D-26-2 samples can be corrected (as described in Green et al. (1986)) to give the approximate age of the thermal event. The corrected age (t_{corr}) is given by: $t_{corr} = (l_o/l) \times t$, where l_o is the unannealed mean track length of the sample, l is the present mean confined track length, and t is the calculated fission track age. The unannealed mean confined track length must be assumed. Green et al. (1986) suggest a mean track length of 14.5 to 15 microns for undisturbed, quickly-cooled volcanic rocks. If $l_o = 15 \pm 1$ microns is used, the corrected ages of the D-26-1 and D-26-2 samples are 108 $\pm$ 14 Ma, and 101 $\pm$ 13 Ma, respectively (Albian). (The error associated with the corrected fission track age is calculated using the errors in the observed mean fission track length (0.2 microns), the mean unannealed fission track length (approximately 1 micron), and in the uncorrected fission track age (8 Ma).)

There is geological evidence of a thermal event in the region during Albian time. Jansa and Pe-Piper (1985) describe Early Cretaceous (Barremian - Albian) volcanic rocks (basaltic sills and volcaniclastics) in Missisauga Formation sediments at a depth of approximately 2.5 km in four wells in the Orpheus Graben and Eastern LaHave Platform. The D-26-1 and D-26-2 samples also contain abundant sulfide mineralization. Euhedral pyrite cubes occur interstitially among detrital quartz and feldspar grains, and microcrystalline pyrite forms

much of the cement in the samples. Although the sulfide mineralization does not imply elevated temperatures, it does indicate fluid flow through the sandstones. The fluids that must have transported the dissolved iron may have been part of a short-lived hydrothermal convection system that was driven by the volcanism that was occurring in the Orpheus Graben.

The C-67-1 sample is interpreted to be at or near its maximum temperature. Because the fission track age of this sample (199 $\pm$ 15 Ma) is much older than the stratigraphic age of the Logan Canyon Formation, the fission tracks in this sample can be considered to be only slightly affected by present-day burial heating. The mean confined track length of 10.8 microns, and the distribution of confined tracks (Figure 4.18) are therefore characteristic of the source rocks of the detrital grains. They can be explained in terms of a slight reduction by recent burial heating of what was originally an "undisturbed basement" type distribution (see Figure 4.23). The age correction from Green et al. (1986) can also be applied to this sample. If l_o = 13 microns is used (13 microns is the mean track length for undisturbed basement type distributions; eg. Figure 4.23 c), the corrected age is 240 + 26 Ma. The significance of this age is unclear, but it clearly indicates the detrital (eg. not authigenic) nature of the grains in the sample.

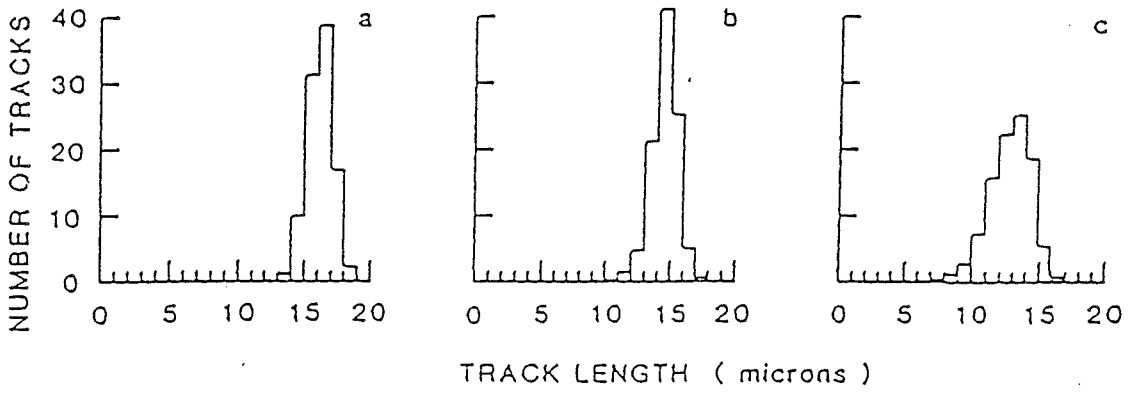

Figure 4.23. Representative distributions of confined fission track lengths (from Green et al., 1986). A represents the distribution of induced track lengths. B represents the distribution of confined track lengths in quickly-cooled volcanic rocks (i.e. Otway Basin samples). C represents the distribution of confined track lengths in basement-type rocks (i.e. Scotian Basin samples).

4.3 Summary and conclusions

The following conclusions can be made based on the fission track data presented in this chapter.

1. Samples that were obtained at depths of greater than 4 km show a very high degree of annealing. These samples indicate that total fission track annealing in apatite may be expected for formation temperatures of greater than approximately 125°C in the Scotian Basin.

2. The levels of thermal maturation of the samples from the Sable Island C-67 well are consistent with a model of simple subsidence heating to the present-day interval temperatures. The fission track age and the distribution of confined tracks in the C-67-1 (Logan Canyon Formation) sample clearly indicate the sediments were derived from basement-type (i.e. not volcanic) rocks.

3. The sample from the Mic Mac J-77 well is more annealed than would be predicted by a model of simple subsidence heating to the present-day interval temperature. The sample is interpreted to have experienced a thermal event (i.e. from warm convecting fluids channeled upwards by salt diapirism). The thermal event was probably intense enough to anneal most (but not all) of the accumulated spontaneous fission tracks.

4. The samples from the Erie D-26 well are also more annealed than would be predicted by a model of simple subsidence heating. These samples are interpreted to have experienced a thermal event at approximately 100 Ma which was intense enough to totally anneal the accumulated spontaneous fission tracks. The thermal event must have been relatively short-lived and have resulted in temperatures of approximately 110 - 120°C.

5 Overview

5.1 Comparison of argon and fission track data with A-I and Ro

Mackenzie et al. (1985) determined the level of completion of steroid aromatization and sterane and hopane isomerization reactions in samples from 10 wells in the Scotian Basin. These included the Erie D-26, Mic Mac J-77, Mic Mac H-86, Sable Island C-67, Venture B-13 (and Venture D-23), and Bluenose G-47 wells, which were also sampled in this study (Bluenose 2G-47 is a redrill of Bluenose G-47). Mackenzie et al. (1985) reported that the A-I reactions at a depth of 2.2 km in the Erie D-26 well were anomalously progressed. The level of completion of the reactions was equivalent to the average depth progression at 3.3 km. The level of completion of the A-I reactions at a depth of 3.3 km in the Mic Mac J-77 well were equivalent to the average depth progression at 3.8 km. In contrast, the level of completion of the A-I reactions in samples from the Venture, Bluenose, and Sable Island wells were at of near the average depth progression.

In Chapter 4 it was observed that the present-day temperatures of the sampled intervals in the Erie D-26, and Mic Mac J-77 wells are too low to account for the degree of fission track annealing, and commensurate reduction in fission track age. This observation is supported by the level of completion of the A-I reactions. Mackenzie et al. (1985) reported that the A-I reactions were all gone to completion in samples that were obtained at depths of greater than 4 km. In Chapter 3 it was observed that the onset of significant diffusion of

radiogenic argon did not occur until burial depths of greater than 4 km had been reached. For this reason A-I and argon data are not comparable.

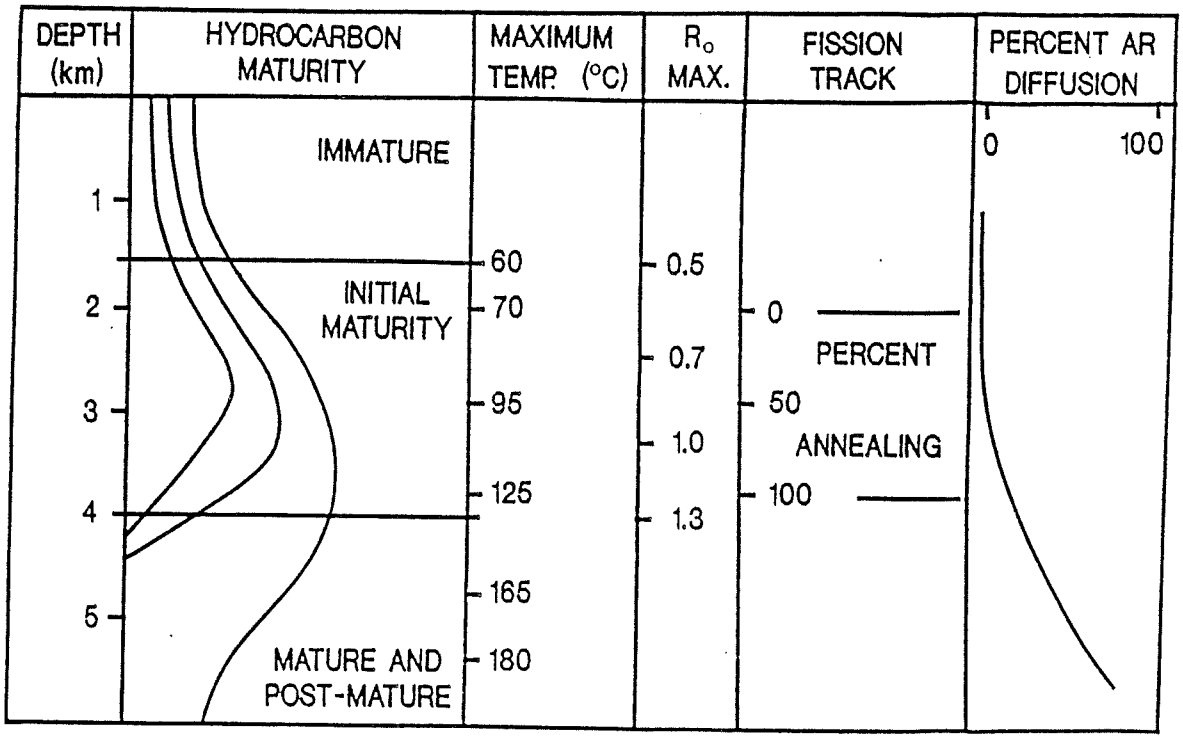

Figure 5.1. Generalized comparison of vitrinite reflectance, annealing of fission tracks in apatite, and K-feldspar argon diffusion with the zones of hydrocarbon generation (modified from Gleadow and Harrison, 1986).

Optical reflectance of vitrinite (Ro) has been measured in samples from many of the wells in the Scotian Basin, including 4 that were sampled in this study, Venture B-43, Venture H-22, Mic Mac H-86, and Venture B-13 (Avery, 1983, 1985, 1986, 1988). Vitrinite reflectance has also been measured on samples from one well drilled on Sable Island (Sable Island 4-H-58, Avery (1978)), which probably has a comparable depth maturation profile to the Sable Island C-67 well. Figure 5.1 shows a generalized comparison of vitrinite reflectance and annealing of fission tracks in apatite with the zones of hydrocarbon generation (from Gleadow and Harrison, 1986). In this figure the degree of annealing of fission tracks in apatite is expressed as a percent age reduction. This implies a knowlege of a fission track age for equivalent but unannealed samples. Such samples are not available for this study however, and unannealed equivalent fission track ages for the partially annealed samples in this study can only be estimated. Therefore only a comparison of apparent fission track ages with vitrinite reflectance can be made.

Figure 5.2 shows the apparent fission track age versus the measured Ro for the 10 samples for which vitrinite data are available (Avery, 1978, 1983, 1985, 1986, 1988). Also shown on the figure is the expected position of the track annealing zone (from Gleadow and Harrison, 1986). There is reasonable agreement between the observed and the expected annealing behavior. However, the data seem to indicate that the transition from 0 % to 50 % annealing occurs over a narrower and somewhat lower range of Ro values (i.e. 0.5 to 0.7) while

the transition from 50 % to 100 % annealing occurs over a somewhat broader range of Ro values (i.e. approximately 0.7 to 1.2). Many more fission track age determinations are needed, especially for samples that have a vitrinite reflectance of 0.8 or less, in order to better define the variation of fission track age with Ro for the Scotian Basin.

Vitrinite reflectance data may also be compared with argon data for the 3 wells for which both are available (Venture B-13, Venture B-43, and Mic Mac H-86). For the intervals sampled in this study the Ro values in the Venture B-43 well are 0.8 - 0.85. The sampled interval in the Venture B-13 well is slightly more mature, with an Ro of 1.0. The sampled interval in the Mic Mac H-86 is much more mature, with an Ro of approximately 2.0. These values are consistent with the estimates of argon loss for these samples (which also indicate that the Mic Mac H-86 sample is considerably more mature than the Venture B-13 or B-43 samples). The fact that the Mic Mac H-86 sample has experienced an argon loss of only 15 to 30 percent at an Ro of 2.0 (below the wet gas floor) indicates that the argon geochronometer is not a sensitive indicator of thermal maturity for sediments that are within the oil window (Ro of 0.5 to 1.35; Dow, 1977).

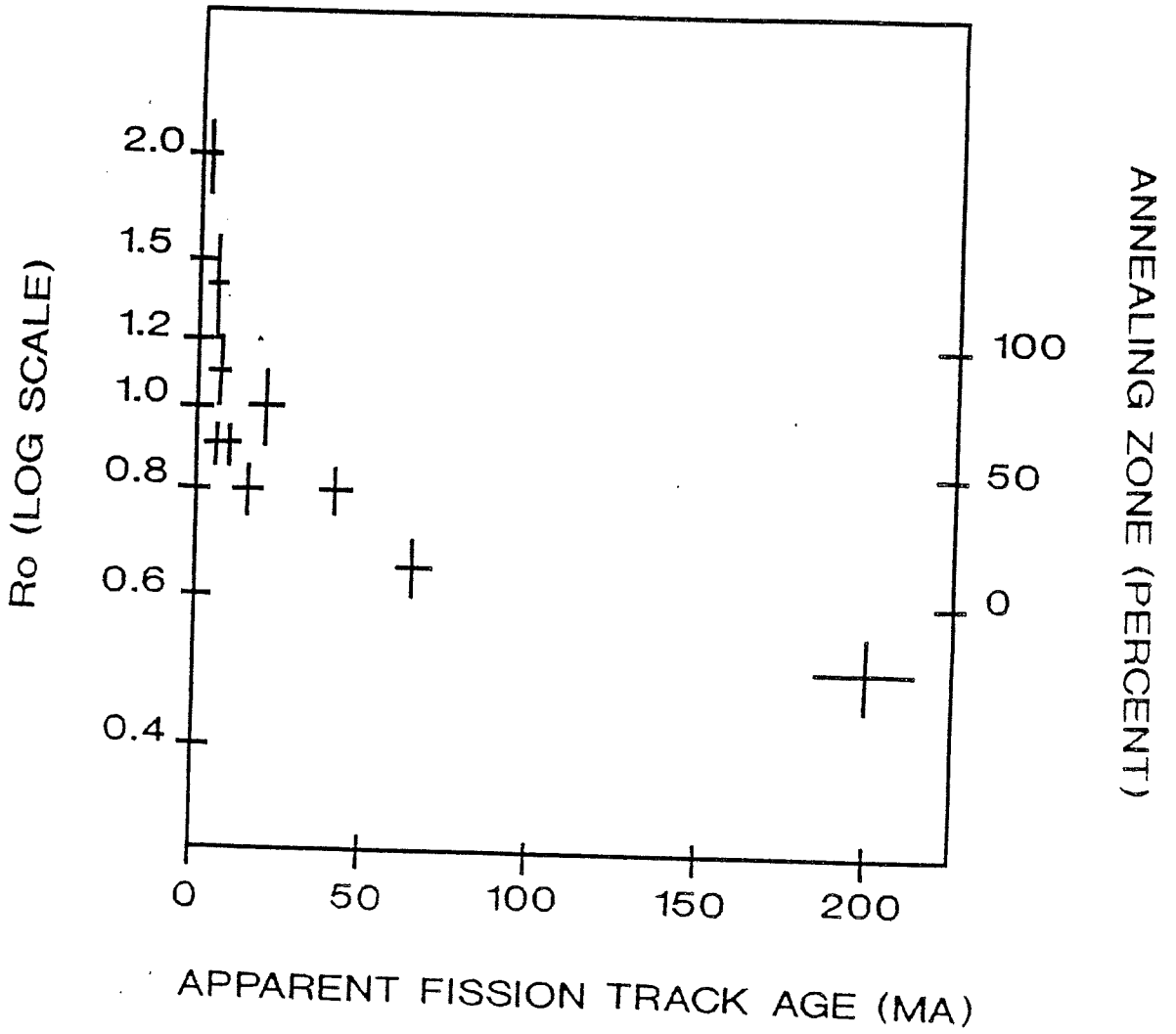

Figure 5.2. A plot of vitrinite reflectance versus fission track age for 10 samples from the Scotian Basin. Ro values are from Avery (1978, 1983, 1985, 1986, 1988).

5.2 Depositional model

The provenance arguments presented in Chapters 3 and 4 are here used to construct depositional models for the Scotian Basin. When these arguments are combined with regional tectonic interpretations based on reflection seismic studies (Marillier et al., 1989, Keen et al., in press) and dynamic finite element modelling studies (Braun and Beaumont, in press) a more complete understanding of the thermal and tectonic evolution of the basin is obtained. To summarize, the main points of the provenance arguments are as follows:

1) The muscovite and K-feldspar argon spectra of the Mohican Formation samples indicate Acadian-age source rocks. Uranium concentrations in apatite from Mohican Formation samples are also similar to those of Acadian-age intrusions on the Nova Scotian mainland, and this area is proposed to have been the source region for the Mohican Formation.

2) The K-feldspar argon spectrum from a Mic Mac Formation sample gave step ages that range from Late Precambrian to Early Devonian. Apatite samples from the Mic Mac Formation are generally intermediate between those of the Mohican and Missisauga Formations.

3) The muscovite argon spectra of the Missisauga Formation samples indicate Taconian-Acadian-age source rocks. The K-feldspar argon spectra gave Late Precambrian ages that indicate Grenvillian-age sources for the Missisauga Formation.

Some justification of the assertion that the source of the Mohican Formation was located on mainland Nova Scotia can be obtained from

the finite element models of Braun and Beaumont (in press). In these models, rifting of passive (Atlantic-type) margins and development of a breakup unconformity (Falvey, 1974) may be accompanied by elevation of the rift flanks. Model predictions indicate that the wavelength of the rift flanks is of the order of 100 - 200 km, and the elevation of the flanks is approximately 1 km. Figure 5.3 (from Braun and Beaumont, in press) diagramatically illustrates this situation. The rift flanks may become the source for syn-rift, and early post-rift sediments. The elevation of the rift flanks may persist for up to 50 Ma after the cessation of active rifting (Weissel and Karner, in press). As was discussed in Chapter 1, within the Scotian Basin the breakup unconformity developed at 190 - 200 Ma, and the age of the Mohican Formation is 180 - 200 Ma (Wade and McLean, in press). Thus, the Mohican Formation represents the earliest regional sedimentation; sedimentation that overlapped both the rift grabens and the intervening basement highs.

Figure 5.4 (modified from Wade and McLean, in press) illustrates the model for sedimentation of the Mohican Formation. In the figure the erosional edge of the top of the Jurassic represents the level of erosion approximately 50 Ma after active rifting ceased. Northwest of this line was the uplifted flank of the rift basin. Southeast of the line is the rift basin, and the arrows indicate the direction of sediment transport (dip direction).

A model for the deposition of the Missisauga Formation and the overlying Logan Canyon Formation is quite different from that

proposed for the Mohican Formation. During the Latest Jurassic and Early Cretaceous, the zones of active rifting had progressed to the eastern edge of the Grand Banks south of Newfoundland, as Iberia and North America began to separate. A major angular (breakup) unconformity (the Avalon Unconformity, Jansa and Wade, 1975) also developed in association with this rifting phase. The uplift and deformation were most severe in the region of the Grand Banks (the Avalon Uplift), over 500 km to the northeast of the Scotian Basin. Below the unconformity are deformed Jurassic sediments preserved in structural basins bounded by faulted basement blocks, while above it are relatively flat-lying Lower Cretaceous (rift flank derived ?) sediments (Wade and McLean, in press). Amoco and Imperial (1973) correlated a Lower Cretaceous sandstone interval above the unconformity with the Missisauga Formation on the Scotian Shelf.

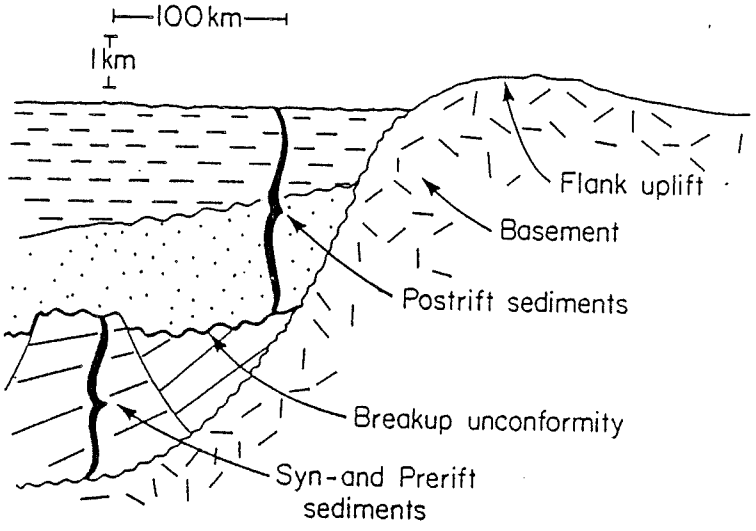

Figure 5.3. Diagrammatic illustration of a simple rifted continental margin showing the relationship between the breakup unconformity and rift flank uplift (from Braun and Beaumont, in press).

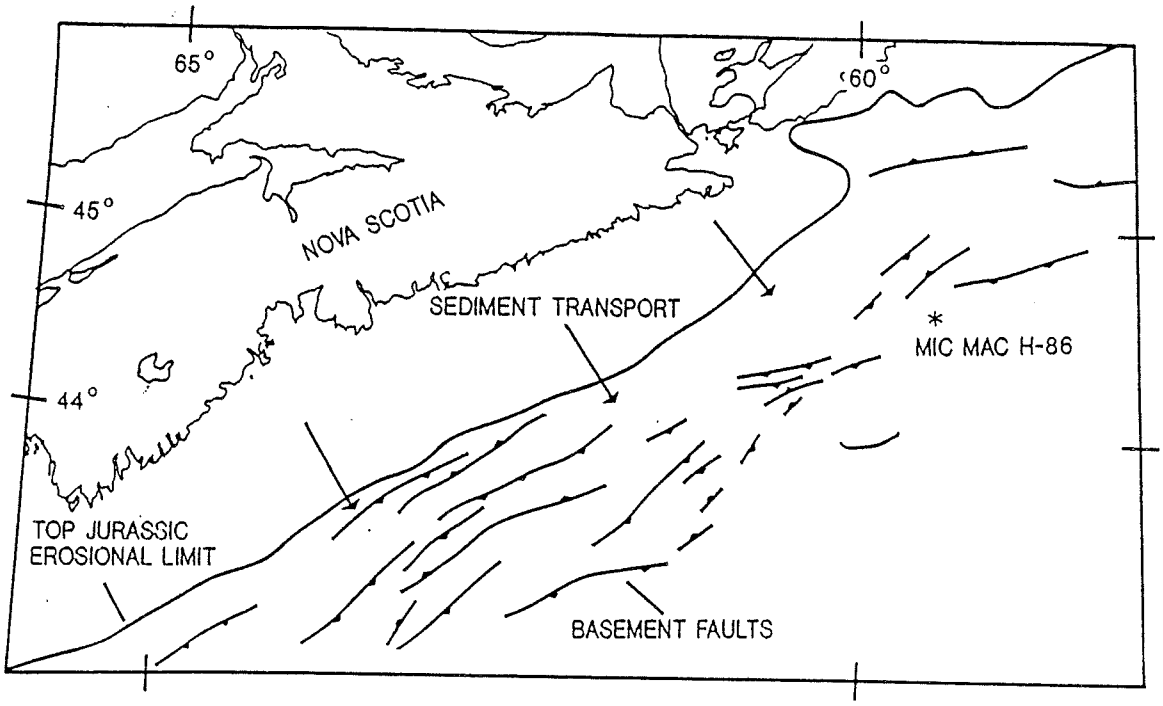

Figure 5.4. Depositional model for the Mohican Formation. The deposition of the Mohican Formation can be approximated by a simple flank uplift model (compare to Figure 5.3).

As was indicated in Chapter 1, the Lower Cretaceous was a time of low relative sea level in the Scotian Basin, and the Missisauga Formation was deposited under alluvial plain and delta facies conditions. The river system that deposited the Missisauga (and Logan Canyon) Formation(s) must have occupied approximately the same channels as the northern portion of the Cabot Strait and Gulf of St. Lawrence, and drained much of the northeast part of the Canadian Shield (Wade and McLean, in press), in particular the Grenville Province, which forms the eastern flank of the Canadian Shield from southern Ontario and New York State to the east coast of Labrador (Wynne-Edwards, 1972; Moore, 1986), thus accounting for the Late Precambrian ages of the Missisauga Formation K-feldspar argon spectra. The southeastern edge of the Grenville Province is presently located approximately 800 km northwest of Sable Island. However, many inliers of Grenvillian aged rocks also occur in the New England States, and Maritime Provinces, indicating that the former extent of the Grenville must have been greater than at present. Within the Maritime Provinces, Barr et al., 1987, ascribe the Blair River Complex in northeastern Cape Breton Island, to the Grenville Province. Barr et al., 1987, also suggest that the Blair River Complex may be correlative with the Grenvillian rocks exposed in the Long Range Inlier and the Indian Head Range Complex of western Newfoundland (Williams, 1978).

Figure 5.5 illustrates the depositional model for the Missisuaga Formation. The figure also shows the approximate distribution of the

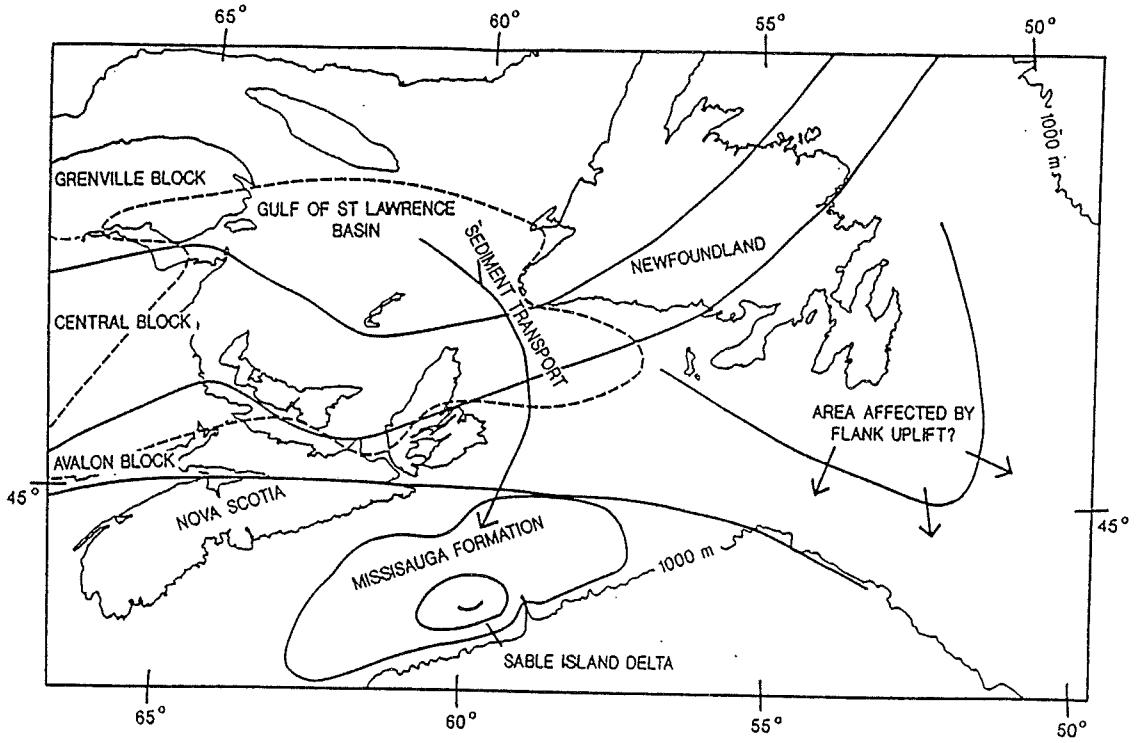

Figure 5.5. Depositional model for the Missisauga Formation. This formation was deposited under fluvio-deltaic conditions, different from those that prevailed during deposition of the Mohican Formation. The figure also shows the positions of the major crustal blocks in the sediment source areas (from Marillier et al. (1989), and the region that may have been affected by flank uplift at this time.

basement terranes in the region proposed as the source area for the Missisauga Formation sediments (from Marillier et al., 1989). Much of this same region is overlain by the Upper Carboniferous Gulf of St.

Lawrence Basin (Bradley, 1982), the approximate outline of which is also shown in Figure 5.5. The Gulf of St. Lawrence Basin contains sediments that have Pennsylvanian - Permian (van de Poll, 1973) depositional ages. The upper surface of the sediments is an erosional unconformity, and based on coal rank studies by Hacquebard (1979, 1986) it has been estimated that between 2.2 and 3.7 km of sediments have been eroded from the basin. Paleocurrent analyses (van de Poll, 1973) indicate that the source of these Carboniferous sediments was located southwest of the basin, but the detrital thermal signature of these sediments is not known. It is possible that they were ultimately derived from Grenville-aged sources located in the Adirondacks and that a fraction of the Missisauga Formation sediments are reworked Gulf of St. Lawrence Basin sediments. The timing of the erosion of the basin is crucial to the feasibility of this hypothesis. If the sediments were eroded during the Permian - Triassic Periods, then the basin could not have been the source of the Early Cretaceous Missisauga Formation. If however, deposition in the Gulf of St. Lawrence continued until the Late Triassic or Early Jurassic period, and uplift and erosion of these sediments did not begin until the Cretaceous, then it is quite likely that the Missisauga Formation would contain a significant fraction of reworked Gulf of St. Lawrence Basin sediments.

It is possible that the Avalon Uplift may have also contributed a fraction of the Missisauga Formation sediments. It is clear from the argon spectra that the sources of the K-feldspars and micas of the Missisauga Formation had different thermal histories. Because the

transport of micas is mainly by flotation, they could be expected to travel further than sediments transported by traction (e.g. feldspars). The Avalon Uplift, which forms part of the Avalon terrane (Williams, 1979) may have been the source of the micas in the Missisauga Formation.

5.3 Conclusions and recommendations

Based on the data presented in this chapter the following conclusions can be made.

1. There is general agreement between the A.I. and fission track geothermometers. Both of these indices record that the level of maturity of the samples from the Mic Mac J-77 and Erie D-26 wells are greater than that that would be predicted by simple burial subsidence heating. The A.I. and fission track data are useful as maturation indices to a depth of approximately 4 km in the Scotian Basin. At depths greater than 4 km A.I. reactions are complete and apatite fission track ages are totally reset.

2. At depths of 4 km or less K-feldspar argon ages are essentially unaffected by burial heating, and therefore the argon maturation index does not overlap with the A.I. (and apatite fission track) indices.

3. There is also good general agreement between the vitrinite reflectance and fission track geothermometers. The fission track annealing zone for the Scotian Basin samples appears to occur over a lower and slightly narrower range of Ro values than does the annealing zone suggested by Gleadow and Harrison (1986), however,

more fission track age determinations are required before the significance of this difference can be properly assessed.

4. A general agreement also exists between the K-feldspar argon and vitrinite maturation indices. Both of these indices record that the interval sampled in the Mic Mac H-86 well is more mature than any other in this study. At depths of greater than 4 km, the K-feldspar argon and vitrinite indices are better suited to determine thermal maturation levels than the A.I. and fission track indices.

5. The deposition of the Mohican Formation conforms well to a model of simple flank uplift of Acadian-age sources on the Nova Scotian mainland.

6. The deposition of the Missisauga Formation can be approximated by a slightly more complex fluviodeltaic model that combines a sediments from two sources. K-feldspars are dominantly derived from the Grenville Province of the Canadian Shield. The micas may be derived from the Avalon Uplift, south of Newfoundland.

This study has attempted to demonstrate the viability of the apatite fission track and K-feldspar argon methods as useful maturation indices for hydrocarbon-bearing strata. To this end the study has achieved some success. However, in attempting to obtain samples from depths where both apatite fission track annealing and K-feldspar argon diffusion could be seen, the optimal track annealing and argon diffusion zones were missed (because they do not substantially overlap). Fission track annealing occurs mainly at depths of less than 4 km, but at this depth argon diffusion is only beginning to occur.

Samples obtained from depths of less than 4 km are needed to better define the track annealing zone. The Mohican I-100, Glennelg N-49 and E-58/E-58A, Alma K-85, and Penobscot B-41 wells (and several others) have conventional sandstone cores between 2 and 4 km depth (see: COGLA, 1987, Offshore Schedule of Wells 1966-1986). In contrast, samples obtained from depths of 4 km or more are needed to better define the zone of K-feldspar argon diffusion. The Venture B-52, and Arcadia J-16 wells both contain conventional cores obtained at depths of greater than 5 km (COGLA, 1987), and appear to be suitable for this purpose. It is also necessary to obtain more samples from relatively shallow depths in order to obtain more information about the provenance of the sampled formations. This information is needed both to constrain models of basin evolution as well as to determine the initial (detrital) fission track or argon signatures to calculate the extent of fission track annealing and argon diffusion for the deeper samples.

It is also necessary to obtain sandstone drillcore from wells drilled in the Gulf of St. Lawrence Basin for apatite fission track study. Fission track (uplift and cooling) ages of samples from this region would determine when the erosion of the Gulf of St. Lawrence Basin occurred, and whether this basin could have acted as a source for the sediments of the Missisauga Formation.

6 Appendix 1: Sample preparation

Hard samples were first crushed to pass through a 1 mm (no. 18 mesh) sieve using a cast-iron mortar and pestle. These samples were then ground and sieved to a maximum grain size of 250 microns (no. 60 mesh) using a large ceramic mortar and pestle. Soft samples were simply crushed and ground down to their constituent grains using the ceramic mortar and pestle. Material finer than 125 microns (no. 120 mesh) was sieved out, and only material ranging in size between 250 and 125 microns (no. 60 to no. 120 mesh) was processed further. Samples were then placed in large beakers and flooded with a jet of water to remove adhering dust and clay particles. After the sample grains had sunk in the muddy water, it was decanted. The procedure was repeated until the water remained clear. The samples were then rinsed with distilled water and left to dry overnight.

Several sandstone samples contained abundant, large (up to 1 cm diameter), detrital grains of mica. One biotite and four muscovite separates were also prepared for argon analysis. (Only one biotite separate was made because biotite was a generally less abundant component of the sandstones than muscovite, and was invariably quite altered.) The micas and other flat grains in the five samples were first concentrated using a paper slide. This method involved pouring a small amount of sand in a line across the top of a piece of paper, which was then held at an angle of about 30° and given several vigorous left-right shakes. Blocky or round grains rolled down the

paper (onto a clean surface) but flat grains did not. The flat grains were then dumped onto another clean surface, and the procedure repeated until the entire sample had been treated in this way.

The concentrates were passed through a Frantz isodynamic magnetic separator (set as follows; current = 0.8 amps, forward tilt = 15°, side tilt = 10°, vib. on 0.9) to separate muscovite from more magnetic grains such as chlorite and biotite. Relatively unaltered muscovite grains were hand-picked at 40X magnification using a Zeiss binocular microscope and a moistened Grumbacher 00 camel's-hair brush. A minimum sample size of 30 mg was obtained for each muscovite separate.

Microcline and orthoclase have specific gravities of 2.54 to 2.57, whereas that of quartz is 2.65 (Hurlbut and Klein, 1977). A solution consisting of 70 wt. percent sodium-polytungstate salt ($3Na_2WO_4 \cdot 9WO_3 \cdot H_2O$) and 30 wt. percent distilled water has a specific gravity of approximately 2.58 at 20°C. In this solution K-feldspars form part of the light fraction, whereas quartz and most other minerals sink, thereby separating the K-feldspars. The actual density of the solutions used to perform density separations were determined with a set of glass density-buttons.

Approximately 500 ml of sodium-polytungstate solution was poured into a sealable 1-liter separatory funnel mounted on a ring stand. The sample grains were then added and the mixture stirred vigorously with a plastic rod for 30 seconds. Enough additional solution was added to

fill the funnel, and the mixture was stirred gently for another 30 seconds. The funnel was then sealed to prevent evaporation and left to stand for 10 minutes, by which time a visible separation of the heavy and light fractions had occurred. Some of the light fraction however, were higher-density grains that floated as a result of surface tension in the solution. The top of the solution was therefore stirred again, very gently, to sink most of these grains, and the funnel was resealed and left to stand for an additional 10 minutes.

The two fractions were then filtered into funnels containing paper basket-type coffee filters. (Evaporation of sodium-polytungstate causes a marked increase in its viscosity and density. The slow filtration rate of conventional filter paper makes it unsuitable for filtering this heavy liquid.) After the filtration was complete, the solid residue was rinsed thoroughly with distilled water to remove all traces of the sodium-polytungstate and allowed to dry overnight. The rinse water was saved in a large beaker, and the heavy liquid in it reclaimed by evaporation.

The following staining technique, using sodium-cobaltinitrate, was employed as an aid to identification of grains of K-feldspar. Sodium-cobaltinitrate stains K-feldspar a bright yellow and sodium-feldspar white. The process involves the use of a strong acid and must be done in a fume-hood. A few drops of mixed epoxy were put on one end of a glass slide. With a second slide, the epoxy was smeared along the length of the first slide to make a very thin, uniform layer. A few (approx. 50 to 200) grains of sample were

sprinkled onto one area of the epoxy layer, and a few grains of a known K-feldspar (used to check that the staining was successful) were sprinkled onto another.

The epoxy was allowed to harden overnight. The mineral grains were then etched by filling a small (30 ml) teflon beaker with 48% hydrofluoric acid (HF) and then placing the slide in the acid fumes (grains downward) on top of the beaker for 2 minutes. The slide was then removed with tweezers and immersed into another small beaker containing a saturated solution of sodium-cobaltinitrate for 15 to 30 seconds. After two quick immersions in a large beaker of water (to rinse off excess stain), the slide was given a final rinse with acetone and allowed to dry.

The results of the staining showed that the purity of the separates was generally less than 100 percent. The samples were therefore hand-picked to improve their purity prior to submission for irradiation. The stained portion of each separate was used as a guide to the amount of hand-picking required in each case. Hand-picking was done at 40X magnification using a Zeiss binocular microscope and a moistened Grumbacher 00 camel's-hair brush. Coalified matter, polymineralic grains, sodium-feldspar, quartz, and highly-altered K-feldspar were removed. A minimum sample size of 30 mg was obtained.

The dried heavy-fractions from the previously-described sodium-polytungstate density separations were treated with the heavy-liq-

uids tetrabromoethane (TBE; specific gravity = 2.96) and methylene-iodide (MI; specific gravity = 3.3), and the Frantz isodynamic magnetic separator to separate apatite. MI, and especially TBE are toxic-carcinogenic liquids (Hauff and Airey, 1980), and therefore must only be used in a fume-hood and while wearing the proper protective clothing (i.e. goggles, filter-mask, lab coat, and rubber gloves).

The samples were first passed through the Frantz (set as follows; current = 1.0 amps, forward tilt = 15°, side tilt = 10°, vib. on 0.7). This was done to remove most of the more magnetic fraction of the sample from the nonmagnetic (apatite-bearing) fraction in order to reduce sample volume and hence the amount of heavy-liquid needed for density separation.

The TBE separation was done using the same procedure as described for sodium-polytungstate, except for the following:

-the liquid was not diluted,

-Whatman #4 filter-paper was used,

-rinsing of the residue was done using copious quantities of acetone (the acetone is saved, and the TBE in it reclaimed),

-samples were left to dry for a minimum of 2 days in the fume-hood. This separation produced large (>90%) light-fractions, and small (<10%) heavy-fractions. The light-fractions were stored in a fume-hood. The heavy-fractions were treated further, using MI.

The procedure for using MI to split the sample at a specific gravity of 3.3 is the same as that used for the TBE, except for the

following:

-due to the small sample size, a 50 ml separatory funnel and smaller-diameter funnel and filter-paper were used. After the samples were dried, the fraction with a specific gravity range of 2.96 to 3.3 (heavy-TBE, light-MI) was passed through the Frantz again (set as follows; current = 1.5 amps, forward tilt = 15°, side tilt = 10°, vib. set at 0.7). Apatite was again concentrated in the nonmagnetic fraction. This fraction was hand-picked for apatite grains.

Apatite grains were hand-picked at 40X magnification using a Zeiss binocular microscope and a moistened Grumbacher 00 camel's-hair brush. Recognition of apatite grains was easily accomplished during hand-picking owing to the prominent hexagonal crystal shape, resinous luster, and relatively low index of refraction of the mineral. In certain cases, where recognition was made more difficult by rounding of the crystal shape, apatite's solubility in weak HCl (grains dissolve in approximately 10 minutes, without producing any gas bubbles) was used as an aid to identification.

7 Appendix 2: Argon age calculations summary sheets

H-86 Biotite

°C	mV 39	% 39	AGE(Ma)	% ATMOS	37/39	40/36	39/36	% IIC
500	87	25	136 +/- 1	50	-	588	8.1	-
550	49	14	172 +/- 1	19	-	1561	27.7	-
600	57	16	204 +/- 1	14	-	2045	31.9	-
650	44	13	213 +/- 1	14	-	2128	32	-
700	20	6	221 +/- 1	15	-	2027	29	-
750	11	3	227 +/- 1	18	-	1647	22	-
800	9	3	235 +/- 2	19	-	1563	19.9	-
850	23	7	250 +/- 1	14	-	2109	26.6	-
900	24	7	250 +/- 1	14	-	2165	27.4	-
950	16	5	245 +/- 1	15	-	1936	24.7	-
1000	8	2	236 +/- 3	27	-	1075	12.2	-

TOTAL GAS AGE = 195 Ma

J = 2.19E-03

ERROR ESTIMATES AT ONE SIGMA LEVEL

37/39,40/36 AND 39/36 Ar RATIOS ARE CORRECTED FOR INTERFERING ISOTOPES

% IIC - INTERFERING ISOTOPES CORRECTION

H-86 Muscovite

°C	mV 39	% 39	AGE(Ma)	% ATMOS	37/39	40/36	39/36	% IIC
500	8	7	133 +/- 4	58	-	509	6.1	-
550	2	2	172 +/- 10	26	-	1116	17.9	-
600	7	6	235 +/- 2	7	-	3948	57.8	-
650	5	5	290 +/- 3	6	-	4676	55.1	-
700	8	6	339 +/- 2	2	-	14610	152.3	-
750	14	12	353 +/- 1	2	-	16882	168.6	-
800	16	14	360 +/- 1	1	-	20667	203	-
850	18	15	363 +/- 1	<1	-	39666	389.1	-
900	17	14	361 +/- 1	2	-	15619	152.2	-
950	20	17	359 +/- 1	3	-	8818	85	-
1000	2	1	349 +/- 8	26	-	1138	8.6	-

TOTAL GAS AGE = 329 Ma

J = 2.2E-03

H-86P K-feldspar

°C	mV 39	% 39	AGE(Ma)	% ATMOS	37/39	40/36	39/36	% IIC
530	65	28	129 +/- 1	26	-	1142	28	-
580	15	6	235 +/- 2	10	-	3080	48.9	-
640	13	5	281 +/- 2	9	-	3359	44.5	-
690	14	6	277 +/- 1	17	-	1724	21	-
740	8	3	280 +/- 3	12	-	2518	32.4	-
790	16	7	278 +/- 1	8	-	3590	48.3	-
840	8	4	270 +/- 3	10	-	2909	39.6	-
890	11	5	274 +/- 1	10	-	2934	39.4	-
940	10	4	276 +/- 2	16	-	1794	22.1	-
990	8	3	277 +/- 2	17	-	1719	20.9	-
1050	13	5	273 +/- 1	14	-	2058	26.4	-
1100	15	6	274 +/- 1	8	-	3575	49	-
1150	19	8	275 +/- 1	7	-	4417	61.3	-
1200	18	8	277 +/- 1	10	-	3083	41.1	-
1250	3	1	279 +/- 4	23	-	1290	14.5	-

TOTAL GAS AGE = 234 Ma

J = 2.45E-03

H-86I K-feldspar

°C	mV 39	% 39	AGE(Ma)	% ATMOS	37/39	40/36	39/36	% IIC
500	47	15	62 +/- 1	21	-	1440	79.6	-
550	15	5	126 +/- 1	7	-	4119	129.1	-
600	33	11	190 +/- 1	5	-	6180	130	-
650	24	8	273 +/- 1	5	-	5582	79.1	-
700	30	10	274 +/- 1	4	-	6793	97.1	-
750	22	7	269 +/- 1	8	-	3838	53.9	-
800	23	7	257 +/- 1	14	-	2101	28.8	-
850	14	4	257 +/- 1	24	-	1252	15.2	-
900	10	3	263 +/- 1	30	-	981	10.7	-
950	18	6	264 +/- 1	45	-	663	5.7	-
1000	16	5	258 +/- 2	71	-	417	1.9	-
1050	7	2	245 +/- 6	82	-	359	1	-
1100	8	3	238 +/- 6	87	-	341	.7	-
1140	10	3	227 +/- 11	90	-	330	.6	-
1300	33	11	-	-	-	-	-	-

J = 2.45E-03

J-77 Muscovite

°C	mV 39	% 39	AGE(Ma)	% ATMOS	37/39	40/36	39/36	% IIC
500	2	2	224 +/- 8	42	-	709	6.9	-
550	<1	<1	406 +/- 13	13	-	2330	17.7	-
600	1	1	476 +/- 10	3	-	8598	60.6	-
650	2	2	474 +/- 5	3	-	9342	66.3	-
700	7	6	473 +/- 2	2	-	16402	118.5	-
750	9	8	466 +/- 1	2	-	15305	112.2	-
800	12	11	452 +/- 1	2	-	19532	148.9	-
850	17	16	439 +/- 1	1	-	20774	163.8	-
900	23	21	459 +/- 1	1	-	22505	169.2	-
950	24	22	459 +/- 1	2	-	11866	88	-
1000	9	8	428 +/- 1	9	-	3153	23.5	-
1050	4	4	416 +/- 4	36	-	827	4.5	-

TOTAL GAS AGE = 449 Ma

J = 2.207E-03

J-77I K-feldspar

°C	mV 39	% 39	AGE(Ma)	% ATMOS	37/39	40/36	39/36	% IIC
500	24	10	631 +/- 1	8	-	3779	20.3	-
550	8	3	642 +/- 2	4	-	8372	46.2	-
600	17	7	714 +/- 3	4	-	7165	34.6	-
650	15	6	732 +/- 1	5	-	6029	28	-
700	28	11	812 +/- 2	3	-	8471	35.2	-
750	13	5	824 +/- 2	9	-	3324	12.8	-
800	6	2	717 +/- 8	28	37.2	1051	3.7	4
850	16	7	886 +/- 4	10	-	2905	10	-
900	22	9	933 +/- 2	12	-	2374	7.5	-
950	13	5	985 +/- 2	15	-	1914	5.4	-
1000	22	9	976 +/- 2	25	-	1177	3	-
1050	15	6	931 +/- 4	41	-	725	1.5	-
1100	12	5	938 +/- 7	49	-	602	1.1	-
1140	10	4	946 +/- 10	55	-	538	.8	-
1300	27	11	-	-	-	-	-	-

J = 2.45E-03

J-77P K-feldspar

°C	mV 39	% 39	AGE(Ma)	% ATMOS	37/39	40/36	39/36	% IIC
500	12	3	761 +/- 2	11	-	2595	10.7	-
550	29	6	599 +/- 1	3	-	8587	51.5	-
600	39	8	707 +/- 1	2	-	13392	66.9	-
650	24	5	803 +/- 1	2	-	14412	61.6	-
700	22	5	845 +/- 2	<1	-	37770	153.6	-
750	35	7	905 +/- 1	<1	-	39306	146.7	-
800	34	7	934 +/- 5	<1	-	32680	116.9	-
850	22	5	956 +/- 1	1	-	28364	98.3	-
900	30	6	995 +/- 1	1	-	25376	83.4	-
950	26	5	1023 +/- 1	2	-	19044	60.2	-
1000	29	6	1020 +/- 1	1	-	23635	75.1	-
1050	23	5	1024 +/- 1	2	-	16464	51.8	-
1100	39	8	1032 +/- 1	1	-	29550	92.7	-
1150	53	11	1037 +/- 1	<1	-	33035	103.3	-
1200	40	8	1041 +/- 1	2	-	13864	42.5	-
1250	16	3	1060 +/- 2	2	-	17218	51.8	-

TOTAL GAS AGE = 935 Ma

J = 2.45E-03

VB-13-2 Muscovite

°C	mV 39	% 39	AGE(Ma)	% ATMOS	37/39	40/36	39/36	% IIC
500	3	1	234 +/- 9	37	-	801	8	-
550	2	<1	293 +/- 9	18	-	1638	16.7	-
600	3	1	367 +/- 6	3	-	9406	88.4	-
650	4	1	356 +/- 5	13	-	2257	19.6	-
700	13	5	366 +/- 1	2	-	14364	137.1	-
750	30	12	369 +/- 1	2	-	19457	184.8	-
800	50	19	366 +/- 1	<1	-	55810	541.8	-
850	43	17	373 +/- 1	<1	-	56104	532.4	-
900	70	27	395 +/- 1	<1	-	34305	304.7	-
950	15	6	369 +/- 1	7	-	4137	37.1	-
1000	15	6	353 +/- 1	8	-	3734	34.8	-
1050	12	5	349 +/- 2	18	-	1616	13.5	-

TOTAL GAS AGE = 372 Ma

J = 2.193E-03

VB-13-5 Muscovite

°C	mV 39	% 39	AGE(Ma)	% ATMOS	37/39	40/36	39/36	% ICC
500	4	2	171 +/- 4	52	-	566	5.9	-
550	3	2	241 +/- 4	21	-	1392	16.8	-
600	4	2	313 +/- 3	18	-	1623	15.3	-
650	6	3	337 +/- 2	5	-	6199	63	-
700	10	5	339 +/- 1	3	-	9096	93.2	-
750	21	11	344 +/- 1	2	-	14297	145.9	-
800	30	16	342 +/- 1	1	-	24675	255.8	-
850	33	17	341 +/- 1	1	-	21959	228.3	-
900	38	20	348 +/- 1	2	-	16932	171.2	-
950	22	12	348 +/- 1	5	-	6421	63	-
1000	9	5	335 +/- 1	8	-	3698	36.5	-
1050	8	4	331 +/- 1	19	-	1576	13.9	-

TOTAL GAS AGE = 337 Ma

J = 2.193E-03

VB-13-1 K-feldspar

°C	mV 39	% 39	AGE(Ma)	% ATMOS	37/39	40/36	39/36	% IIC
510	29	4	453 +/- 1	15	-	1999	12.9	-
560	60	8	315 +/- 1	3	-	9064	99.9	-
600	57	8	458 +/- 1	1	-	20109	149	-
650	66	9	591 +/- 1	<1	-	32387	180.1	-
700	63	9	677 +/- 1	<1	-	29763	140.6	-
750	49	7	753 +/- 2	<1	-	32817	136.6	-
800	68	9	808 +/- 2	<1	-	55690	213.1	-
850	23	3	840 +/- 1	1	-	22837	82.7	-
900	40	5	862 +/- 3	1	-	25665	90	-
950	26	3	886 +/- 1	1	-	28078	95.2	-
1000	25	3	905 +/- 1	1	-	21544	70.9	-
1050	41	6	926 +/- 3	<1	-	189348	613	-
1100	33	5	936 +/- 1	1	-	26898	85	-
1150	37	5	951 +/- 3	1	-	22068	68.2	-
1200	76	10	967 +/- 2	<1	-	37518	114.1	-
1250	35	5	1008 +/- 1	1	-	26644	76.5	-
1300	5	<1	1053 +/- 5	5	-	6194	16.1	-

TOTAL GAS AGE = 761 Ma

J = 2.175E-03

VB-13-2 K-feldspar

°C	mV 39	% 39	AGE(Ma)	% ATMOS	37/39	40/36	39/36	% IIC
450	12	6	563 +/- 3	67	-	443	.9	-
480	9	5	334 +/- 1	15	-	1927	19.8	-
510	12	6	385 +/- 1	10	-	2858	26.5	-
540	12	6	489 +/- 2	8	-	3867	28.3	-
570	11	6	597 +/- 3	8	-	3756	21.7	-
600	10	5	676 +/- 2	5	-	6080	31.4	-
630	15	8	737 +/- 2	11	-	2739	11.9	-
660	9	5	769 +/- 4	13	-	2215	8.9	-
690	11	6	820 +/- 3	8	-	3799	15	-
720	19	9	888 +/- 4	4	-	7186	26.7	-
750	12	6	935 +/- 4	6	-	4571	15.5	-
800	11	5	968 +/- 5	8	-	3577	11.4	-
850	10	5	994 +/- 8	8	-	3562	10.9	-
900	11	6	997 +/- 6	8	-	3832	11.8	-
950	14	7	979 +/- 4	9	-	3469	10.8	-
1000	6	3	1003 +/- 5	11	-	2751	8.1	-
1050	6	3	1030 +/- 9	25	-	1182	2.8	-
1100	6	3	1023 +/- 10	47	-	630	1	-

TOTAL GAS AGE = 790 Ma

J = 2.47E-03

VB-43-1 K-feldspar

°C	mV 39	% 39	AGE(Ma)	% ATMOS	37/39	40/36	39/36	% IIC
450	4	<1	1423 +/- 8	13	-	2198	3.4	-
480	3	<1	727 +/- 8	14	-	2109	7.9	-
520	8	1	805 +/- 3	6	-	4713	17	-
550	9	2	545 +/- 2	6	-	4772	27.6	-
580	18	3	564 +/- 1	4	-	7726	44	-
610	16	3	660 +/- 2	4	-	7720	36.5	-
640	10	2	720 +/- 2	4	-	7320	31.1	-
670	16	3	773 +/- 2	2	-	13009	51.6	-
700	23	4	799 +/- 1	1	-	22215	85.5	-
750	26	4	851 +/- 1	1	-	27106	96.7	-
800	33	5	893 +/- 1	2	-	17911	59.7	-
850	27	4	920 +/- 1	2	-	17870	57.4	-
900	41	7	933 +/- 2	1	-	23357	74	-
950	44	7	961 +/- 3	<1	-	148789	458.8	-
1000	24	4	990 +/- 1	1	-	24199	71.1	-
1050	53	9	1031 +/- 2	1	-	21673	60.2	-
1100	74	12	1074 +/- 2	<1	-	31543	83.4	-
1160	66	11	1119 +/- 2	<1	-	42185	106	-
1200	49	8	1147 +/- 3	1	-	26653	64.5	-
1250	42	7	1161 +/- 3	1	-	27204	64.8	-
1300	11	2	1148 +/- 3	4	-	6679	15.6	-

TOTAL GAS AGE = 986 Ma

J = 2.175E-03

VB-43-4 K-feldspar

°C	mV 39	% 39	AGE(Ma)	% ATMOS	37/39	40/36	39/36	% IIC
500	12	2	649 +/- 2	11	-	2597	11.5	-
530	12	2	295 +/- 2	8	-	3930	44.5	-
560	23	4	357 +/- 1	3	-	9343	89.8	-
600	26	5	479 +/- 1	2	-	14888	104.2	-
650	41	7	579 +/- 1	2	-	19400	109.6	-
700	37	7	669 +/- 1	1	-	23177	110.7	-
750	28	5	739 +/- 1	1	-	23979	101.6	-
800	21	4	773 +/- 1	<1	-	48035	194	-
850	32	6	786 +/- 1	2	-	13081	50.9	-
950	43	8	810 +/- 1	2	-	11859	44.3	-
1000	37	7	823 +/- 1	4	-	6914	24.8	-
1050	38	7	849 +/- 2	3	-	11426	40.2	-
1100	58	11	878 +/- 2	2	-	15509	52.7	-
1150	58	11	888 +/- 2	2	-	16351	54.9	-
1200	48	9	925 +/- 2	1	-	24182	77.5	-
1250	31	6	980 +/- 1	3	-	11469	33.6	-

TOTAL GAS AGE = 773 Ma

J = 2.175E-03

C-67-1A K-feldspar

°C	mV 39	% 39	AGE(Ma)	% ATMOS	37/39	40/36	39/36	% IIC
450	24	3	750 +/- 5	18	-	1664	6.5	-
480	12	2	647 +/- 2	2	-	15210	85.3	-
510	16	2	654 +/- 3	1	-	21497	119.8	-
540	22	3	701 +/- 2	<1	-	84288	436.4	-
570	32	4	763 +/- 5	<1	-	52874	246.7	-
600	41	5	798 +/- 5	<1	-	37937	167	-
630	47	6	846 +/- 15	<1	-	40614	166.3	-
660	43	5	858 +/- 8	1	-	29039	116.6	-
690	55	7	829 +/- 8	<1	-	87064	367.5	-
720	122	15	819 +/- 5	<1	-	39372	168	-
750	15	2	830 +/- 5	<1	-	31387	131.3	-
800	39	5	825 +/- 6	1	-	21122	88.7	-
850	40	5	834 +/- 6	2	-	17450	72	-
900	52	6	840 +/- 4	2	-	19190	78.7	-
950	54	7	868 +/- 5	2	-	11971	46.6	-
1000	38	5	900 +/- 6	4	-	8108	29.8	-
1050	30	4	904 +/- 6	7	-	4031	14.1	-
1140	45	6	913 +/- 11	9	-	3312	11.3	-
1300	87	11	-	-	-	-	-	-

J = 2.47E-03

C-67-1B K-feldspar

°C.	mV 39	% 39	AGE(Ma)	% ATMOS	37/39	40/36	39/36	% IIC
450	1	<1	842 +/- 52	56	-	526	.9	-
480	<1	<1	818 +/- 65	51	-	585	1.2	-
510	1	<1	876 +/- 18	32	-	909	2.4	-
540	3	1	817 +/- 6	12	-	2376	8.9	-
590	5	2	770 +/- 4	12	-	2568	10.5	-
650	13	5	825 +/- 2	5	-	5423	21.8	-
700	23	9	882 +/- 1	4	-	6866	25.7	-
750	11	5	910 +/- 3	6	-	4620	16.2	-
800	27	11	918 +/- 1	5	-	6217	22	-
850	16	6	928 +/- 13	10	-	3072	10.1	-
900	14	6	935 +/- 5	18	-	1643	4.9	-
950	19	8	954 +/- 10	19	-	1551	4.4	-
1000	18	7	984 +/- 8	13	-	2334	6.9	-
1050	16	6	983 +/- 4	6	-	5301	17	-
1100	12	5	993 +/- 5	8	-	3791	11.7	-
1150	13	5	1003 +/- 5	9	-	3442	10.4	-
1200	12	5	1017 +/- 4	11	-	2573	7.4	-
1250	28	11	993 +/- 5	15	-	1964	5.6	-
1300	15	6	976 +/- 8	19	-	1594	4.4	-

TOTAL GAS AGE = 944 Ma

J = 2.47E-03

C-67-2 K-feldspar

°C	mV 39	% 39	AGE(Ma)	% ATMOS	37/39	40/36	39/36	% IIC
450	13	2	838 +/- 15	32	-	913	2.5	-
480	10	1	673 +/- 6	4	-	7512	39.3	-
510	18	2	679 +/- 10	2	-	14591	77.1	-
540	12	2	740 +/- 15	<1	-	41407	200.2	-
570	13	2	775 +/- 3	<1	-	80222	367.7	-
600	47	6	805 +/- 11	<1	-	55415	241.8	-
630	46	6	830 +/- 6	<1	-	47733	200.5	-
660	36	5	838 +/- 10	2	-	18406	75.6	-
690	39	5	864 +/- 8	<1	-	59246	236.9	-
720	65	8	865 +/- 7	<1	-	140514	563.2	-
750	42	5	850 +/- 6	<1	-	89437	365.7	-
825	46	6	870 +/- 9	<1	-	29893	117.9	-
900	51	7	883 +/- 9	1	-	28850	111.6	-
975	90	12	913 +/- 13	1	-	25605	94.9	-
1050	79	10	916 +/- 3	2	-	14009	51.1	-
1140	90	12	924 +/- 4	4	-	7111	25.1	-
1300	83	11	-	-	-	-	-	-

J = 2.47E-03

D-26-1 K-feldspar

°C	mV 39	% 39	AGE(Ma)	% ATMOS	37/39	40/36	39/36	% IIC
500	12	4	395 +/- 30	75	-	394	.9	-
550	16	5	348 +/- 3	45	-	662	4.2	-
600	32	10	403 +/- 1	24	-	1241	9.3	-
650	34	11	443 +/- 1	24	-	1227	8.2	-
700	32	10	462 +/- 1	22	-	1320	8.6	-
750	28	9	487 +/- 1	18	-	1601	10.4	-
800	19	6	517 +/- 6	15	-	1957	12.3	-
850	13	4	564 +/- 3	22	-	1370	7.2	-
900	14	4	597 +/- 6	22	-	1363	6.7	-
950	9	3	616 +/- 7	25	-	1161	5.2	-
1000	9	3	644 +/- 3	28	-	1068	4.4	-
1050	18	6	658 +/- 6	23	-	1287	5.5	-
1100	23	7	670 +/- 13	24	-	1238	5.1	-
1150	28	9	658 +/- 5	23	-	1291	5.5	-
1200	15	5	658 +/- 5	22	-	1322	5.7	-
1250	16	5	635 +/- 5	27	-	1106	4.7	-

TOTAL GAS AGE = 535 Ma

J = 2.471E-03

ERROR ESTIMATES AT ONE SIGMA LEVEL

37/39,40/36 AND 39/36 Ar RATIOS ARE CORRECTED FOR INTERFERING ISOTOPES

% IIC - INTERFERING ISOTOPES CORRECTION

K-90-2 K-feldspar

°C	mV 39	% 39	AGE(Ma)	% ATMOS	37/39	40/36	39/36	% IIC
450	7	<1	486 +/- 13	82	-	358	.5	-
480	11	2	581 +/- 3	25	-	1166	5.6	-
510	11	2	514 +/- 3	29	-	1024	5.4	-
540	29	4	498 +/- 1	11	-	2691	18.5	-
570	36	5	578 +/- 1	4	-	8009	50.4	-
630	83	12	739 +/- 1	1	-	19926	95.8	-
660	53	7	849 +/- 1	1	.1	20108	81.4	0
690	43	6	876 +/- 2	3	.1	11521	44.3	0
720	24	3	885 +/- 1	3	-	9795	37	-
750	30	4	882 +/- 1	1	-	22648	87.6	-
800	63	9	877 +/- 7	1	-	28663	111.9	-
850	28	4	879 +/- 1	<1	-	122267	479.9	-
900	32	5	871 +/- 1	1	-	24077	94.6	-
950	39	6	883 +/- 1	1	-	22426	86.5	-
1000	26	4	902 +/- 1	1	-	20213	75.9	-
1050	38	5	901 +/- 2	1	-	20049	75.3	-
1100	41	6	914 +/- 1	3	-	11411	41.6	-
1150	36	5	912 +/- 1	3	-	9942	36.2	-
1200	25	4	904 +/- 1	2	-	15445	57.5	-
1250	36	5	918 +/- 4	2	-	15792	57.7	-
1300	14	2	926 +/- 2	3	-	8883	31.6	-

TOTAL GAS AGE = 829 Ma

J = 2.471E-03

8 Appendix 3: Fission track zeta and age calculations summary sheets

Sample C-67-1

CRYSTAL	NS	NI	RATIO	RHO S	RHO I	[U] ppm	AGE (MA)
1	35	21	1.667	8.96E+05	5.38E+05	7	217.0 ± 59.9
2	33	24	1.375	8.45E+05	6.14E+05	8	179.6 ± 48.2
3	20	19	1.053	5.12E+05	4.86E+05	6	137.9 ± 44.2
4	18	20	0.900	4.61E+05	5.12E+05	7	118.1 ± 38.4
5	32	23	1.391	8.19E+05	5.89E+05	8	181.7 ± 49.7
6	33	29	1.138	8.45E+05	7.42E+05	10	149.0 ± 37.9
7	8	7	1.143	2.05E+05	1.79E+05	2	149.6 ± 77.4
8	23	28	0.821	9.81E+05	1.19E+06	16	107.9 ± 30.4
9	120	62	1.935	3.07E+06	1.59E+06	21	251.3 ± 39.3
10	49	27	1.815	1.25E+06	6.91E+05	9	236.0 ± 56.6
11	51	26	1.962	1.31E+06	6.66E+05	9	254.7 ± 61.4
12	32	28	1.143	8.19E+05	7.17E+05	10	149.6 ± 38.7
13	98	50	1.960	2.51E+06	1.28E+06	17	254.5 ± 44.2
14	152	92	1.652	3.89E+06	2.36E+06	31	215.2 ± 28.4
15	25	21	1.190	6.40E+05	5.38E+05	7	155.8 ± 46.1
16	4	3	1.333	1.02E+05	7.68E+04	1	174.2 ± 133.0
	733	480		1.20E+06	7.88E+05	11	

SUMMARY OF STATISTICS

Variance of Square root of NS = 7.7133
Variance of Square root of NI = 3.3865
Correlation coefficient (R for NS vs. NI) = 0.9685

Chi^2 = 19.46507 with 15 degrees of freedom. TEST PASS

AGE CALCULATION

Zeta factor used = 10594.0± 439.0
Glass dosimeter = SRM614
ND counted = 1600
RHOD D for glass = 2.500E+04 ± 0.625E+03
Area of 1 QUAD = 1.5625E-06
Pooled NS/NI = 1.527 ± 0.090
Mean NS/NI = 1.405 ± 0.098

POOLED AGE

199 ± 15.2 MA

MEAN AGE

183 ± 15.6 MA

Sample D-26-1

CRYSTAL	NS	NI	RATIO	RHO S	RHO I	[U] ppm	AGE (MA)
1	5	8	0.625	1.28E+05	2.05E+05	3	81.6 ± 46.5
2	43	70	0.614	1.10E+06	1.79E+06	24	80.2 ± 15.5
3	41	57	0.719	1.05E+06	1.46E+06	20	93.8 ± 19.2
4	26	40	0.650	6.66E+05	1.02E+06	14	84.8 ± 21.4
5	11	21	0.524	2.82E+05	5.38E+05	7	68.4 ± 25.5
6	5	4	1.250	1.28E+05	1.02E+05	1	162.2 ± 108.8
7	83	121	0.686	2.12E+06	3.10E+06	42	89.5 ± 12.8
8	70	94	0.745	1.79E+06	2.41E+06	32	97.1 ± 15.3
9	17	14	1.214	4.35E+05	3.58E+05	5	157.6 ± 56.9
10	3	8	0.375	7.68E+04	2.05E+05	3	49.1 ± 33.2
	304	437		7.78E+05	1.12E+06	15	

SUMMARY OF STATISTICS

Variance of Square root of NS = 6.9031
Variance of Square root of NI = 9.9860
Correlation coefficient (R for NS vs. NI) = 0.9905

Chi^2 = 5.418117 with 9 degrees of freedom. TEST PASS

AGE CALCULATION

Zeta factor used = 10594.0± 439.0
Glass dosimeter = SRM614
ND counted = 1600
RHOD D for glass = 2.480E+04 ± 0.620E+03
Area of 1 QUAD = 1.5625E-06
Pooled NS/NI = 0.696 ± 0.052
Mean NS/NI = 0.740 ± 0.093

POOLED AGE

90.7 ± 8.1 MA

MEAN AGE

96.5 ± 13.0 MA

Sample D-26-2

CRYSTAL	NS	NI	RATIO	RHO S	RHO I	[U] ppm	AGE (MA)
1	35	41	0.854	8.96E+05	1.05E+06	14	110.7 ± 25.5
2	51	67	0.761	1.31E+06	1.72E+06	23	98.8 ± 18.4
3	34	47	0.723	8.70E+05	1.20E+06	16	94.0 ± 21.2
4	44	75	0.587	1.13E+06	1.92E+06	26	76.3 ± 14.5
5	43	77	0.558	1.10E+06	1.97E+06	27	72.7 ± 13.8
6	34	67	0.507	8.70E+05	1.72E+06	23	66.1 ± 13.9
7	70	105	0.667	1.79E+06	2.69E+06	36	86.6 ± 13.4
8	7	12	0.583	1.79E+05	3.07E+05	4	75.9 ± 36.1
9	16	18	0.889	4.10E+05	4.61E+05	6	115.3 ± 39.6
	334	509		9.50E+05	1.45E+06	20	

SUMMARY OF STATISTICS

Variance of Square root of NS = 2.8502
Variance of Square root of NI = 4.9112
Correlation coefficient (R for NS vs. NI) = 0.9451

Chi^2 = 5.565425 with 8 degrees of freedom. TEST PASS

AGE CALCULATION

Zeta factor used = 10594.0± 439.0
Glass dosimeter = SRM614
ND counted = 1600
RHOD D for glass = 2.470E+04 ± 0.618E+03
Area of 1 QUAD = 1.5625E-06
Pooled NS/NI = 0.656 ± 0.046
Mean NS/NI = 0.681 ± 0.048

POOLED AGE
85.3 ± 7.3 MA

MEAN AGE
88.5 ± 7.5 MA

Sample J-77I

CRYSTAL	NS	NI	RATIO	RHO S	RHO I	[U] ppm	AGE (MA)
1	7	11	0.636	1.79E+05	2.82E+05	5	66.4 ± 32.1
2	15	21	0.714	1.92E+05	2.69E+05	5	74.5 ± 25.2
3	10	9	1.111	2.56E+05	2.30E+05	4	115.5 ± 53.1
4	3	5	0.600	7.68E+04	1.28E+05	2	62.6 ± 45.7
5	4	10	0.400	1.02E+05	2.56E+05	4	41.8 ± 24.7
6	3	5	0.600	7.68E+04	1.28E+05	2	62.6 ± 45.7
7	7	12	0.583	8.96E+04	1.54E+05	3	60.9 ± 29.0
8	3	8	0.375	7.68E+04	2.05E+05	3	39.2 ± 26.5
9	8	10	0.800	2.05E+05	2.56E+05	4	83.4 ± 39.5
10	13	28	0.464	3.33E+05	7.17E+05	12	48.5 ± 16.3
11	15	14	1.071	3.84E+05	3.58E+05	6	111.4 ± 41.4
12	16	34	0.471	1.37E+05	2.90E+05	5	49.2 ± 14.9
13	9	13	0.692	2.30E+05	3.33E+05	6	72.2 ± 31.3
14	5	8	0.625	1.28E+05	2.05E+05	3	65.2 ± 37.2
15	6	20	0.300	1.54E+05	5.12E+05	9	31.4 ± 14.6
16	13	23	0.565	3.33E+05	5.89E+05	10	59.0 ± 20.5
17	14	26	0.538	1.79E+05	3.33E+05	6	56.2 ± 18.6
18	21	35	0.600	1.34E+05	2.24E+05	4	62.6 ± 17.3
19	15	29	0.517	1.92E+05	3.71E+05	6	54.0 ± 17.2
20	14	20	0.700	1.79E+05	2.56E+05	4	73.0 ± 25.4
21	21	27	0.778	1.79E+05	2.30E+05	4	81.1 ± 23.6
22	7	9	0.778	1.79E+05	2.30E+05	4	81.1 ± 40.9
23	8	13	0.615	1.02E+05	1.66E+05	3	64.2 ± 28.9
24	2	7	0.286	5.12E+04	1.79E+05	3	29.9 ± 24.0
25	5	9	0.556	1.28E+05	2.30E+05	4	58.0 ± 32.4
26	10	29	0.345	8.53E+04	2.47E+05	4	36.1 ± 13.2
27	3	6	0.500	7.68E+04	1.54E+05	3	52.2 ± 36.9
28	5	7	0.714	1.28E+05	1.79E+05	3	74.5 ± 43.6
29	40	40	1.000	2.56E+05	2.56E+05	4	104.0 ± 23.3
30	4	15	0.267	1.02E+05	3.84E+05	6	27.9 ± 15.7
31	3	7	0.429	7.68E+04	1.79E+05	3	44.8 ± 30.9
32	7	12	0.583	1.79E+05	3.07E+05	5	60.9 ± 29.0
33	6	11	0.545	1.54E+05	2.82E+05	5	57.0 ± 28.9
34	17	18	0.944	4.35E+05	4.61E+05	8	98.3 ± 33.2
35	9	13	0.692	2.30E+05	3.33E+05	6	72.2 ± 31.3
	348	564		1.68E+05	2.72E+05	5	

SUMMARY OF STATISTICS

Variance of Square root of NS = 1.1161
Variance of Square root of NI = 1.3123
Correlation coefficient (R for NS vs. NI) = 0.8370

AGE CALCULATION

Zeta factor used = 10594.0± 439.0
Glass dosimeter = SRM614
ND counted = 1200
RHOD D for glass = 1.980E+04 ± 0.572E+03
Area of 1 QUAD = 1.5625E-06
Pooled NS/NI = 0.617 ± 0.042
Mean NS/NI = 0.611 ± 0.036

POOLED AGE

64.4 ± 5.5 MA

MEAN AGE

63.8 ± 4.9 MA

Sample J-77P

CRYSTAL	NS	NI	RATIO	RHO S	RHO I	[U] ppm	AGE (MA)
1	15	13	1.154	3.84E+05	3.33E+05	6	119.4 ± 45.2
2	4	5	0.800	1.02E+05	1.28E+05	2	83.0 ± 55.7
3	46	97	0.474	1.18E+06	2.48E+06	42	49.3 ± 8.8
4	10	20	0.500	2.56E+05	5.12E+05	9	52.0 ± 20.1
5	7	13	0.538	1.79E+05	3.33E+05	6	56.0 ± 26.3
6	7	8	0.875	1.79E+05	2.05E+05	3	90.8 ± 47.0
7	3	10	0.300	7.68E+04	2.56E+05	4	31.3 ± 20.6
8	11	10	1.100	2.82E+05	2.56E+05	4	113.9 ± 49.8
9	10	15	0.667	2.56E+05	3.84E+05	6	69.3 ± 28.3
10	18	27	0.667	4.61E+05	6.91E+05	12	69.3 ± 21.1
11	3	10	0.300	7.68E+04	2.56E+05	4	31.3 ± 20.6
12	2	3	0.667	5.12E+04	7.68E+04	1	69.3 ± 63.2
13	7	7	1.000	1.79E+05	1.79E+05	3	103.6 ± 55.4

SUMMARY OF STATISTICS

Variance of Square root of NS = 1.9885
Variance of Square root of NI = 4.1073
Correlation coefficient (R for NS vs. NI) = 0.9638

Chi^2 = 11.24001 with 12 degrees of freedom. TEST PASS

AGE CALCULATION

Zeta factor used = 10594.0± 439.0
Glass dosimeter = SRM614
ND counted = 1200
RHOD D for glass = 1.972E+04 ± 0.569E+03
Area of 1 QUAD = 1.5625E-06
Pooled NS/NI = 0.601 ± 0.064
Mean NS/NI = 0.696 ± 0.081

POOLED AGE

62.5 ± 7.3 MA

MEAN AGE

72.2 ± 9.1 MA

Sample C-67-2

CRYSTAL	NS	NI	RATIO	RHO S	RHO I	[U] ppm	AGE (MA)
1	7	15	0.467	1.79E+05	3.84E+05	5	61.0 ± 27.9
2	4	14	0.286	1.02E+05	3.58E+05	5	37.4 ± 21.2
3	2	59	0.034	5.12E+04	1.51E+06	20	4.5 ± 3.2
4	6	13	0.462	1.54E+05	3.33E+05	4	60.3 ± 29.8
5	4	17	0.235	1.02E+05	4.35E+05	6	30.8 ± 17.1
6	5	16	0.313	1.28E+05	4.10E+05	6	40.9 ± 21.0
7	2	4	0.500	5.12E+04	1.02E+05	1	65.4 ± 56.6
8	5	16	0.313	1.28E+05	4.10E+05	6	40.9 ± 21.0
9	4	74	0.054	1.02E+05	1.89E+06	25	7.1 ± 3.6
10	2	11	0.182	5.12E+04	2.82E+05	4	23.8 ± 18.3
11	4	14	0.286	1.02E+05	3.58E+05	5	37.4 ± 21.2
12	2	5	0.400	5.12E+04	1.28E+05	2	52.3 ± 43.8
13	5	12	0.417	1.28E+05	3.07E+05	4	54.5 ± 29.0
14	2	5	0.400	5.12E+04	1.28E+05	2	52.3 ± 43.8
15	2	5	0.400	5.12E+04	1.28E+05	2	52.3 ± 43.8
16	7	16	0.438	1.79E+05	4.10E+05	6	57.2 ± 25.9
	63	296		1.01E+05	4.74E+05	6	

SUMMARY OF STATISTICS

Variance of Square root of NS = 0.2127
Variance of Square root of NI = 3.2706
Correlation coefficient (R for NS vs. NI) = 0.0066

Chi^2 = 31.42755 with 15 degrees of freedom. TEST FAIL

AGE CALCULATION

Zeta factor used = 10594.0± 439.0
Glass dosimeter = SRM614
ND counted = 1600
RHOD D for glass = 2.480E+04 ± 0.620E+03
Area of 1 QUAD = 1.5625E-06
Pooled NS/NI = 0.213 ± 0.030
Mean NS/NI = 0.324 ± 0.036

POOLED AGE

27.9 ± 4.1 MA

MEAN AGE

42.4 ± 5.2 MA

Sample VB-43-1A

CRYSTAL	NS	NI	RATIO	RHO S	RHO I	[U] ppm	AGE (MA)
1	1	5	0.200	2.56E+04	1.28E+05	4	12.3 ± 13.4
2	1	3	0.333	2.56E+04	7.68E+04	2	20.4 ± 23.6
3	0	3	0.000	0.00E+00	7.68E+04	2	0.0 ± INFINITE
4	8	21	0.381	2.56E+05	6.72E+05	19	23.4 ± 9.7
5	1	5	0.200	2.56E+04	1.28E+05	4	12.3 ± 13.4
6	0	3	0.000	0.00E+00	7.68E+04	2	0.0 ± INFINITE
7	0	3	0.000	0.00E+00	7.68E+04	2	0.0 ± INFINITE
8	1	7	0.143	2.56E+04	1.79E+05	5	8.8 ± 9.4
9	1	6	0.167	2.56E+04	1.54E+05	4	10.2 ± 11.1
10	1	4	0.250	2.56E+04	1.02E+05	3	15.3 ± 17.2
11	1	7	0.143	2.56E+04	1.79E+05	5	8.8 ± 9.4
12	2	5	0.400	5.12E+04	1.28E+05	4	24.5 ± 20.5
13	1	5	0.200	2.56E+04	1.28E+05	4	12.3 ± 13.4
14	0	5	0.000	0.00E+00	1.28E+05	4	0.0 ± INFINITE
	18	82		3.34E+04	1.52E+05	5	

SUMMARY OF STATISTICS

Variance of Square root of NS = 0.5611
Variance of Square root of NI = 0.5283
Correlation coefficient (R for NS vs. NI) = 0.9560

Chi^2 = 5.97007 with 13 degrees of freedom. TEST PASS

AGE CALCULATION

Zeta factor used = 10594.0± 439.0

POOLED AGE

Glass dosimeter = SRM614
ND counted = 380 13.5 ± 3.6 MA
RHOD D for glass = 1.160E+04 ± 0.595E+03
Area of 1 QUAD = 1.5625E-06
Pooled NS/NI = 0.220 ± 0.057

MEAN AGE

Mean NS/NI = 0.173 ± 0.038
10.6 ± 2.5 MA

Sample VB-43-1B

CRYSTAL	NS	NI	RATIO	RHO S	RHO I	[U] ppm	AGE (MA)
1	2	8	0.250	5.12E+04	2.05E+05	6	15.5 ± 12.2
2	1	2	0.500	2.56E+04	5.12E+04	1	30.9 ± 37.9
3	0	1	0.000	0.00E+00	2.56E+04	1	0.0 ± INFINITE
4	2	14	0.143	5.12E+04	3.58E+05	10	8.8 ± 6.7
5	1	4	0.250	2.56E+04	1.02E+05	3	15.5 ± 17.3
6	0	2	0.000	0.00E+00	5.12E+04	1	0.0 ± INFINITE
7	1	5	0.200	2.56E+04	1.28E+05	4	12.4 ± 13.6
8	5	8	0.625	1.28E+05	2.05E+05	6	38.6 ± 22.0
	12	44		3.84E+04	1.41E+05	4	

SUMMARY OF STATISTICS

Variance of Square root of NS = 0.5529
Variance of Square root of NI = 0.8401
Correlation coefficient (R for NS vs. NI) = 0.5949

Chi^2 = 4.167366 with 7 degrees of freedom. TEST PASS

AGE CALCULATION

Zeta factor used = 10594.0± 439.0
Glass dosimeter = SRM614
ND counted = 380
RHOD D for glass = 1.170E+04 ± 0.600E+03
Area of 1 QUAD = 1.5625E-06
Pooled NS/NI = 0.273 ± 0.089
Mean NS/NI = 0.246 ± 0.084

POOLED AGE

16.9 ± 5.6 MA

MEAN AGE

15.2 ± 5.3 MA

Sample VB-43-8

CRYSTAL	NS	NI	RATIO	RHO S	RHO I	[U] ppm	AGE (MA)
1	0	4	0.000	0.00E+00	1.02E+05	3	0.0 ± INFINITE
2	0	17	0.000	0.00E+00	4.35E+05	12	0.0 ± INFINITE
3	0	33	0.000	0.00E+00	8.45E+05	24	0.0 ± INFINITE
4	0	10	0.000	0.00E+00	2.56E+05	7	0.0 ± INFINITE
5	0	5	0.000	0.00E+00	1.28E+05	4	0.0 ± INFINITE
6	0	7	0.000	0.00E+00	1.79E+05	5	0.0 ± INFINITE
7	1	7	0.143	2.56E+04	1.79E+05	5	9.0 ± 9.7
8	2	16	0.125	5.12E+04	4.10E+05	11	7.9 ± 5.9
9	3	9	0.333	7.68E+04	2.30E+05	6	21.1 ± 14.0
10	4	19	0.211	1.02E+05	4.86E+05	14	13.3 ± 7.3
11	1	5	0.200	2.56E+04	1.28E+05	4	12.6 ± 13.9
12	0	6	0.000	0.00E+00	1.54E+05	4	0.0 ± INFINITE
13	1	9	0.111	2.56E+04	2.30E+05	6	7.0 ± 7.4
14	0	8	0.000	0.00E+00	2.05E+05	6	0.0 ± INFINITE
15	0	6	0.000	0.00E+00	1.54E+05	4	0.0 ± INFINITE
16	4	14	0.286	1.02E+05	3.58E+05	10	18.1 ± 10.2
17	2	5	0.400	5.12E+04	1.28E+05	4	25.3 ± 21.1
18	2	9	0.222	5.12E+04	2.30E+05	6	14.1 ± 11.0
19	1	13	0.077	2.56E+04	3.33E+05	9	4.9 ± 5.1
20	0	6	0.000	0.00E+00	1.54E+05	4	0.0 ± INFINITE
21	0	3	0.000	0.00E+00	7.68E+04	2	0.0 ± INFINITE
22	0	29	0.000	0.00E+00	7.42E+05	21	0.0 ± INFINITE
23	0	5	0.000	0.00E+00	1.28E+05	4	0.0 ± INFINITE
	21	245		2.34E+04	2.73E+05	8	

SUMMARY OF STATISTICS

Variance of Square root of NS = 0.5686
Variance of Square root of NI = 1.0991
Correlation coefficient (R for NS vs. NI) = 0.1307

Chi² = 31.58962 with 22 degrees of freedom. TEST PASS

AGE CALCULATION

Zeta factor used = 10594.0± 439.0
Glass dosimeter = SRM614
ND counted = 380
RHOD D for glass = 1.195E+04 ± 0.613E+03
Area of 1 QUAD = 1.5625E-06
Pooled NS/NI = 0.086 ± 0.019
Mean NS/NI = 0.092 ± 0.027

POOLED AGE
5.4 ± 1.3 MA

MEAN AGE
5.8 ± 1.7 MA

Sample VH-22-1

CRYSTAL	NS	NI	RATIO	RHO S	RHO I	[U] ppm	AGE (MA)
1	0	7	0.000	0.00E+00	1.79E+05	5	0.0 ± INFINITE
2	1	6	0.167	2.56E+04	1.54E+05	4	10.3 ± 11.1
3	0	6	0.000	0.00E+00	1.54E+05	4	0.0 ± INFINITE
4	1	4	0.250	2.56E+04	1.02E+05	3	15.5 ± 17.3
5	0	7	0.000	0.00E+00	1.79E+05	5	0.0 ± INFINITE
6	0	6	0.000	0.00E+00	1.54E+05	4	0.0 ± INFINITE
7	1	2	0.500	2.56E+04	5.12E+04	1	30.9 ± 37.9
8	1	5	0.200	2.56E+04	1.28E+05	4	12.4 ± 13.6
9	0	5	0.000	0.00E+00	1.28E+05	4	0.0 ± INFINITE
10	1	3	0.333	2.56E+04	7.68E+04	2	20.6 ± 23.8
11	1	3	0.333	2.56E+04	7.68E+04	2	20.6 ± 23.8
12	3	5	0.600	7.68E+04	1.28E+05	4	37.1 ± 27.1
13	0	5	0.000	0.00E+00	1.28E+05	4	0.0 ± INFINITE
14	1	2	0.500	2.56E+04	5.12E+04	1	30.9 ± 37.9
15	0	4	0.000	0.00E+00	1.02E+05	3	0.0 ± INFINITE
16	4	28	0.143	1.02E+05	7.17E+05	20	8.8 ± 4.7
	14	98		2.24E+04	1.57E+05	4	

SUMMARY OF STATISTICS

Variance of Square root of NS = 0.4534
Variance of Square root of NI = 0.7772
Correlation coefficient (R for NS vs. NI) = 0.6370

Chi^2 = 14.18231 with 15 degrees of freedom. TEST PASS

AGE CALCULATION

Zeta factor used = 10594.0± 439.0
Glass dosimeter = SRM614
ND counted = 380
RHOD D for glass = 1.170E+04 ± 0.600E+03
Area of 1 QUAD = 1.5625E-06
Pooled NS/NI = 0.143 ± 0.041
Mean NS/NI = 0.189 ± 0.054

POOLED AGE

8.8 ± 2.6 MA

MEAN AGE

11.7 ± 3.4 MA

Sample VH-22-9

CRYSTAL	NS	NI	RATIO	RHO S	RHO I	[U] ppm	AGE (MA)
1	0	19	0.000	0.00E+00	4.86E+05	14	0.0 ± INFINITE
2	0	7	0.000	0.00E+00	1.79E+05	5	0.0 ± INFINITE
3	0	6	0.000	0.00E+00	1.54E+05	4	0.0 ± INFINITE
4	4	90	0.044	1.02E+05	2.30E+06	67	2.7 ± 1.4
5	3	23	0.130	7.68E+04	5.89E+05	17	7.9 ± 4.9
6	0	5	0.000	0.00E+00	1.28E+05	4	0.0 ± INFINITE
7	2	44	0.045	5.12E+04	1.13E+06	33	2.8 ± 2.0
8	0	5	0.000	0.00E+00	1.28E+05	4	0.0 ± INFINITE
9	1	4	0.250	2.56E+04	1.02E+05	3	15.2 ± 17.0
10	5	31	0.161	1.28E+05	7.94E+05	23	9.8 ± 4.7
11	3	10	0.300	7.68E+04	2.56E+05	7	18.2 ± 12.0
12	2	40	0.050	5.12E+04	1.02E+06	30	3.0 ± 2.2
13	1	5	0.200	2.56E+04	1.28E+05	4	12.2 ± 13.3
14	0	7	0.000	0.00E+00	1.79E+05	5	0.0 ± INFINITE
15	1	8	0.125	2.56E+04	2.05E+05	6	7.6 ± 8.1
16	0	7	0.000	0.00E+00	1.79E+05	5	0.0 ± INFINITE
17	2	6	0.333	5.12E+04	1.54E+05	4	20.3 ± 16.6
18	3	11	0.273	7.68E+04	2.82E+05	8	16.6 ± 10.8
19	3	43	0.070	7.68E+04	1.10E+06	32	4.2 ± 2.5
20	1	17	0.059	2.56E+04	4.35E+05	13	3.6 ± 3.7
21	0	19	0.000	0.00E+00	4.86E+05	14	0.0 ± INFINITE
	31	407		3.78E+04	4.96E+05	14	

SUMMARY OF STATISTICS

Variance of Square root of NS = 0.6533
Variance of Square root of NI = 3.9245
Correlation coefficient (R for NS vs. NI) = 0.6073

Chi^2 = 26.80817 with 20 degrees of freedom. TEST PASS

AGE CALCULATION

Zeta factor used = 10594.0± 439.0
Glass dosimeter = SRM614
ND counted = 380
RHOD D for glass = 1.150E+04 ± 0.590E+03
Area of 1 QUAD = 1.5625E-06
Pooled NS/NI = 0.076 ± 0.014
Mean NS/NI = 0.097 ± 0.025

POOLED AGE

4.6 ± 0.9 MA

MEAN AGE

5.9 ± 1.6 MA

Sample VB-13-1

CRYSTAL	NS	NI	RATIO	RHO S	RHO I	[U] ppm	AGE (MA)
1	0	6	0.000	0.00E+00	1.54E+05	2	0.0 ± INFINITE
2	1	6	0.167	2.56E+04	1.54E+05	2	21.6 ± 23.3
3	2	3	0.667	5.12E+04	7.68E+04	1	85.9 ± 78.5
4	1	9	0.111	2.56E+04	2.30E+05	3	14.4 ± 15.2
5	0	6	0.000	0.00E+00	1.54E+05	2	0.0 ± INFINITE
6	1	7	0.143	2.56E+04	1.79E+05	2	18.5 ± 19.8
7	0	4	0.000	0.00E+00	1.02E+05	1	0.0 ± INFINITE
8	1	6	0.167	2.56E+04	1.54E+05	2	21.6 ± 23.3
9	3	8	0.375	7.68E+04	2.05E+05	3	48.5 ± 32.8
10	2	8	0.250	5.12E+04	2.05E+05	3	32.4 ± 25.6
11	1	8	0.125	2.56E+04	2.05E+05	3	16.2 ± 17.2
12	2	9	0.222	5.12E+04	2.30E+05	3	28.8 ± 22.5
13	2	8	0.250	5.12E+04	2.05E+05	3	32.4 ± 25.6
14	1	7	0.143	2.56E+04	1.79E+05	2	18.5 ± 19.8
15	0	9	0.000	0.00E+00	2.30E+05	3	0.0 ± INFINITE
16	0	3	0.000	0.00E+00	7.68E+04	1	0.0 ± INFINITE
17	0	4	0.000	0.00E+00	1.02E+05	1	0.0 ± INFINITE
	17	111		2.56E+04	1.67E+05	2	

SUMMARY OF STATISTICS

Variance of Square root of NS = 0.4034
Variance of Square root of NI = 0.1816
Correlation coefficient (R for NS vs. NI) = 0.3941

Chi^2 = 11.03407 with 16 degrees of freedom. TEST PASS

AGE CALCULATION

Zeta factor used = 10594.0± 439.0
Glass dosimeter = SRM614
ND counted = 1600
RHOD D for glass = 2.450E+04 ± 0.613E+03
Area of 1 QUAD = 1.5625E-06
Pooled NS/NI = 0.153 ± 0.040
Mean NS/NI = 0.154 ± 0.043

POOLED AGE

19.8 ± 5.3 MA

MEAN AGE

20.0 ± 5.7 MA

Sample VB-13-4A

CRYSTAL	NS	NI	RATIO	RHO S	RHO I	[U] ppm	AGE (MA)
1	1	4	0.250	2.56E+04	1.02E+05	3	15.7 ± 17.5
2	1	4	0.250	2.56E+04	1.02E+05	3	15.7 ± 17.5
3	0	6	0.000	0.00E+00	1.54E+05	4	0.0 ± INFINITE
4	0	3	0.000	0.00E+00	7.68E+04	2	0.0 ± INFINITE
5	2	3	0.667	5.12E+04	7.68E+04	2	41.7 ± 38.1
6	0	6	0.000	0.00E+00	1.54E+05	4	0.0 ± INFINITE
7	1	5	0.200	2.56E+04	1.28E+05	4	12.5 ± 13.7
8	0	5	0.000	0.00E+00	1.28E+05	4	0.0 ± INFINITE
9	2	6	0.333	5.12E+04	1.54E+05	4	20.9 ± 17.1
10	1	7	0.143	2.56E+04	1.79E+05	5	9.0 ± 9.6
11	4	6	0.667	1.02E+05	1.54E+05	4	41.7 ± 26.9
12	0	3	0.000	0.00E+00	7.68E+04	2	0.0 ± INFINITE
13	6	31	0.194	1.54E+05	7.94E+05	22	12.1 ± 5.4
14	1	5	0.200	2.56E+04	1.28E+05	4	12.5 ± 13.7
15	2	5	0.400	5.12E+04	1.28E+05	4	25.1 ± 21.0
16	0	5	0.000	0.00E+00	1.28E+05	4	0.0 ± INFINITE
17	0	6	0.000	0.00E+00	1.54E+05	4	0.0 ± INFINITE
18	0	4	0.000	0.00E+00	1.02E+05	3	0.0 ± INFINITE
19	0	7	0.000	0.00E+00	1.79E+05	5	0.0 ± INFINITE
20	2	23	0.087	5.12E+04	5.89E+05	17	5.5 ± 4.0
21	1	10	0.100	2.56E+04	2.56E+05	7	6.3 ± 6.6
22	0	6	0.000	0.00E+00	1.54E+05	4	0.0 ± INFINITE
23	0	13	0.000	0.00E+00	3.33E+05	9	0.0 ± INFINITE
24	0	4	0.000	0.00E+00	1.02E+05	3	0.0 ± INFINITE
25	0	6	0.000	0.00E+00	1.54E+05	4	0.0 ± INFINITE
26	0	3	0.000	0.00E+00	7.68E+04	2	0.0 ± INFINITE
27	8	114	0.070	2.05E+05	2.92E+06	82	4.4 ± 1.6
28	0	6	0.000	0.00E+00	1.54E+05	4	0.0 ± INFINITE
29	0	8	0.000	0.00E+00	2.05E+05	6	0.0 ± INFINITE
30	0	14	0.000	0.00E+00	3.58E+05	10	0.0 ± INFINITE
	32	328		2.73E+04	2.80E+05	8	

SUMMARY OF STATISTICS

Variance of Square root of NS = 0.6914
Variance of Square root of NI = 2.9324
Correlation coefficient (R for NS vs. NI) = 0.7879

Chi^2 = 39.92941 with 29 degrees of freedom. TEST PASS

AGE CALCULATION

Zeta factor used = 10594.0± 439.0
Glass dosimeter = SRM614
ND counted = 380
RHOD D for glass = 1.185E+04 ± 0.608E+03
Area of 1 QUAD = 1.5625E-06
Pooled NS/NI = 0.098 ± 0.018
Mean NS/NI = 0.119 ± 0.035

POOLED AGE

6.1 ± 1.2 MA

MEAN AGE

7.4 ± 2.2 MA

Sample VB-13-4B

CRYSTAL	NS	NI	RATIO	RHO S	RHO I	[U] ppm	AGE (MA)
1	3	19	0.158	7.68E+04	4.86E+05	14	10.0 ± 6.2
2	4	12	0.333	1.02E+05	3.07E+05	9	21.1 ± 12.2
3	1	11	0.091	2.56E+04	2.82E+05	8	5.8 ± 6.0
4	1	5	0.200	2.56E+04	1.28E+05	4	12.6 ± 13.9
5	0	5	0.000	0.00E+00	1.28E+05	4	0.0 ± INFINITE
6	0	9	0.000	0.00E+00	2.30E+05	6	0.0 ± INFINITE
7	0	5	0.000	0.00E+00	1.28E+05	4	0.0 ± INFINITE
8	1	7	0.143	2.56E+04	1.79E+05	5	9.0 ± 9.7
9	1	8	0.125	2.56E+04	2.05E+05	6	7.9 ± 8.4
10	0	7	0.000	0.00E+00	1.79E+05	5	0.0 ± INFINITE
11	0	4	0.000	0.00E+00	1.02E+05	3	0.0 ± INFINITE
12	0	5	0.000	0.00E+00	1.28E+05	4	0.0 ± INFINITE
13	0	8	0.000	0.00E+00	2.05E+05	6	0.0 ± INFINITE
14	0	5	0.000	0.00E+00	1.28E+05	4	0.0 ± INFINITE
15	0	6	0.000	0.00E+00	1.54E+05	4	0.0 ± INFINITE
16	0	2	0.000	0.00E+00	5.12E+04	1	0.0 ± INFINITE
17	0	8	0.000	0.00E+00	2.05E+05	6	0.0 ± INFINITE
18	0	6	0.000	0.00E+00	1.54E+05	4	0.0 ± INFINITE
19	1	4	0.250	2.56E+04	1.02E+05	3	15.8 ± 17.7
20	0	4	0.000	0.00E+00	1.02E+05	3	0.0 ± INFINITE
	12	140		1.54E+04	1.79E+05	5	

SUMMARY OF STATISTICS

Variance of Square root of NS = 0.4309
Variance of Square root of NI = 0.4132
Correlation coefficient (R for NS vs. NI) = 0.7191

Chi^2 = 15.78545 with 19 degrees of freedom. TEST PASS

AGE CALCULATION

Zeta factor used = 10594.0± 439.0
Glass dosimeter = SRM614
ND counted = 380
RHOD D for glass = 1.195E+04 ± 0.613E+03
Area of 1 QUAD = 1.5625E-06
Pooled NS/NI = 0.086 ± 0.026

POOLED AGE

5.4 ± 1.7 MA

Sample 2G-47-1

CRYSTAL	NS	NI	RATIO	RHO S	RHO I	[U] ppm	AGE (MA)
1	0	4	0.000	0.00E+00	1.02E+05	1	0.0 ± INFINITE
2	3	4	0.750	1.28E+05	1.71E+05	2	97.4 ± 74.4
3	6	17	0.353	1.54E+05	4.35E+05	6	46.0 ± 21.8
4	3	16	0.188	7.68E+04	4.10E+05	6	24.5 ± 15.4
5	1	14	0.071	2.56E+04	3.58E+05	5	9.3 ± 9.7
6	2	11	0.182	5.12E+04	2.82E+05	4	23.7 ± 18.3
7	7	35	0.200	1.79E+05	8.96E+05	12	26.1 ± 10.8
8	3	25	0.120	7.68E+04	6.40E+05	9	15.7 ± 9.6
9	0	8	0.000	0.00E+00	2.05E+05	3	0.0 ± INFINITE
10	2	16	0.125	5.12E+04	4.10E+05	6	16.3 ± 12.3
11	4	24	0.167	1.02E+05	6.14E+05	8	21.8 ± 11.8
12	4	15	0.267	1.02E+05	3.84E+05	5	34.8 ± 19.6
13	4	11	0.364	1.02E+05	2.82E+05	4	47.4 ± 27.7
14	2	24	0.083	5.12E+04	6.14E+05	8	10.9 ± 8.0
15	0	17	0.000	0.00E+00	4.35E+05	6	0.0 ± INFINITE
16	1	25	0.040	2.56E+04	6.40E+05	9	5.2 ± 5.3
17	0	28	0.000	0.00E+00	7.17E+05	10	0.0 ± INFINITE
18	0	10	0.000	0.00E+00	2.56E+05	3	0.0 ± INFINITE
19	0	16	0.000	0.00E+00	4.10E+05	6	0.0 ± INFINITE
20	1	10	0.100	2.56E+04	2.56E+05	3	13.1 ± 13.7
21	4	92	0.043	1.02E+05	2.36E+06	32	5.7 ± 2.9
22	1	20	0.050	2.56E+04	5.12E+05	7	6.5 ± 6.7
23	2	10	0.200	6.40E+04	3.20E+05	4	26.1 ± 20.2
24	2	13	0.154	5.12E+04	3.33E+05	4	20.1 ± 15.3
25	0	5	0.000	0.00E+00	1.28E+05	2	0.0 ± INFINITE
26	0	9	0.000	0.00E+00	2.30E+05	3	0.0 ± INFINITE
27	14	96	0.146	3.58E+05	2.46E+06	33	19.1 ± 5.5
28	0	14	0.000	0.00E+00	3.58E+05	5	0.0 ± INFINITE
29	1	12	0.083	2.56E+04	3.07E+05	4	10.9 ± 11.3
30	1	32	0.031	2.56E+04	8.19E+05	11	4.1 ± 4.1
	68	633		5.92E+04	5.51E+05	7	

SUMMARY OF STATISTICS

Variance of Square root of NS = 0.9284
Variance of Square root of NI = 3.1771
Correlation coefficient (R for NS vs. NI) = 0.6806

Chi^2 = 48.85868 with 29 degrees of freedom. TEST FAIL

AGE CALCULATION

Zeta factor used = 10594.0± 439.0
Glass dosimeter = SRM614
ND counted = 1600
RHOD D for glass = 2.470E+04 ± 0.618E+03
Area of 1 QUAD = 1.5625E-06
Pooled NS/NI = 0.107 ± 0.014
Mean NS/NI = 0.124 ± 0.029

POOLED AGE

14.0 ± 1.9 MA

MEAN AGE

16.2 ± 3.9 MA

Sample K-90-1

CRYSTAL	NS	NI	RATIO	RHO S	RHO I	[U] ppm	AGE (MA)
1	1	4	0.250	2.56E+04	1.02E+05	1	33.5 ± 37.5
2	0	6	0.000	0.00E+00	1.54E+05	2	0.0 ± INFINITE
3	1	10	0.100	2.56E+04	2.56E+05	3	13.4 ± 14.1
4	1	78	0.013	2.56E+04	2.00E+06	26	1.7 ± 1.7
5	1	70	0.014	2.56E+04	1.79E+06	24	1.9 ± 1.9
6	1	8	0.125	2.56E+04	2.05E+05	3	16.8 ± 17.8
7	0	18	0.000	0.00E+00	4.61E+05	6	0.0 ± INFINITE
8	0	31	0.000	0.00E+00	7.94E+05	10	0.0 ± INFINITE
9	1	13	0.077	2.56E+04	3.33E+05	4	10.3 ± 10.7
	6	238		1.71E+04	6.77E+05	9	

SUMMARY OF STATISTICS

Variance of Square root of NS = 0.2500
Variance of Square root of NI = 6.3407
Correlation coefficient (R for NS vs. NI) = 0.2157

$Chi^{2\prime}$ = 14.70266 with 8 degrees of freedom. TEST PASS

AGE CALCULATION

Zeta factor used = 10594.0± 439.0
Glass dosimeter = SRM614
ND counted = 1600
RHOD D for glass = 2.540E+04 ± 0.635E+03
Area of 1 QUAD = 1.5625E-06
Pooled NS/NI = 0.025 ± 0.010
Mean NS/NI = 0.064 ± 0.030

POOLED AGE
3.4 ± 1.4 MA

MEAN AGE
8.6 ± 4.0 MA

Sample H-86I

CRYSTAL	NS	NI	RATIO	RHO S	RHO I	[U] ppm	AGE (MA)
1	0	67	0.000	0.00E+00	1.72E+06	29	0.0 ± INFINITE
2	0	77	0.000	0.00E+00	1.97E+06	33	0.0 ± INFINITE
3	0	62	0.000	0.00E+00	1.59E+06	27	0.0 ± INFINITE
4	0	78	0.000	0.00E+00	2.00E+06	34	0.0 ± INFINITE
5	3	34	0.088	7.68E+04	8.70E+05	15	9.2 ± 5.6
6	3	139	0.022	7.68E+04	3.56E+06	60	2.3 ± 1.3
7	4	208	0.019	1.02E+05	5.32E+06	90	2.0 ± 1.0
8	1	62	0.016	2.56E+04	1.59E+06	27	1.7 ± 1.7
9	2	81	0.025	5.12E+04	2.07E+06	35	2.6 ± 1.9
10	1	338	0.003	2.56E+04	8.65E+06	146	0.3 ± 0.3
	14	1146		3.58E+04	2.93E+06	49	

SUMMARY OF STATISTICS

Variance of Square root of NS = 0.6797
Variance of Square root of NI = 14.0610
Correlation coefficient (R for NS vs. NI) = 0.2456

Chi^2 = 23.49561 with 9 degrees of freedom. TEST FAIL

AGE CALCULATION

Zeta factor used = 10594.0± 439.0
Glass dosimeter = SRM614
ND counted = 1200
RHOD D for glass = 1.980E+04 ± 0.572E+03
Area of 1 QUAD = 1.5625E-06
Pooled NS/NI = 0.012 ± 0.003
Mean NS/NI = 0.017 ± 0.009

POOLED AGE

1.3 ± 0.4 MA

MEAN AGE

1.8 ± 0.9 MA

9 References cited

Alexander, E. C. (Jr.), Mickelson, G. M., and Lanphere, M. A. 1978. MMHb-1: A new $^{40}Ar/^{39}Ar$ dating standard. U. S. Geol. Surv. Open-File Rept. **78-701**, p. 6-8.

Amoco Canada Petroleum Company Ltd., and Imperial Oil Ltd. 1973. Regional Geology of the Grand Banks. Bull. Can. Petrol. Geol. **21**, p. 479-503.

Avery, M. P. 1978. Vitrinite reflectance measurements of Mobil Tetco Sable Island 4-H-58. Geol. Surv. Can. Report No. EPGS-DOM.5-78MPA.

Avery, M. P. 1983. Vitrinite reflectance (Ro) on the dispersed organics in Mobil-Texaco-Pex Venture B-43. Geol. Surv. Can. Report No. EPGS-DOM.9-83MPA.

Avery, M. P. 1985. Vitrinite reflectance (Ro) of a single sample from Core no. 7 in Mobil et al., Venture H-22. Geol. Surv. Can. Report No. EPGS-DOM.8-85MPA. 15 p.

Avery, M. P. 1986. Vitrinite reflectance (Ro) of dispersed organics from Shell Mic Mac H-86. Geol. Surv. Can. Report No. EPGS-DOM.5-86MPA.

Avery, M. P. 1988. Vitrinite reflectance (Ro) of dispersed organics from Mobil-Texaco-Pex Venture B-13. Geol. Surv. Can. Report No. EPGS-DOM.1-88MPA.

Barr, S.M., Raeside, R.P., and van Breemen, O. 1987. Grenvillian basement in the northern Cape Breton Highlands, Nova Scotia. Can. J. Earth Sci. **24**, p. 992-997.

Beaumont, C., Boutilier, R., Mackenzie, A. S., and Rullkötter, J. 1985. Isomerization and aromatization of hydrocarbons and the paleothermometry and burial history of the Alberta foreland basin. Am. Assoc. Petrol. Geol. Bulletin 69, p. 546-566.

Bradley, D. C. 1982. Subsidence in Late Paleozoic basins in the northern Appalachians. Tectonics, **1**, no. 1, p. 107-123.

Braun, J. and Beaumont, C. (in press). A physical explanation of the relationship between flank uplifts and the breakup unconformity at rifted continental margins. Submitted to Geology, December, 1988

Canada Oil and Gas Lands Administration. 1987. Offshore Schedule of Wells 1966-1986; Energy Mines and Resources, Canada, Indian and Northern Affairs, Canada, Ottawa.

Check, G. 1989. $^{40}Ar/^{39}Ar$ thermochronology of the Britt Domain, Grenville Province - Georgian Bay, Ontario. B.Sc. Honors Thesis, Dalhousie University. 78 p.

Crank, J. 1975. The mathmatics of diffusion, 2nd ed. Clarendon, Oxford.

Dodson, M. H. 1973. Closure temperature in cooling geochronological and petrological systems. Contr. Mineral. and Petrol. **40**, p. 259-274.

Donelick, R. A. 1988. Etchable fission track length reduction in apatite: experimental observations, theory, and geological applications. Ph.D. thesis, Renssalaer Polytechnic Institute, New York, 414 p.

Dow, W. G. 1977. Kerogen studies and geological interpretation. Journal of Geochemical Exploration **7**, p. 79-99.

Falvey, D. A. 1974. The development of continental margins in plate tectonic theory. Australian Petroleum Exploration Journal, **14**, p. 95-106.

Farrar, S. S. and Glover, L. III. 1983. Grenville basement in the Piedmont east of the pre-Appalachian (pre-Caledonian) edge (?) of the North American craton: Geological Society of America, Abstracts with Programs, **15**, no. 3, p. 123.

Faure, G. 1986. Principles of isotope geology, 2nd ed. J. Wiley and Sons, New York.

Fleischer, R., Price, P. B., and Walker, R. M. 1965. Tracks of charged particles in solids. Science, **149**, p. 383-393.

Gibling, M. R., Boehner, R. C., and Rust, B. R. 1987. The Sydney Basin of Atlantic Canada: an upper Paleozoic strike-slip basin in a collisional setting In Sedimentary basins amd basin forming mechanisms. (Eds. C. Beaumont and A. J. Tankard) Can. Soc. Petrol. Geol. Memoir 12, p. 269-285.

Given, M. M. 1977. Mesozoic and Early Cenozoic geology of offshore Nova Scotia. Bull. Can. Petrol. Geol. **25**, p. 63-91.

Gleadow, A. J. W., Duddy, I. R., and Lovering, J. F. 1983. Fission track analysis: A new tool for the evaluation of thermal histories and hydrocarabon potential. Australian Petroleum Exploration Association Journal **23**, p. 93-102.

Gleadow, A. J. W., Duddy, I. R., Green, P. F., and Lovering, J. F. 1986. Confined fission track lengths in apatite: a diagnostic tool for thermal history analysis. Contrib. Mineral. Petrol. **94**, p. 405-415.

Gradstein, G. M., Williams, G. L., Jenkins, W. A. M., and Ascoli, P. 1975. Mesozoic and Cenozoic stratigraphy of the Atlantic continental margin, Eastern Canada. In Canada's Continental Margins and Offshore Petroleum Exploration. (Ed. C. J. Yorath, E. R. Parker, and D. J. Glass). Can. Soc. Petrol. Geol. Memoir 4, p. 103-131.

Grant, A. C., McAlpine, K. D., and Wade, J. A. 1986. The continental margin of eastern Canada: geological framework and petroleum potential. In Future Petroleum Provinces of the World. (Ed. M. T. Halbouty). Bull. Am. Assoc. Petrol. Geol. Memoir 40, p. 177-205.

Green, P. F., Duddy, I. R., Gleadow, A. J. W., Tingate, P. R., and Laslett, G. M. 1986. Thermal annealing of fission tracks in apatite 1. A qualitative description. Chemical Geology (Isotope geoscience section), **59**, p. 237-253.

Green, P. F., Duddy, I. R., Gleadow, A. J. W., and Lovering, J. F. 1989. Apatite fission track analysis as a paleotemperature indicator for

hydrocarbon exploration. In Thermal history of sedimentary basins: Methods and case histories. (Eds. N. D. Naeser, and T. H. McCulloh) Springer-Verlag, New York, 319 p.

Hacquebard, P.A. 1979. Geologic development and economic evaluation of the Sydney coal basin, Nova Scotia, Canada. In Neuvieme Congres International de Stratigraphie et de Geologie du Carbonifere (Eds. M. Gordon Jr., E. S. Belt, A. T. Cross, J. T. Dutro Jr., H. H. J. Geldsetzer, W. L. Manger, R. W. Macqueen, W. W. Nassichuk, H. W. Pfeffercorn, and P. S. Sutherland) Southern Illinois University Press, Carbondale and Edwardsville, (1984) 712 p.

Hacquebard, P. A. 1986. The Gulf of St. Lawrence Carboniferous Basin; the largest coalfield of eastern Canada. CIM Bulletin, **79**, No. 891, p. 67-78.

Hanes, J. A., Clark, S. J., and Archibald, D. A. 1988. An $^{40}Ar/^{39}Ar$ geochronological study of the Elzevir batholith and its bearing on the tectonothermal history of the southwestern Grenville Province, Canada. Can. J. Earth Sci. **25**, p. 1834-1845.

Harrison, T. M. 1983. Some observations on the interpretation of $^{40}Ar/^{39}Ar$ age spectra. Isot. Geosci. **1**, p. 319-338.

Harrison, T. M. and Be, K. 1983. $^{40}Ar/^{39}Ar$ age spectrum analysis of detrital microclines from the southern San Joaquin Basin, California: An approach to determining the thermal evolution of sedimentary basins. Earth Planet. Sci. Lett. **64**, p. 244-256.

Harrison, T. M. and Burke, K. 1989. $^{40}Ar/^{39}Ar$ thermochronology of sedimentary basins using detrital feldspars: Examples from the San Joaquin Valley, California, Rio Grande Rift, New Mexico, and North Sea. In Thermal history of sedimentary basins: Methods and case histories. (Eds. N. D. Naeser, and T. H. McCulloh) Springer-Verlag, New York, 319 p.

Harrison, T. M. and McDougall, I. 1980. Investigations of an intrusive contact, northwest Nelson, New Zealand-I: Thermal, chronological and isotopic constraints. Geochim. Cosmochim. Acta **44**, p. 1985-2003.

Harrison, T. M. and McDougall, I. 1982. The thermal significance of potassium feldspar K-Ar ages inferred from $^{40}Ar/^{39}Ar$ age spectrum results. Geochim. Cosmochim. Acta **46**, pp. 1811-1820.

Harrison, T. M., Duncan, I., and McDougall, I. 1985. Diffusion of ^{40}Ar in biotite: Temperature, pressure and compositional effects. Geochim. Cosmochim. Acta **49**, p. 2461 - 2468.

Hauff, P. L. and Airey, J. 1980. The handling, hazards, and maintenance of heavy liquids in the geologic laboratory. Geol. Surv. Can. circular 827, 24 p.

Hodych, J. P. and Hayatsu, A. 1989. Paleomagnetism and K-Ar isochron dates of Early Jurassic basalt flows and dikes of Atlantic Canada. Can. J. Earth Sci. **25**, p. 1972-1989.

Hurford, A. J. and Green, P. F. 1982. A users' guide to fission track calibration. Earth and Planet. Sci. Lett. **59**, p. 343-354.

Hurford, A. J. and Green, P. F. 1983. The Zeta calibration of fission track dating. Isotope Geoscience, **1**, p. 285-317.

Hurford, A. J. and Hammerschmidt, K. 1985. $^{40}Ar/^{39}Ar$ and K/Ar dating of the Bishop and Fish Canyon tuffs: Calibraton ages for fission track dating standards. Chemical Geology (Isotope Geoscience Section), **58**, p. 23-32.

Hurlbut, C. S. Jr. and Klein, C. 1977. Manual of mineralogy (after J. D. Dana) 19th ed., J. Wiley and Sons, New York, 532 p.

Hayatsu, A. 1979. K-Ar isochron age of the North Mountain basalt, Nova Scotia; Can. Jour. Earth Sci. **16**, p. 973-975.

Huneke, J. C. 1976. Diffusion artifacts in dating by stepwise thermal release of rare gases. Earth Planet. Sci. Lett. **28**, p. 407-417.

Issler, D. R. 1982. Calculation of organic maturation levels from downhole temperatures/burial history curves, Scotian shelf. B.Sc. thesis, University of Waterloo, Ontario, 129 p.

Issler, D. R. 1984. Calculation of organic maturation levels for offshore eastern Canada-implications for general application of Lopatin's method. Can. J. Earth Sci. **21**, p. 477-488.

Jain, S. C. 1958. Simple solutions of the partial differential equation for diffusion (or heat conduction). R. Soc. Lond., Proc. **A243**, p. 359-374.

Jansa, L. F. and Wade, J. A. 1975. Geology of the continental margin off Nova Scotia and Newfoundland. Geol. Surv. Can. Paper 74-30, p. 51-105.

Jost, W. 1960. Diffusion in solids, liquids, and gases. Academic Press, New York.

Keen, C. E., Loncarevic, B. D., Ried, I., Woodside, J., Haworth, R. T., and Williams, H. (in press) Tectonic and geophysical overview. In The geology of the continental margin of eastern Canada (Eds. M. J. Keen and G. Williams) Geological Society of America.

Marillier, F., Keen, C. E., Stockmal, G. S., Quinlan, G., Williams, H., Coleman-Sadd, S. P., and O'Brien, S. J. 1989. Crustal structure and surface zonation of the Canadian Appalachians: implications of deep seismic reflection data. Can. J. Earth Sci. **26**, p. 305-321.

Mackenzie, A. S., Beaumont, C., and Rullkötter, J. 1985. The aromatization and isomerization of hydrocarbons and the thermal and subsidence history of the Nova Scotia margin. Phil. Trans. R. Soc. Lond. A, **315**, p. 203-232.

Mackenzie, A. S. and McKenzie, D. 1983. Isomerization and aromatization of hydrocarbons in sedimentary basins formed by extension. Geological Magazine, **120**, p. 417-528.

McCulloh, T. H. and Naeser, N. D. 1989. Thermal history of sedimentary basins: Introduction and overview. In Thermal history of sedimentary basins. (Ed. N. D. Naeser and T. H. McCulloh). Springer-Verlag, New York, 319 p.

McDougall, I. and Harrison, T. M. 1988. Geochronology and Thermochronology by the $^{40}Ar/^{39}Ar$ method. Clarendon Press, New York. 212 p.

McIver, N. L. 1972. Cenozoic and Mesozoic stratigraphy of the Nova Scotia Shelf. Can. Jour. Earth Sci. **9**, p. 54-70

McWhae, J. R. H. 1981. Structure and spreading history of the north western Atlantic region from the Scotian Shelf to Baffin Bay. In Geology of the North Atlantic Borderlands. (Ed. J. W. Kerr and A. J. Ferguson). Can. Soc. Petrol. Geol. Memoir 7, p. 299-332.

Merrihue, C. and Turner, G. 1966. Potassium-argon dating by activation with fast neutrons. Jour. Geophys. Res. **71**, p. 2852-2857.

Mitchell, J. G. 1968. The argon-40/argon-39 method for potassium-argon age determination. Geochim. Cosmochim. Acta **32**, p. 781-790.

Moore, J. M. 1986. Introduction: The "Grenville Problem" then and now. In The Grenville Province: (Eds. J. M. Moore, A. Davidson, and A. J. Baer) Geological Association of Canada Special Paper 31 p. 1-11.

Noguera Urrea, V. H. 1987. Geology and diagenetic history of overpressured siliciclastic reservoirs in the Lower Missisauga-Mic Mac Formations of the Venture gas field, Scotian Shelf, Nova Scotia. M.Sc. thesis, Dalhousie University, Nova Scotia, 208 p.

Olszewski, W. J. Jr. and Gaudette, H. E. 1982. Age of the Brookville gneiss and associated rocks, southeastern New Brunswick: Can. J. Earth Sci. **19**, p. 2158-2166.

Ozima, M., Kaneoka, I., and Yanagisawa, M. 1989. Temperature and pressure effects on ^{40}Ar-^{39}Ar systematics. Earth Planet. Sci. Lett., **42**, p. 463-472.

Powell, T. G. 1982. Petroleum geochemistry of the Verrill Canyon Formation; a source for Scotian Shelf hydrocarbons: Bulletin of Canadian Petroleum Geology, **30**, p. 167-179.

Price, P. B. and Walker, R. M. 1962. Chemical etching of charged-particle tracks in solids. Jour. Appl. Phys. **33**, p. 3407-3412.

Price, P. B. and Walker, R. M. 1963. Fossil tracks of charged particles in mica and the age of minerals. Jour. of Geophys. Res. **68**, No. 16, p. 4847-4862.

Reichenburg, D. 1953. Properties of ion-exchange resins in relation to their structure. III. Kinetics of exchange. Am. Chem. Soc. J. **75**, p. 589-597.

Reynolds, P. H., Elias, P., Muecke, G. K., and Grist, A. M. 1987. Thermal history of the southwestern Meguma zone, Nova Scotia, from an $^{40}Ar/^{39}Ar$ and fission track dating study of intrusive rocks. Can. J. Earth Sci. **24**, p. 1952-1965.

Silk, E. C. H. and Barnes, R. S. 1959. Phil. Mag. **4**, p. 970.

Turner, G. 1968. The distribution of potassium and argon in chondrites. In Origin and distribution of elements (Ed. L. H. Aherns) Pergammon, London. p. 387-398.

van de Poll, H. W. 1973. Stratigraphy, sediment dispersal and gacies analysis of the Pennsylvanian Pictou Group in New Brunswick. Maritime Sediments, **9**, No. 3, p. 72-77.

Wade, J. A. 1981. Geology of the Canadian Atlantic margin from Georges Bank to the Grand Banks. In Geology of the North Atlantic Borderlands. (Eds. J. W. Kerr and A. J. Ferguson). Can. Soc. Petrol. Geol. Memoir 7, p. 447-460.

Wade, J. A. 1988. The Mesozoic-Cenozoic history of the northwestern margin of North America: Offshore Technological Conference Proceedings, **3**, p. 1849-1859.

Wade, J. A. (in press). The stratigraphy of Georges Bank Basin and relationships to the Scotian Basin. In The geology of the continental margin of eastern Canada (Eds. M. J. Keen and G. Williams) Geological Society of America.

Wade, J. A. and McLean B. C. (in press). Aspects of the geology of the Scotian Basin from recent seismic and well data. In The geology of the continental margin of eastern Canada (Eds. M. J. Keen and G. Williams) Geological Society of America.

Wark, J. M. and Clarke, D. B. 1980. Geochemical discriminators and the paleotectonic environment of the North Mountain basalts, Nova Scotia. Can Jour. Earth Sci. **17**, p. 1740-1745.

Weissel, J. K. and Karner, G. D. (in press). Flexural uplift of rift flanks due to tectonic denudation of the lithosphere during extension.

Williams, H. 1978. Tectonic lithofacies map of the Appalachian Orogen. Memorial University Newfoundland, Map 1, scale 1 : 1,000,000

Williams, H. 1979. Appalachian Orogen in Canada. Can Jour. Earth Sci. **16**, p. 792-807.

Wynne-Edwards, H.R. 1972. The Grenville Province, In Variations in tectonic styles in Canada (Eds. R. A. Price and R. J. W. Douglas): Geological Association of Canada Special Paper 11, p. 263-334.

York, D. 1969. Least squares fitting of a straight line with correlated errors. Earth Planet. Sci. Lett. **39**, p. 94-97.

Zeitler, P. K. 1987. Argon diffusion in partially outgassed alkali feldspars: insights from $^{40}Ar/^{39}Ar$ analysis. Chemical Geology (Isotope Geoscience Section), **65**, p. 167-181.

Zeitler, P. K. and Fitzgerald, J. D. 1986. Saddle-shaped $^{40}Ar/^{39}Ar$ age spectra from young, microstructurally complex potassium feldspars. Geochim. Cosmochim. Acta **50**, p. 1185-1199.